THE INTERSTELLAR MEDIUM NEAR STAR FORMING REGIONS

THE INTERSTELLAR MEDIUM NEAR STAR FORMING REGIONS

By

GLEN R. PETITPAS, B.Sc.

A Thesis

Submitted to the School of Graduate Studies

in Partial Fulfilment of the Requirements for the Degree

Master of Science

McMaster University

MASTER OF SCIENCE (1997)

Department of Physics and Astronomy

McMaster University

Hamilton, Ontario

TITLE: The Interstellar Medium Near Star Forming Regions

AUTHOR: Glen R. Petitpas, B.Sc. (Saint Mary's University)

SUPERVISOR: Dr. Christine D. Wilson

NUMBER OF PAGES: xi, 114

Abstract

This thesis presents C I ($^3P_1-^3P_0$), ^{12}CO J=4−3, and ^{12}CO J=3−2 maps of the barred spiral galaxy M83 taken at the 15-m James Clerk Maxwell Telescope (JCMT). We have also observed the ^{12}CO J=2−1 and J=3−2 lines for molecular clouds in the dwarf irregular galaxies IC 10 and NGC 6822. Additionally, we have observed the ^{13}CO J=2−1 line for IC 10 and made the first detection of the ^{13}CO J=3−2 transition in a Local Group galaxy. In M83, all maps exhibit a similar morphology with a double peaked appearance which is consistent with gas inflow along the bar collecting at the inner Lindblad resonance. This indicates that nuclear starbursts may occur even in galaxies where this phenomenon transpires. The observations cannot rule out that the double peaked emission is the result of a rotating molecular ring out of the plane of the galaxy nearly perpendicular to the main disk. The twelve [C I]/^{12}CO J=4−3 line ratios are uniform, which indicates that the [C I] emission is originating from the same hot regions as the ^{12}CO J=4−3 emission. The ^{12}CO J=4−3/J=3−2 line ratios are higher along an arc of active star forming regions. The high line ratios likely indicate optically thin gas, created by the high temperatures caused by star forming regions in the nucleus of this starburst galaxy.

In IC 10, the CO line ratios are uniform and are consistent with the average line ratios observed in M33 (a spiral galaxy in the Local Group). The ^{12}CO J=3−2/J=2−1 ratio for NGC 6822 is higher than those found for IC 10 and M33 and

suggests that the ^{12}CO emission is optically thin in this region. This high line ratio is likely the result of its location inside a large H II region. The ^{12}CO/^{13}CO J=3−2 line ratio in the molecular clouds MC 1/2 in IC 10 indicates that the gas must have a rather high kinetic temperature of about 100 K. In IC 10 we observe structures on a variety of size scales that all appear to be gravitationally bound. The existence of large gravitationally bound objects may help explain the rather high star formation rate in IC 10.

Acknowledgements

First, I'd like to thank my supervisor Christine Wilson for allowing me the chance to work for her. Her patience and insight has made my trip up the learning curve as simple as humanly possible. Without her wisdom (and knowledge of grammar), this work would not have been possible.

I'd also like to thank my office-mates during the last two years, namely Pat Durrell, Dean McLaughlin, Denise Kaisler, Andy Rorabeck and more recently Brenda Matthews, Tracy Webb and Sean Woodworth, for putting up with me and (rarely) accepting my choices in music. They made long days in the office unquestionably more bearable. I'd especially like to thank Dean for his stimulating discussions on molecular cloud structure, and without Andy's help in quantum, I may not have made it this far! Special thanks to Brenda for helping me with my comma fetish.

Last, but far from least, I thank my parents. I thank my Mom for her continued support and encouragement throughout my life to follow my dreams, even when things weren't going well. I must of course thank my Dad who did not live to see the completion of this project. At times I think everything I accomplished in life I did solely to see the look of pride on his face. Worry not, I'll never forget it. For all observing runs past and future to exotic locations, the most memorable telescope time will be the trips into the back yard with my father. He made me who I am today.

For my Father

Contents

1 Introduction **1**

2 The Nuclear Interstellar Medium of M83 **15**

2.1 Introduction 15

2.2 Observations and Data Reduction 18

2.3 Morphology and Dynamics 19

2.3.1 Gas Collection at Inner Lindblad Resonances? 26

2.3.2 Rotating Gas Disk and Torus Out of the Plane of the Galaxy? 34

2.4 Physical Conditions 37

2.4.1 Column Densities from Line Intensities 39

2.4.2 Line Ratios 45

2.5 Conclusions 50

3 Molecular Clouds in IC 10 and NGC 6822 **52**

3.1 Introduction 52

3.2 Observations and Data Reduction 55

3.3 Molecular Cloud Properties 62

3.3.1 MC 1/2 and MC 6/7/8 in IC 10 62

3.3.2 MC 2 in NGC 6822 69

3.3.3 Molecular Masses 75

3.4 Implications for the CO-to-H_2 Conversion Factor 80

3.5 Conclusions 82

4 Recapitulation **85**

A Calibration and Temperature Scales **89**

B The CO-to-H_2 Conversion Factor **94**

C Local Thermodynamic Equilibrium **98**

D Large Velocity Gradient **105**

References **108**

List of Figures

1.1 **Optical Images of the Galaxies in this Thesis** 9

2.1 **Individual ^{12}CO J=3−2 Spectra for M83** 20

2.2 **Individual ^{12}CO J=4−3 Spectra for M83** 21

2.3 **Individual [C I] Spectra for M83** 22

2.4 **Integrated ^{12}CO J=3−2 Intensity Map for M83** 23

2.5 **Integrated ^{12}CO J=4−3 Intensity Map for M83** 24

2.6 **Integrated [C I] Intensity Map for M83** 25

2.7 **^{12}CO J=3−2 Channel Map for M83** 27

2.8 **^{12}CO J=4−3 Channel Map for M83** 28

2.9 **^{12}CO J=4−3/^{12}CO J=3−2 Line Ratios** 43

2.10 **[C I]/^{12}CO J=4−3 Line Ratios** 48

3.1 **CO Spectral Lines** 57

3.2 **^{13}CO J=3−2 Emission from IC 10:MC 1/2** 58

3.3 **CO Line Ratios** 60

3.4 **LVG Solutions for IC 10:MC 1/2** 65

3.5 **LVG Solutions for IC 10 MC 6/7/8** 68

3.6 **LVG Solutions for NGC 6822 MC 2** 74

List of Tables

2.1 **Properties of Starburst Galaxies** 45

3.1 **CO Line Ratios of Molecular Clouds in IC 10 and NGC 6822** 59

3.2 **Masses of Molecular Clouds in IC 10 and NGC 6822** 77

Chapter 1

Introduction

" And from above the thin squeaks of radio static,

The captured fume of space, foams in our ears ..."

Hart Crane, *The Bridge*, 1929[1]

The regions of space between the stars (the interstellar medium, or ISM) is predominantly filled with neutral hydrogen and helium (Spitzer 1978). Star formation occurs in regions where the ISM has collected into higher density agglomerations of gas and dust. Inside these high density regions, the column density (number of particles in a column along a line of sight) is high enough to shield the inner parts of the cloud from the ionizing ultraviolet (UV) flux, allowing molecules to form (Genzel 1992).

The study of molecular clouds plays a crucial role in our understanding of star formation. Inside giant molecular clouds (GMCs), molecular gas is cycled into the

[1] It wasn't until two years *later* (1931) that Karl Jansky began the initial experiments that subsequently gave birth to the field we now know as radio astronomy.

next generation of stars. Deep inside these clouds, dark dense cores collapse to form massive clusters of stars that in turn heat and eventually dissipate the surrounding molecular gas (Young & Scoville 1991). It is for this reason optical wavelength studies of the early stages of star formation are difficult due to the heavy obscuration caused by the initial surrounding gas and dust cloud. It isn't until the stars have formed and blown away the remaining gas and dust that the stars become visible to the naked eye.

It is believed that the stellar winds created by the formation of new, hot stars can trigger star formation in other nearby molecular clouds or even other parts of the same cloud. It is expected that massive stars should affect nearby star formation since they a) ionize nearby gas which drives shocks into the rest of the cloud, b) shock nearby gas through stellar winds, and c) heat and accelerate gas through subsequent supernova explosions (Elmegreen & Lada 1977). Understanding how star formation influences the physical conditions of molecular gas provides valuable insight into the processes that trigger subsequent bursts of star formation.

Inside these molecular clouds, the main constituent is molecular hydrogen (H_2). This is unfortunate because H_2 is a homonuclear diatomic molecule which means it has no permanent electric dipole moment, hence no dipole radiation. As a result, we must find an alternate way of tracing the mass of molecular clouds. The second most abundant molecule is carbon monoxide (CO, Turner 1988) which fortunately has many possible rotational transitions which are readily excited through collisions with

H_2 (*e.g.* Green & Thaddeus 1976). The lowest of these rotational (J) transitions is the ^{12}CO J=1$-$0 transition which emits radiation at a wavelength of 2.6 millimeters (115 GHz). This wavelength is much larger than the size of the dust grains ($10^{-4} - 10^{-5}$ mm, Spitzer 1978) responsible for the absorption (or reddening) of visual light, hence it is not affected by the same problems that plague studies of star formation at optical wavelengths. It does however suffer from optical depth complications (see Appendix C). ^{12}CO J=1$-$0 emission is usually considered optically thick, which means that we are only seeing emission from the *surface* of the cloud we are observing. Determining if an emission line is optically thick or thin can be accomplished by looking at the line profile. Emission lines that are very optically thick will have a flat topped appearance caused by line saturation. They may also have a dip in the central peak, which is a result of self-absorption caused by the large number of CO molecules along the line of sight in very optically thick gas (*e.g.* Park & Hong 1995). For extragalactic molecular clouds that do not fill the beam[2], the emission line is normally very weak and any line profile structures may get washed out by the noise in the spectra, or smeared out by the superposition of emission at different velocities. Hence, this technique is generally applied to Galactic molecular clouds that fill the beam.

One way to avoid needing line profiles to determine optical depth is to observe some of the rarer isotopomers of CO such as ^{13}CO or C^{18}O. These rarer isotopomers

[2]The beam is the region on the sky from which the telescope collects emission. The sensitivity pattern of the beam can be approximated by a Gaussian distribution so the beam size is often characterized by a full-width at half-maximum.

are generally considered optically thin which allows us to see emission from all depths of the cloud, rather than just the surface. The higher J transitions of CO could potentially be optically thin since they are not as easily excited as the J=1−0 transition, but for the purposes of studying hot, dense star forming regions, this may not be a valid assumption. Another technique involves creating integrated intensity line ratios which eliminate the unknown filling factor of the molecular cloud in the beam. Models (see Appendix C) indicate that CO line ratios greater than one are not allowed for optically thick emission. Unfortunately, line ratios of less than one are predicted for both optically thin and thick gas so we can only determine with any certainty if a cloud is optically thin.

It has been found empirically that there exists a CO-to-H_2 conversion factor (α) that relates CO line intensity ($I_{\rm CO}$) to the column density (N) of H_2 (namely $N({\rm H_2}) = \alpha I_{\rm CO}$). The oldest technique for determining α uses extinction measurements to derive $N({\rm H_2})$. By counting the number of stars we can see in our own Galaxy[3] in a given direction, we can estimate the amount of extinction caused by dust particles. With this information, we can estimate the amount of dust in a region of space. By assuming a gas-to-dust ratio, we then estimate the amount of gas (hence $N({\rm H_2})$). By measuring the CO intensity in that direction we obtain an estimate of

[3]It should be noted that the galaxy we live in is called the Milky Way and is often referred to as the Galaxy. Throughout this thesis, the word 'Galaxy' (capitalized) will refer to the galaxy we live in and 'galaxy' (lower case) will be a generic term for galaxies other than our own. Oddly enough, the term used to describe objects outside of our Galaxy is 'extragalactic' with a lower case 'g'.

α.

A second method for determining α compares diffuse gamma-ray emission with CO and H I data from large scale surveys. The gamma-ray emission is modeled as a linear combination of $N(\mathrm{H\ I})$ and I_{CO} to solve for the cosmic ray distribution (cosmic rays interact with H nucleons to create gamma-rays) and α that best fit the data (Bloeman 1989).

The technique used to derive the CO-to-H_2 conversion factors used in this thesis involves assuming that the clouds are in virial equilibrium. By measuring the width of the clouds' spectral lines, we can estimate the kinetic energy (KE) of the cloud. The virial assumption ($2KE + W = 0$) allows us to convert this kinetic energy into a gravitational potential (W), which in turn allows calculation of the cloud mass. Measuring the cloud size (through interferometry) and assuming most of the mass is in the form of molecular hydrogen allows us to calculate an H_2 column density. This can be compared to the CO line strength to calculate α.

All of the above techniques give values for α (in our own Galaxy) in the range of $1 - 5 \times 10^{20}$ cm^{-2} [K km s^{-1}]$^{-1}$ (Young & Scoville 1991). The current best value is $\alpha_{\mathrm{Gal}} = 3 \times 10^{20}$ cm^{-2} [K km s^{-1}]$^{-1}$ with an uncertainty of $\sim$30%. There are problems with adopting the Galactic value for α when studying other galaxies. It is believed that α depends on the physical conditions inside the molecular clouds such as density, temperature and metallicity. This makes adopting the Galactic value in low metallicity, hot, dense, starburst galaxies a perilous procedure (see Appendix B).

The physical conditions of molecular clouds can be determined by studying the strengths of different molecular emission lines. The kinetic temperature and density of the gas will determine the energy of the collisions with H_2, which in turn determines the rotational energy level (J) to which the CO gas will be excited. By measuring the strengths of emission from the different J transitions of CO, we can estimate the physical conditions within the molecular clouds (Genzel 1992).

One problem with measuring the CO flux of extragalactic molecular clouds is that we do not know the filling factor of the cloud in the beam. Any region of space that is in our beam but is not emitting acts to dilute the strength of the signal. This problem is compounded by the fact that molecular clouds are irregular, clumpy objects (Stutzki & Güsten 1990). Unless we know how much of the material in the beam is emitting, we cannot correct our observed line strengths to true temperatures and fluxes. For the submillimeter wavelength CO emission we are studying in this thesis, the beam size at the 15-m James Clerk Maxwell Telescope (JCMT) is at best $12''$. For a galaxy as far away as M83 (4.7 Mpc[4], de Vaucouleurs 1979), this corresponds to a region of the galaxy that is 270 pc (=890 light years) in diameter. The typical diameters of molecular clouds in our own Galaxy are tens of parsecs. This means that we cannot hope to resolve molecular clouds with the single dish of the JCMT in galaxies that are as distant as M83.

A technique used to eliminate this problem is to create line ratios. By assum-

[4] 1 pc = 3.08×10^{16} m

ing that the same material within the beam is emitting all of the molecular emission, we can divide the integrated intensities of the spectral lines, thus eliminating the unknown filling factor (see Appendix C). By modeling line ratios rather than line intensities, we are able to study the physical conditions in molecular clouds in distant galaxies without knowing the sizes and shapes of the emitting regions.

By measuring large scale CO emission, we can determine the morphology and dynamics of the molecular gas in the galaxy. All emission that we observe is redshifted (receding) or blueshifted (approaching) by the object's motion though space. For example, when we observe a galaxy outside our own, we see the centre of the galaxy's emission redshifted to a new frequency as a result of the entire galaxy's motion away from us (caused by the Hubble expansion of the universe). If the galaxy is rotating, we will see the emission from the side moving away from us redshifted to a greater extent than the centre. Looking at the side of the galaxy moving toward us, we will see the emission redshifted to a lesser extent than the centre. By making maps of galaxies in CO emission we can measure the redshift of the peak of the emission line in different regions of the galaxy with respect to the motion of the centre of the galaxy. Combining the velocity information with the known orientation of the galaxy allows us to determine the motions of the molecular gas. Integrating the emission over all velocities allows us to determine the overall structure of the gas distribution.

This thesis studies the physical conditions of molecular clouds near the star forming regions of two different types of galaxies; barred spirals and dwarf irregulars.

First we look at the nucleus of the barred spiral galaxy M83 (see Chapter 2). It is undergoing a rather strong nuclear starburst (Global Star Formation Rate (GSFR) of 6 solar masses per year ($M_\odot$ yr^{-1})). Its close proximity, pronounced bar structure (see Figure 1.1) and nearly face-on orientation make it one of the best galaxies for studying the gas response to a bar potential. It was first studied in ^{12}CO J=1−0 by Combes *et al.* (1978) who found that the CO was concentrated towards the nucleus, whereas the H I surface density drops toward the center. Their map consisted of only ten positions over the entire galaxy and had a beam size of 64″, which prevented them from finding anything but large scale distribution and kinematics. Twelve years later, Handa *et al.* (1990) took a closer look at the CO gas in M83. They obtained higher resolution maps of ^{12}CO J=1−0 emission (16″ beam) that were fully sampled over the entire optical bar (3.5′× 1′). They found a ridge of CO emission on the leading edge of the bar that is coincident with the observed dust lanes (see Figure 1.1, dust lanes appear lighter in this negative image). They also found that ~40% of the CO emission originates from a region within a radius of 0.4 kpc around the center of the galaxy (equivalent to an area ~10% of the total region mapped), again suggesting concentrations of molecular gas in the nuclear regions of M83.

That same year, Wiklind *et al.* (1990) studied the arm and interarm regions of M83 in ^{12}CO J=1−0 and J=2−1 emission at 43″ and 23″ resolution respectively. They found that the molecular gas showed a well-defined spiral arm structure that was offset 300 pc downstream (*i.e.* in the wake of the spiral arm) from the observed

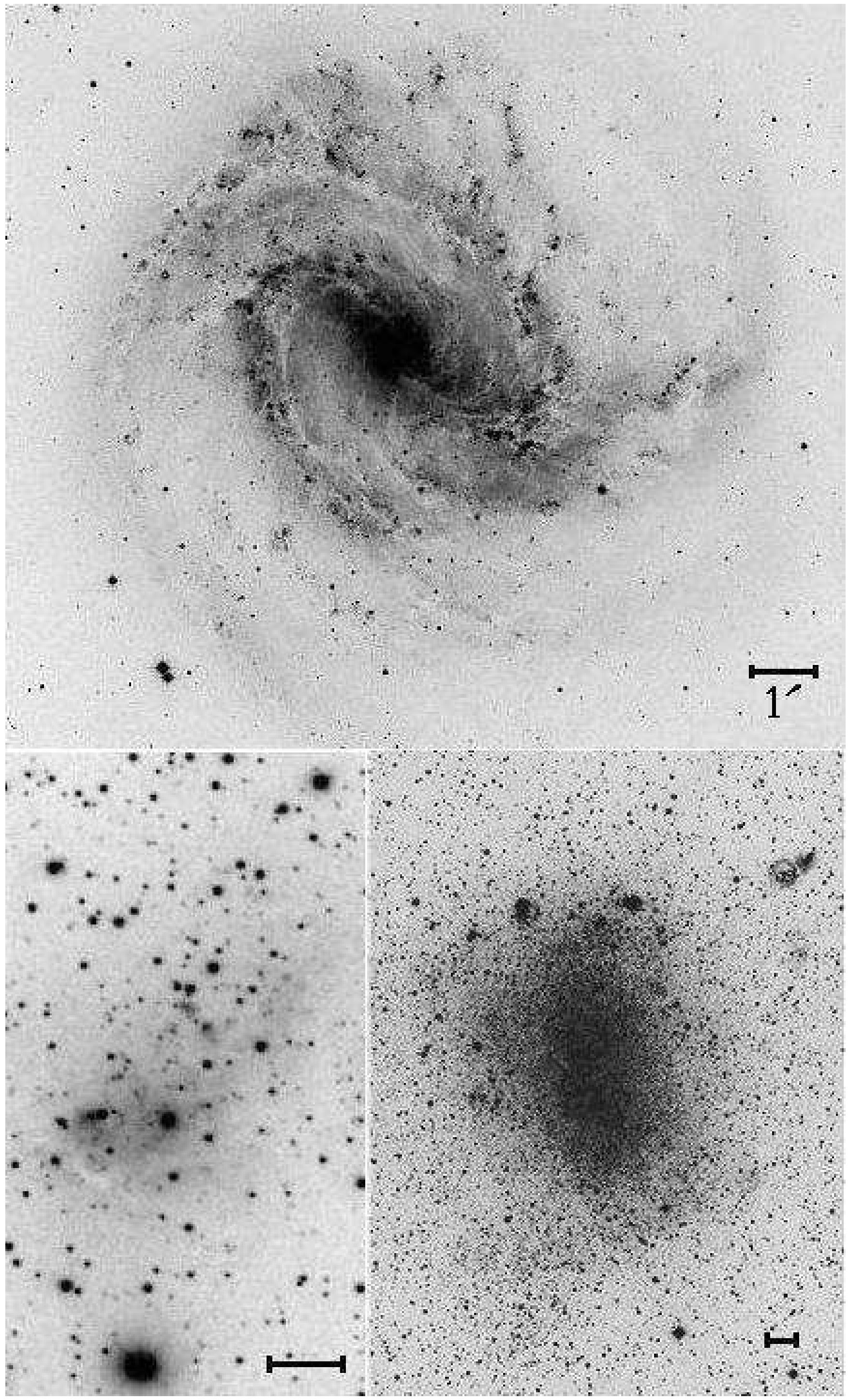

Figure 1.1: **Optical Images of the Galaxies in this Thesis**
The top image is the barred spiral M83. The lower left image is the dwarf irregular galaxy IC 10. The lower right image is the dwarf irregular galaxy NGC 6822. The M83 and NGC 6822 images were taken at the Anglo Australian Observatory. The IC 10 image was taken at the Observatorium Hoher List at Bonn.

dust lanes. This differs from what is found in the spiral galaxy M51, where the molecular gas is coincident with the dust lanes (Vogel *et al.* 1988). In M83, streaming motions along the bar have been detected in the H I and Hβ maps of Tilanus & Allen (1993) but they are not as strong as those seen in M51 (Rand & Kulkarni 1990). This indicates that M83 may lack the very strong density wave shock that is seen in other spiral galaxies and may be a key to explaining the observed offset between the molecular spiral arms and the dust ridges. Still, even with only a moderate strength bar potential, the gas is still being disrupted by the bar potential, causing the gas to flow inward toward the nucleus, possibly fueling the nuclear starburst (*e.g.* Gallais *et al.* 1991).

Kenney *et al.* (1992) studied ^{12}CO J=1−0 emission in the nuclei of four barred spiral galaxies at $\sim 2\farcs5$ resolution and found that a double peaked structure was common among the three galaxies that are *not* undergoing a nuclear starburst. The galaxy that *was* undergoing a nuclear starburst did not exhibit this double peak, but the emission was instead centrally concentrated. The double peaked structure seen in the non-starburst galaxies is consistent with crowding of gas streamlines near the inner Lindblad resonances (Binney & Tremaine 1987, also see §2.3). The starburst galaxy with the single peak of emission at the centre can be explained if strong tidal forces disrupted the molecular gas at the inner Lindblad resonance, causing it to fall into the nucleus where it becomes fuel for the starburst.

The second type of galaxy we consider is the dwarf irregular galaxy. Dwarf irregular galaxies are relatively gas poor but yet are able to produce stars at a rate comparable to that of starburst galaxies (*e.g.* Hunter *et al.* 1989). This is puzzling considering our belief that large amounts of molecular gas must be present in order to fuel star formation in a galaxy. In this thesis we have studied IC 10 and NGC 6822 (see Chapter 3). They lack the large scale structures seen in M83 (see Figure 1.1) and are free from the complicated dynamics that exist in barred spiral galaxies. CO was first detected near the star forming regions of IC 10 by Ohta *et al.* (1988). Becker (1990) mapped six regions of molecular gas in ^{12}CO J=1−0 and ^{12}CO J=2−1 with a maximum of 12″ resolution and found the CO line strengths of IC 10 are greater than those of the LMC, SMC, and NGC 6822 (*e.g.* Israel *et al.* 1993, Wilson 1994). The simplest explanation of these strong CO lines is that IC 10 contains large amounts of molecular gas (Wilson & Reid 1991), but a more likely answer lies in the star formation activity of IC 10. Previous studies find that IC 10 is undergoing unusually high rates of star formation (GSFR = 0.15 $M_\odot$ yr^{-1}, Thronson *et al.* 1990, Massey & Armandroff 1995) and the location of the CO peaks generally correspond with the peaks in the H I maps (Shostak & Skillman 1989). This indicates some connection between the molecular gas and the star forming regions. Maloney & Black (1988) find that the ratio of CO intensity to excitation temperature is constant for ensembles of identical clouds. Hence, higher temperatures will result in brighter CO emission, which could explain the strength of the CO lines in IC 10.

More recently, Wilson (1995) re-mapped the molecular emission originally mapped by Becker (1990) with much higher resolution ($5\farcs5 \times 9\farcs5$) and found that the larger regions resolved into a series of smaller clouds with diameters as small as $\sim$5″. Using these data to calculate the CO-to-H_2 conversion factor in this low metallicity environment yielded a value that was on average almost three times (2.7 $\alpha_{\rm Gal}$) as high as the value obtained for our own Galaxy. This possibly indicates that the apparent paucity of molecular gas is not the result of an absence of gas, but that CO is not tracing it as well as it does in our own Galaxy. In fact, recent studies using C II (Madden *et al.* 1997) find that a value for the CO-to-H_2 conversion factor of $\sim 100\times$ that of our own Galaxy may be appropriate. This would also explain the ability of dwarf galaxies to form stars in conditions seemingly deprived of molecular gas based on CO observations.

In contrast to IC 10, NGC 6822 has relatively weak CO emission (Wilson 1992) and has star formation activity that is much lower ($\sim 5-9$ times) than is found in IC 10 (GSFR = 0.03 $M_\odot$ yr^{-1}, Gallagher *et al.* 1991, Massey & Armandroff 1995). It is one of the few non-interacting dwarf irregular galaxies resolved in the far-infrared by *IRAS* and is believed to be relatively transparent due to its low metallicity (hence reduced dust-to-gas ratio, Gallagher *et al.* 1991). After a failed attempt by Elmegreen *et al.* (1980), CO emission was first detected in NGC 6822 around the bright H II region Hubble V by Israel (1991). He concluded that the weak line strength was possibly the result of CO being photodissociated by the hot stars in the H II regions, suggesting a CO-to-H_2 conversion factor that is much larger than our own Galaxy.

Molecular gas in NGC 6822 was first mapped by Wilson (1992). The data for four under-resolved molecular regions were used to estimate that the CO-to-H_2 conversion factor for NGC 6822 was comparable to the value found for Galactic giant molecular clouds. Ohta *et al.* (1993) obtained a single spectrum for one position in Hubble V and found line strengths much weaker than in IC 10. By noting NGC 6822's metallicity was similar to that of IC 10, but its CO lines are much weaker, they concluded that the CO-to-H_2 conversion factor must be much higher in NGC 6822 than it is in IC 10. The following year, Wilson (1994) used the Owens Valley Millimeter Wave Interferometer to resolve individual molecular clouds in NGC 6822. She found that the clouds were on average less massive than those found in other Local Group galaxies. Resolving the clouds allowed direct measurement of the CO-to-H_2 conversion factor, and she obtained $\alpha < (2.2 \pm 1.3)\alpha_{\rm Gal}$. This value is not as high as the value obtained for IC 10 using the same techniques but the large uncertainty allows for values larger than that found in IC 10 as well as values that are consistent with the Galactic value. Most recently Israel (1997) used the Swedish-ESO Submillimeter Telescope (43$''$ main beam) to obtain individual spectra for 4 positions in NGC 6822. By combining the CO data with H I and infrared data, he estimates the CO-to-H_2 conversion factor to be 40$\pm$15 times the Galactic value. The large number of assumptions that went into this estimate make the value seem even more uncertain than quoted.

This thesis uses observations of different rotational transitions of CO and its isotopomers to determine the physical conditions in three starburst galaxies. Chapter

2 presents CO and C I maps of the barred spiral galaxy M83. In §2.2 we discuss the observations of M83 and in §2.3 we use the maps to examine the structure and dynamics of the molecular gas and in §2.4 we use the spectral line intensities and line ratios to study the physical conditions of the molecular gas within the nuclear starburst. The results for M83 are summarized in §2.5. In Chapter 3 we study the physical conditions in the low metallicity, dwarf irregular galaxies IC 10 and NGC 6822. The observations and data reduction are discussed in §3.2. In §3.3.1 we discuss the conditions in the molecular gas in two regions in IC 10 derived from CO line ratios and in §3.3.2 we perform a similar analysis for the molecular cloud observed in NGC 6822. In §3.2 we use line intensities to determine the molecular masses of the clouds in IC 10 and NGC 6822. We discuss some of the possible implications that varying the CO-to-H_2 conversion factor may have on our results in §3.4 and the results for the dwarf irregular galaxies are summarized in §3.5. The chief results of this thesis are recapitulated in §4.

I attempt to clarify some of the jargon used in the individual chapters though a series of appendices. The many temperature scales used in radio and submillimeter astronomy and their applications and calculations are summarized in Appendix A. A brief note on the existence and pitfalls of the CO-to-H_2 conversion factor is presented in Appendix B. The commonly used but rarely discussed Local Thermodynamic Equilibrium approximation is outlined in Appendix C, and finally the Large Velocity Gradient model is detailed in Appendix D.

Chapter 2

The Physical Conditions and Dynamics of the Interstellar Medium in the Nucleus of M83: Observations of CO and CI

2.1 Introduction

The circumnuclear regions of galaxies are very often the setting for starbursts and other extraordinary events. Observations of the gas kinematics and distribution indicate that bars, resonances, gas inflow, and tidal shear play important roles in the formation and evolution of nuclear starbursts (*e.g.* Handa *et al.* 1990, Kenney *et al.* 1992). Previous observations show that the molecular gas in the central regions of barred spiral galaxies does not extend all the way into the centre of the nucleus. It accumulates some distance away from the centre, giving the emission a double peaked appearance with each peak occurring where the bar meets the nucleus (Kenney *et al.* 1992, Ishizuki *et al.* 1990). Dynamical models indicate that in the presence of a barred potential, gas will flow inward along the bar and slow its descent temporarily near stellar inner Lindblad resonances (ILR, *e.g.* Combes 1988, Shlosman, Frank & Begelman 1989). At these locations the gas will start to accumulate into larger complexes of molecular clouds.

In addition to complex dynamics, there is most likely a profusion of complicated photo-chemistry occurring within the nucleus of this barred spiral galaxy. It is possibly enhanced by the extreme conditions molecular clouds within a nuclear starburst must endure. Interstellar clouds are believed to consist of smaller high density dark cores interspersed throughout a larger region of lower density. These high density regions are self-shielded from ultraviolet (UV) flux that tends to dissociate molecular gas. The result is the population of the diffuse region by hydrogen atoms (H I), atomic and ionized carbon (C I, C II), and many other atomic and ionized species (*e.g.* Morton *et al.* 1973) while the dark cores can contain molecular species such as H_2 and CO.

It is believed that atomic carbon can exist only in a small energy window, outside of which it will either be ionized or combined with oxygen to form CO. Inside the dense cores, most of the carbon combines to form CO while outside, the UV radiation acts to ionize atomic carbon. It is therefore expected that C I is the dominant species near the edges of dense, self-shielding cloud cores.

This simple model fails to explain the extended [C I] emission observed in molecular clouds in our own Galaxy (Plume, Jaffe, & Keene 1994, Keene *et al.* 1985).

One possible explanation is found in the clumpy structure of molecular clouds (*e.g.* Stutzki & Güsten 1990). This clumpiness would allow UV radiation to penetrate much deeper into the cloud allowing C I to exist at depths greater than would be allowed by a simple spherical model of molecular clouds (*e.g.* Boisse 1990). More recently, many alternative explanations have been proposed to explain the extended [C I] emission. These include ideas which range from complicated chemical processes involving H^+ (where the H^+ can pilfer oxygen from CO leaving atomic carbon) to simpler ideas such as a C/O ratio greater than one (leaving left over C). For a quick review, see Keene *et al.* (1985).

This chapter presents [C I] and CO maps of the barred spiral galaxy M83. Its low inclination angle ($i = 24°$, Comte 1981) and close proximity ($D = 4.7$ Mpc, Tully 1988) make it one of the best locations for studying the response of gas to a barred potential. It is believed to be undergoing a nuclear starburst (*e.g.* Talbot *et al.* 1979) which may be triggered by molecular gas inflow along the bar potential. This nuclear starburst would produce higher temperatures which should readily excite the higher J-transitions in the CO gas. Also, strong UV flux has been detected in the nucleus (Bohlin *et al.* 1983) which would help dissociate the CO into C I. By studying the CO and [C I] data on scales larger than individual molecular clouds, we hope to better understand the dynamics of the gas and its role in fueling the nuclear starburst and also learn about the conditions conducive to the formation of C I.

2.2 Observations and Data Reduction

[C I] and ^{12}CO J=4−3 observations of M83 were taken using the 15 m James Clerk Maxwell Telescope (JCMT) over the period of 1996 April 5 – 10. The half-power beam width of the JCMT is 12″ at 492 GHz ([C I]) and 461 GHz (^{12}CO J=4−3) and 14″ at 345 GHz (^{12}CO J=3−2). The galaxy was mapped using 5″ sampling then averaged over 5×5 cells resulting in 25″ resolution for the final maps. All observations were obtained using the Dwingeloo Autocorrelation Spectrometer.

The data were reduced using the data reduction package SPECX and were binned to 4 km s^{-1} resolution. The raw spectra were converted into FITS files using SPECX and then the Bell Labs data reduction package COMB was used to convolve the ^{12}CO J=4−3 to the same beam size as the ^{12}CO J=3−2 data. The ^{12}CO J=3−2 data were taken in *raster* mode at the JCMT, which scans along an entire row before spending time on the 'off-source' position. It was later discovered that a loose wire was causing poor baselines for spectra taken in this manner so the ^{12}CO J=4−3 data were taken in *beam-switched* mode, which toggles between 'on' and 'off-sources' (by chopping secondary mirror) at each location on the map. The result is that the ^{12}CO J=3−2 data required third order (polynomial fitted) baseline removal while the ^{12}CO J=4−3 and [C I] data required zeroth order. The calibration was monitored by frequently observing both planets and spectral line calibrators. The spectral line calibrators for the CO data had integrated intensities that were within ∼10% of the published values while observations of the [C I] calibrators were not integrated long enough to obtain detections. We therefore adopt the published values of $\eta_{\rm MB} = 0.58$ for ^{12}CO J=3−2 and $\eta_{\rm MB} = 0.52$ for the ^{12}CO J=4−3 and [C I] data.

Since the line strengths we are comparing are measured with (or convolved to) the same beam diameter, using the $T_{\rm R}^\star$ temperature scale (see Appendix A) would ensure that our observed line ratios are equal to the true radiation temperature ratios. However, conversion to $T_{\rm R}^\star$ from $T_{\rm A}^\star$ requires knowledge of the forward scattering and spillover ($\eta_{\rm FSS}$), which is difficult to measure and was not attempted during the observing run. We do have good values for the main beam efficiencies and so an accurate conversion to main beam temperature ($T_{\rm MB}$) is possible. Using the $T_{\rm MB}$ scale instead of $T_{\rm R}^\star$ scale only changes the ^{12}CO J=4−3/J=3−2 line ratio by ∼10% under normal calibration conditions. For this reason, we will use the main beam temperature scale for the line ratios throughout this thesis. The maps are plotted in the $T_{\rm MB}$ temperature scale. The individual ^{12}CO J=3−2, ^{12}CO J=4−3, and [C I] spectra are shown in Figures 2.1, 2.2, and 2.3 respectively.

2.3 Morphology and Dynamics

The integrated intensity maps (^{12}CO J=3−2, Figure 2.4; ^{12}CO J=4−3 Figure 2.5; [C I], Figure 2.6) indicate a double (possibly triple) peaked structure in the emission. Within the pointing uncertainty of the JCMT (2″ rms), each map exhibits the

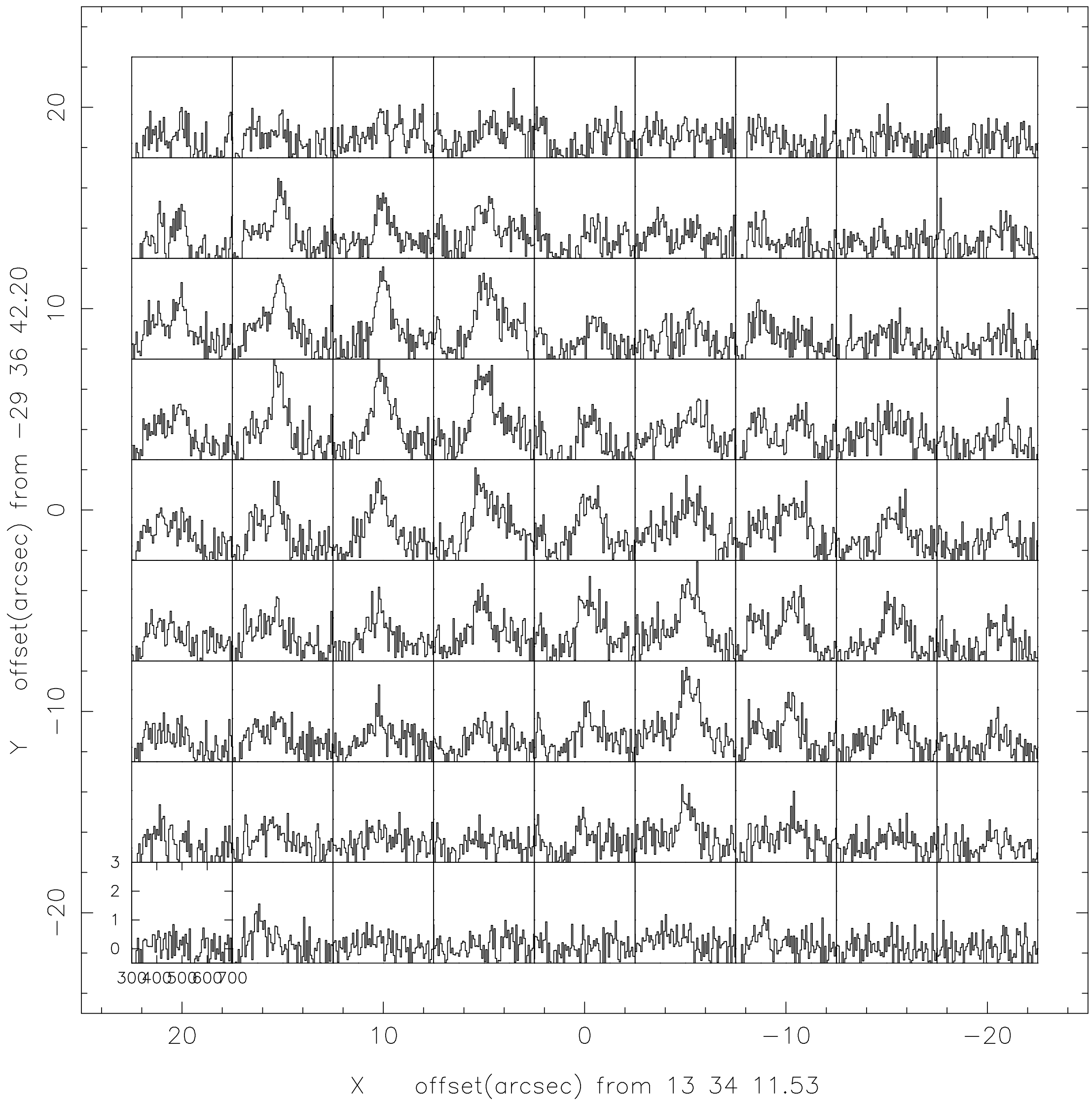

Figure 2.1: **Individual ^{12}CO J=3−2 Spectra for M83**

Individual ^{12}CO J=3−2 spectra for the galaxy M83. The orientation is such that north corresponds to an angle 135° couter-clockwise from the negative horizontal axis. The bar runs along the x-axis. The temperature scale is main beam temperature ($T_{\rm MB}$). The map is centred at $\alpha = 13^{\rm h}34^{\rm m}11\overset{\rm s}{.}53$, $\delta = -29°36'42\overset{''}{.}20$. The velocity range plotted is from 300 km s^{-1} to 700 km s^{-1} at a resolution of 16.2 km s^{-1} (18.75 MHz).

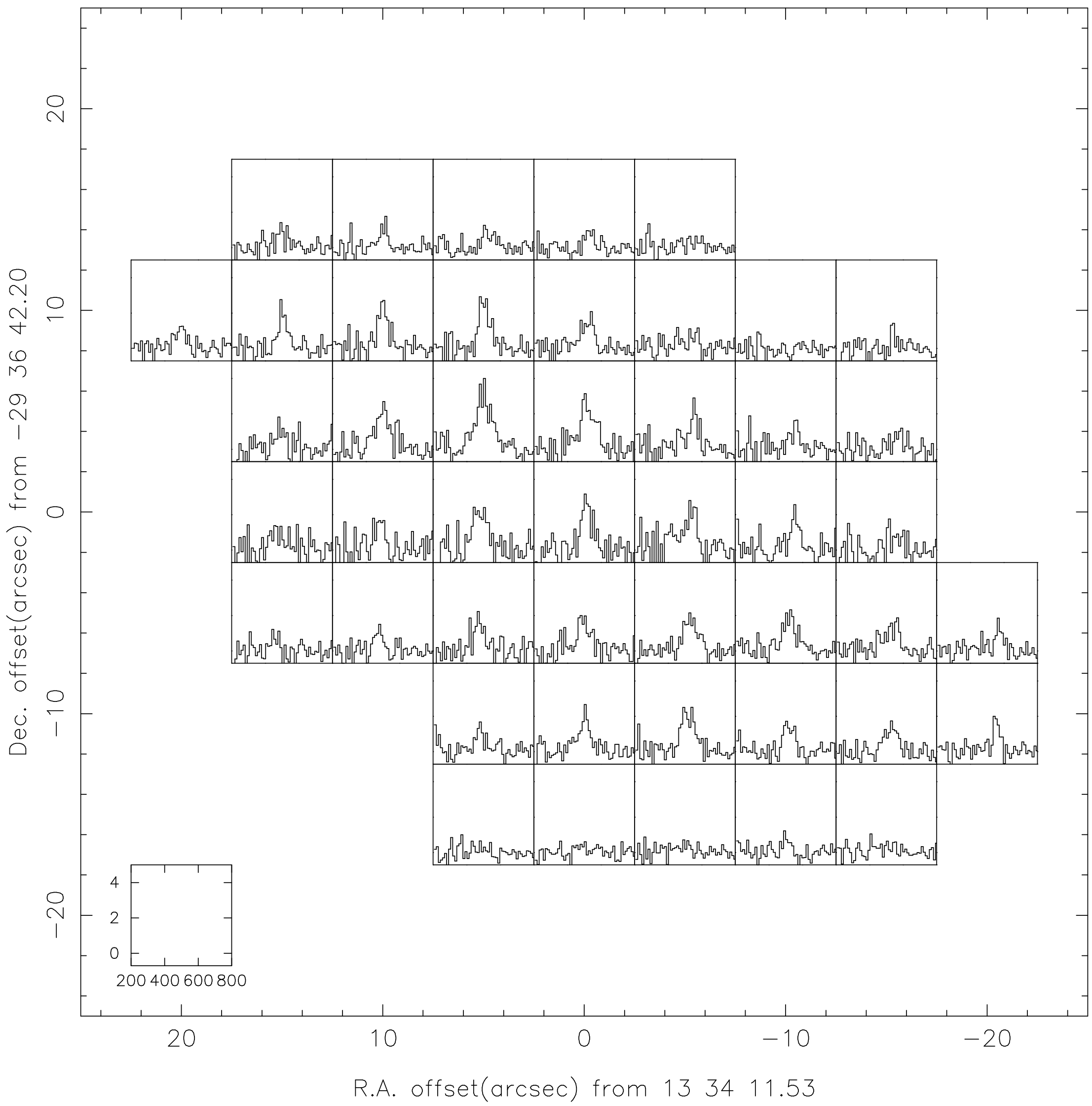

Figure 2.2: **Individual ^{12}CO J=4−3 Spectra for M83**
Individual ^{12}CO J=4−3 spectra for the galaxy M83. The temperature scale is main beam temperature ($T_{\rm MB}$). The map centre and orientation is the same as Figure 2.1. The velocity range plotted is from 200 km s^{-1} to 800 km s^{-1} at a resolution of 12.2 km s^{-1} (18.75 MHz).

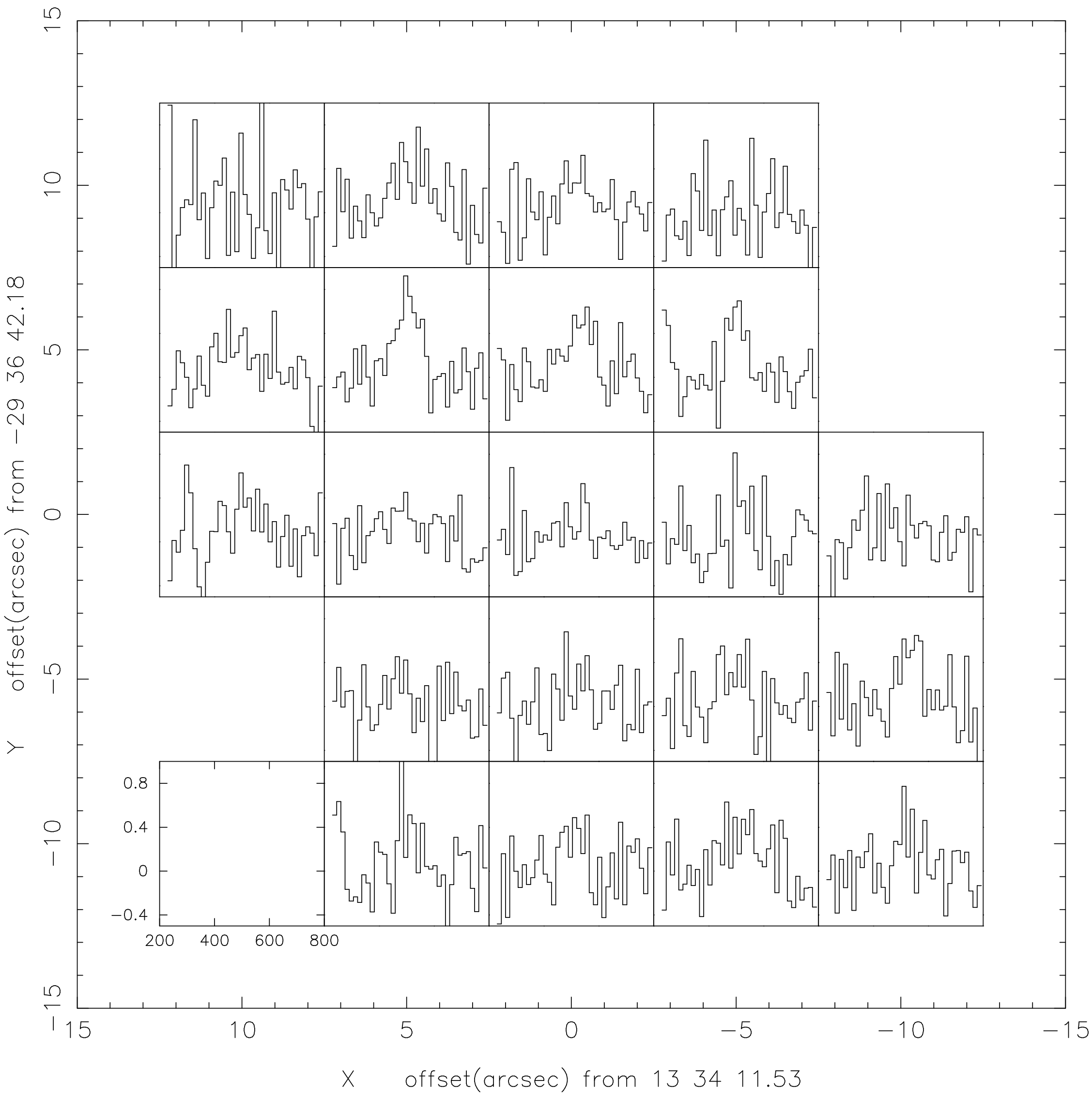

Figure 2.3: **Individual [C I] Spectra for M83**

Individual [C I] spectra for the galaxy M83. The temperature scale is main beam temperature ($T_{\rm MB}$). The map centre and orientation is the same as Figure 2.1. The velocity range plotted is from 200 km s^{-1} to 800 km s^{-1} at a resolution of 15.1 km s^{-1} (25 MHz).

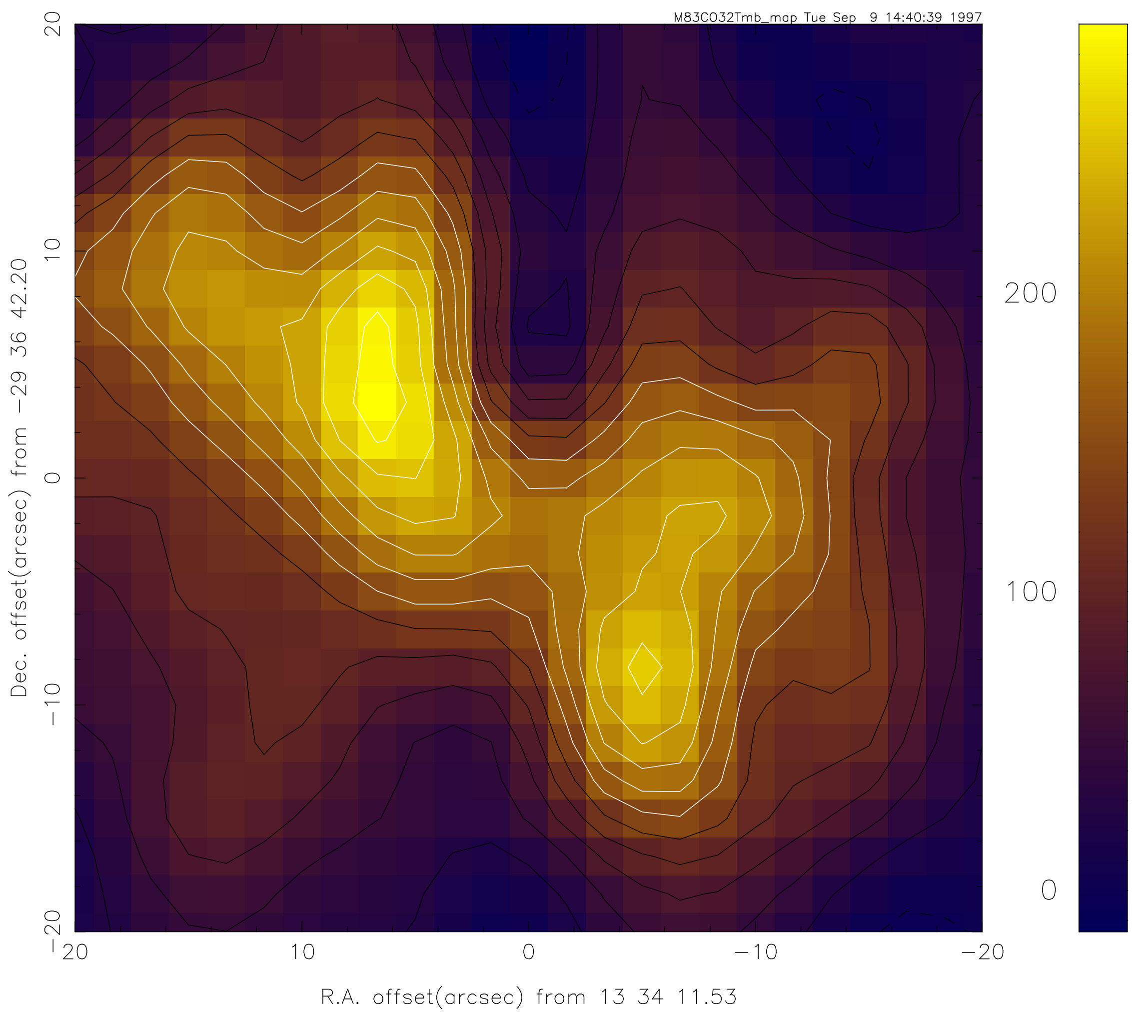

Figure 2.4: **Integrated ^{12}CO J=3−2 Intensity Map for M83**
Integrated intensity map for the ^{12}CO J=3−2 transition in M83. The emission is integrated from 400 km s^{-1} to 600 km s^{-1} and is given in K km s^{-1} ($T_{\rm MB}$). The contour interval is 25 K km s^{-1} with the lowest contour being −25 K km s^{-1}. The maximum and minimum values are 290.07 K km s^{-1} and −13.85 K km s^{-1} respectively. The emission shows a double peaked structure that is consistent with gas inflow along the bar collecting at the inner Lindblad resonance, or a molecular ring of gas seen at an oblique angle.

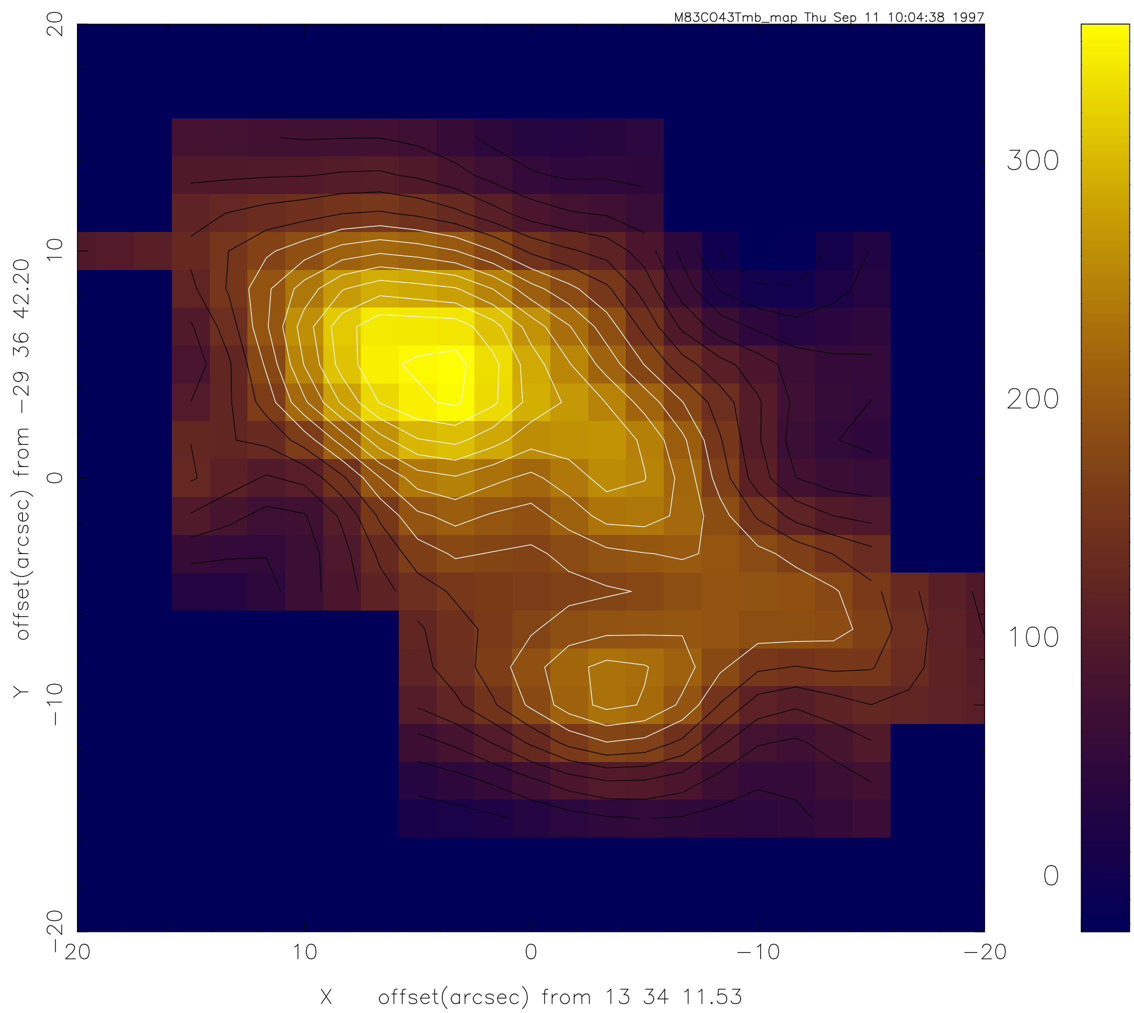

Figure 2.5: **Integrated ^{12}CO J=4−3 Intensity Map for M83**
Integrated intensity map for the ^{12}CO J=4−3 transition in M83. The emission is integrated from 400 km s^{-1} to 600 km s^{-1} and is given in K km s^{-1} ($T_{\rm MB}$). The contour interval is 25 K km s^{-1} with the lowest contour being −25 K km s^{-1}. The maximum and minimum values are 357.23 K km s^{-1} and −23.45 K km s^{-1} respectively. This data also shows the same double peaked structure as the ^{12}CO J=3−2 data, although it is not as symmetric. Note the bent 'elbow'-like emission joining the two strongest peaks.

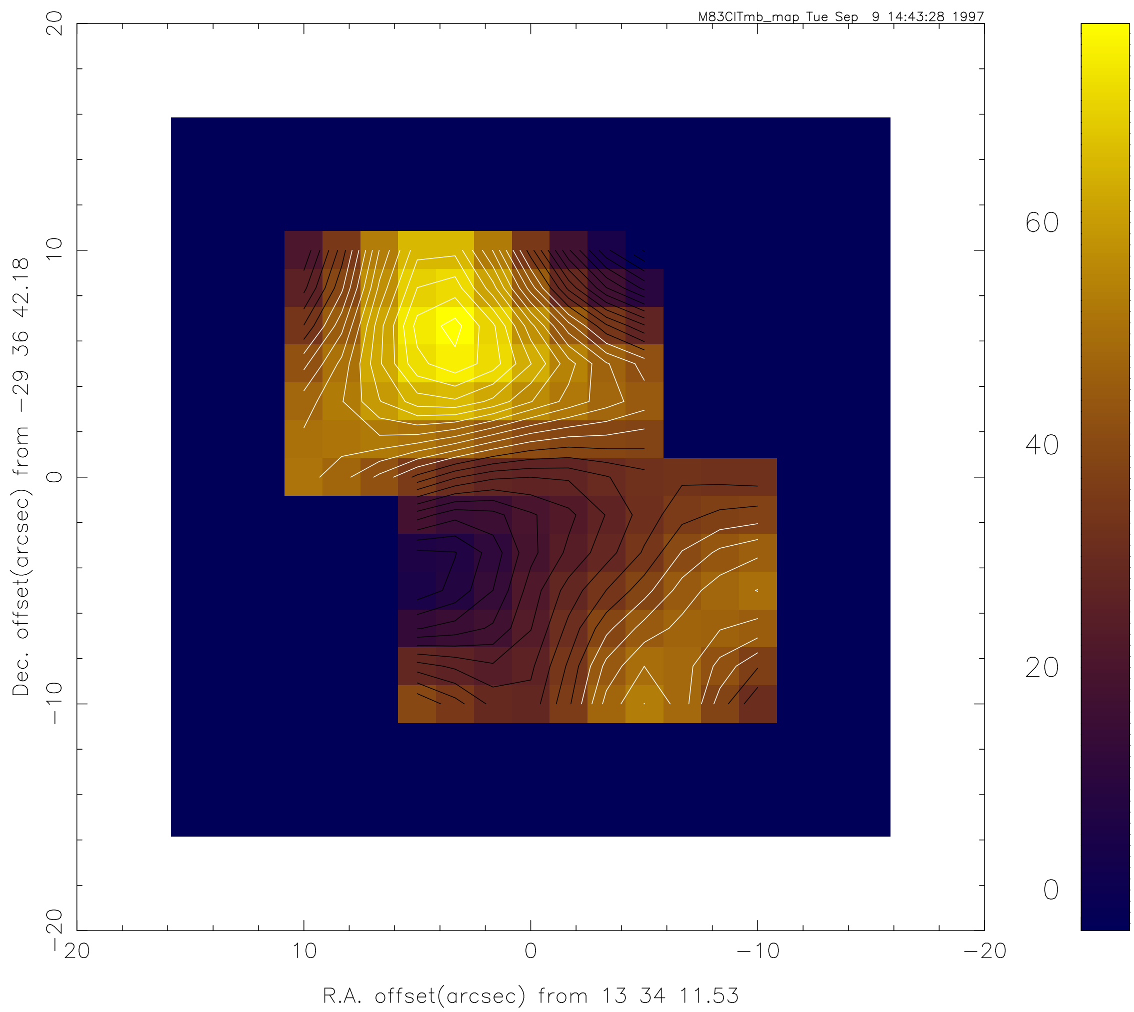

Figure 2.6: **Integrated [C I] Intensity Map for M83**
Integrated intensity map for the [C I] transition in M83. The emission is integrated from 400 km s^{-1} to 600 km s^{-1} and is given in K km s^{-1} (T_{MB}). The contour interval is 3.33 K km s^{-1} with the lowest contour being −6.67 K km s^{-1}. The maximum and minimum values are 77.91 K km s^{-1} and −3.66 K km s^{-1} respectively. This data shows a similar 'elbow' structure as the ^{12}CO J=4−3 data. The peaks overlap (within pointing uncertainties) the two peaks and bend in the ^{12}CO J=4−3 data.

strongest emission peak at (+5″, +5″) with the second strongest at (−5″, −10″). These two emitting regions peak at different velocities. It can be seen in the channel maps (^{12}CO J=3−2, Figure 2.7; ^{12}CO J=4−3, Figure 2.8) that the emission at (+5″, +5″) peaks at approximately 500 km s^{-1} in both the ^{12}CO J=3−2 and ^{12}CO J=4−3 maps while the emission at (−5″, −10″) peaks at ∼550 km s^{-1}. In the integrated intensity maps (especially the [C I] and ^{12}CO J=4−3), there are indications of a third, weaker peak at approximately (−10″, −5″) but the channel maps do not indicate a separate clump of emission at a velocity different from the two main emission peaks. This seems to indicate that the hints of a third emission peak are likely just an extension of the (−5″, −10″) peak or a diffuse cloud of molecular gas that is evenly distributed in velocity space, hence not seen until the emission is integrated over all velocities. The [C I] emission is too weak to obtain reliable channel maps.

2.3.1 Gas Collection at Inner Lindblad Resonances?

The [C I] emission appears to follow the ^{12}CO J=4−3 emission much more closely than it does the ^{12}CO J=3−2 emission. The ^{12}CO J=4−3 and [C I] emission appear asymmetric, with the two main peaks to the north and south of the centre, connected by an "elbow" of weaker emission that undergoes a ∼90° bend. Irregular structure was also seen in M83 in the ^{12}CO J=1−0 emission by Handa *et al.* (1990). Numerical simulations predict that a shock front will form at the leading edge of bar of a barred galaxy (*e.g.* Sørensen *et al.* 1976). At this shock front, interstellar gas is compressed

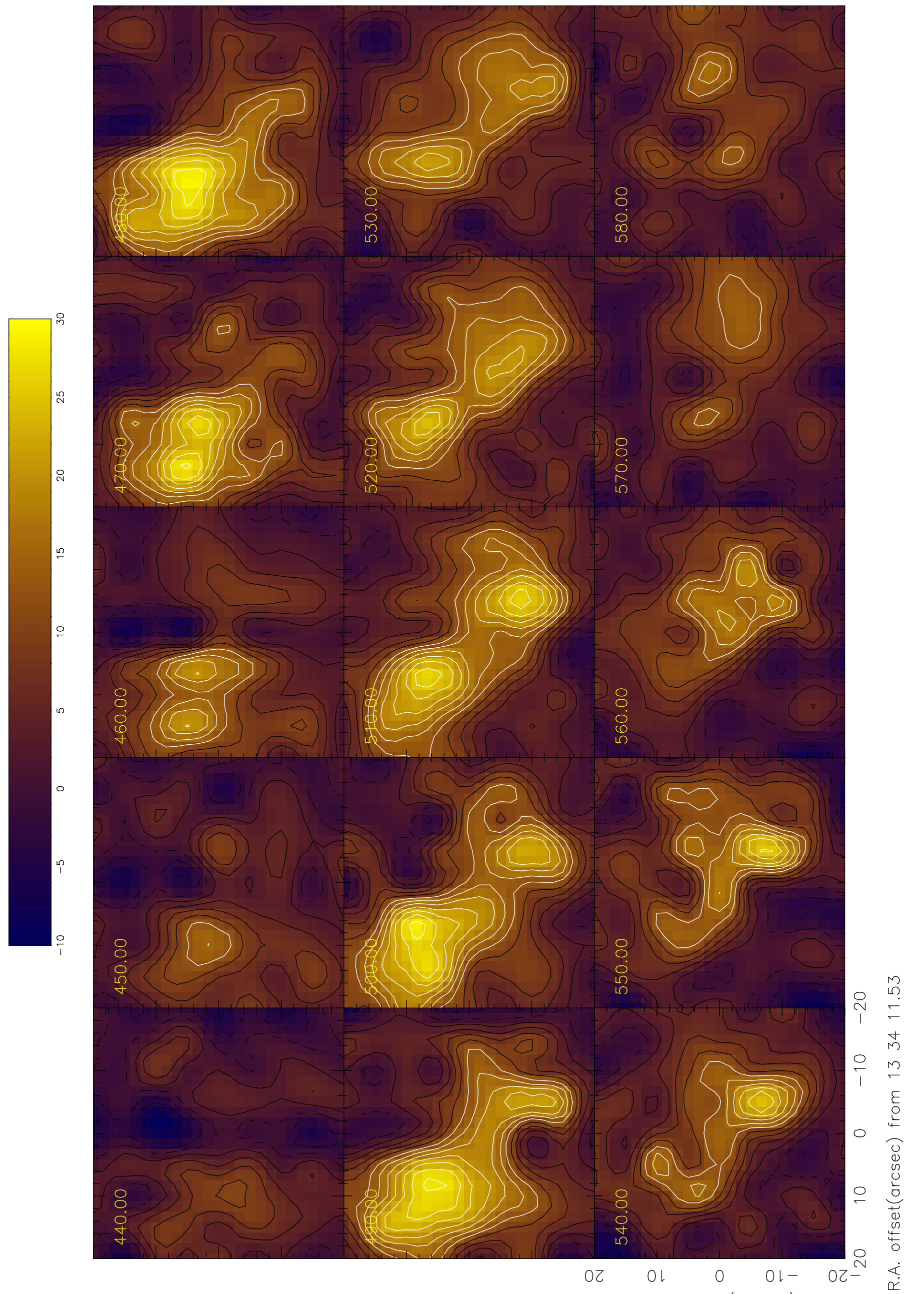

Figure 2.7: ^{12}**CO** J**=3−2 Channel Map for M83**

Integrated intensity channel map for the ^{12}CO J=3−2 transition in M83. The integrated emission is given in K km s^{-1} ($T_{\rm MB}$). The velocity interval is 10 km s^{-1} with the first panel centred at 440 km s^{-1}. Contour levels are shown at 2.5 K km s^{-1} intervals with the base level at −7.5 K km s^{-1}. In this figure we can see the emission to the north peak at velocities lower than the emission to the south. This can be explained by gas collecting at ILRs or by a ring of rotating molecular gas. Note that in order to make the best use of space, this and subsequent figures are rotated so that the x-axis runs vertically.

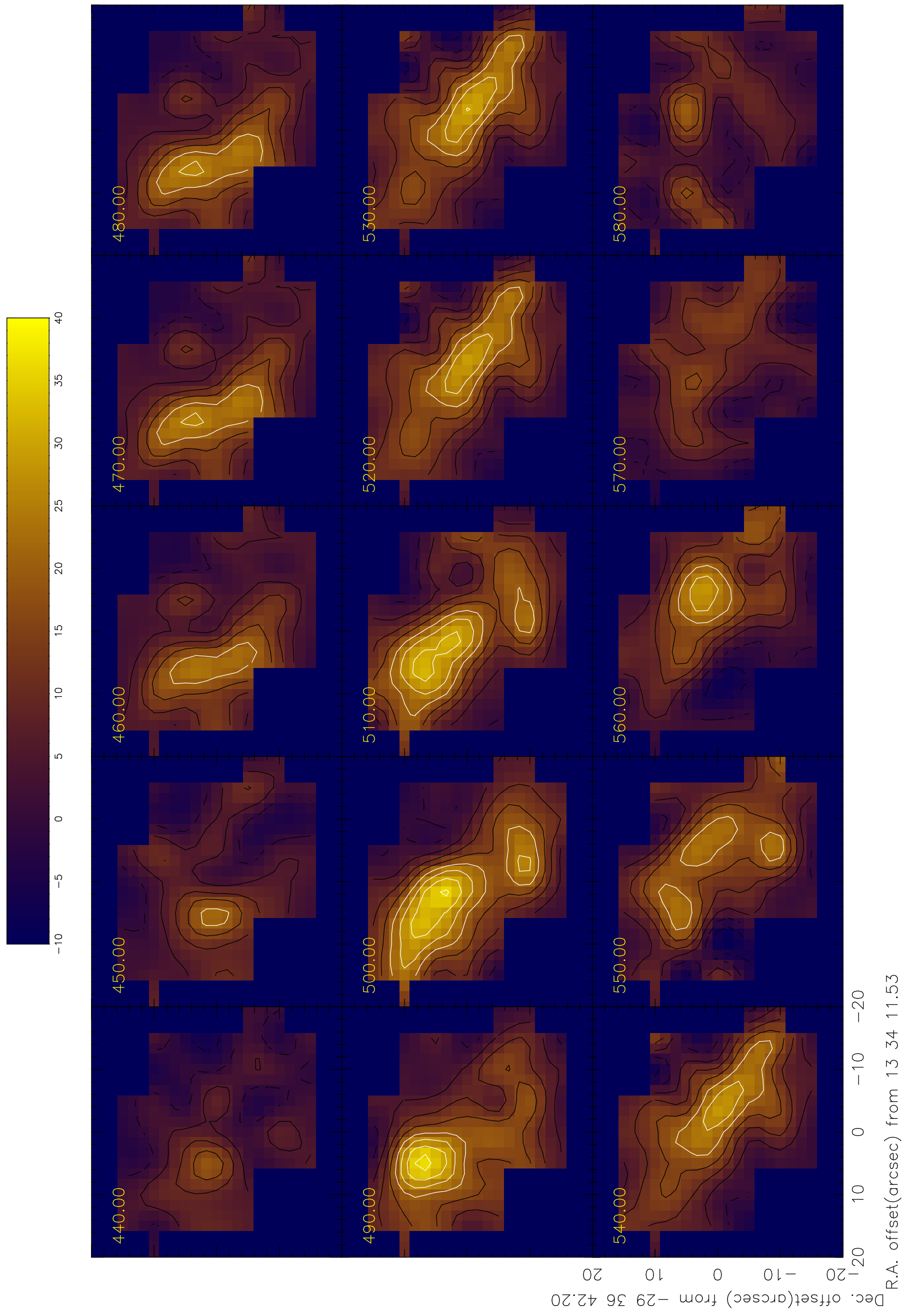

Figure 2.8: ^{12}**CO** J**=4−3 Channel Map for M83**

Integrated intensity channel map for the ^{12}CO J=4−3 transition in M83. The integrated emission is given in K km s^{-1} ($T_{\rm MB}$). The velocity interval is 10 km s^{-1} with the first panel centred at 440 km s^{-1}. Contour levels are shown at 5.0 K km s^{-1} intervals with the base level at −5.0 K km s^{-1}.In this figure we can see the emission peak shift to the south due to the rotation of the molecular gas. Note how it peaks at the centre near velocities of ∼520 km s^{-1}. This indicates that the ^{12}CO J=4−3 emission may originate from a disk of gas rather than a torus.

and loses kinetic energy causing it to flow toward the nucleus. The star formation is thought to be triggered by such an inflow. In the figures, the galactic bar of M83 runs along the x-axis. This indicates that the emission is originating on the leading edge of the bar potential (as first seen by Handa *et al.* 1990) as predicted by theoretical models of barred galaxies.

This raises the question as to why the gas does not continue to flow into the centre rather than stopping to form the double peaked structure we see. One answer potentially lies in the location of the inner Lindblad resonances (ILRs). Stars and molecular clouds orbiting the centre of a galaxy oscillate radially in addition to their tangential orbits around the galactic nucleus. The frequency of these radial oscillations are called epicycle frequencies (κ_0). The objects' orbital frequencies about the galactic nucleus are called their circular frequencies (Ω_0). In a barred spiral galaxy, the bar will rotate at a (usually) different frequency called the pattern speed ($\Omega_{\rm b}$). Lindblad resonances occur in barred potentials when an object (star or cloud) encounters successive crests of the bar potential at a frequency that coincides with epicycle frequency, namely

$$m(\Omega_0 - \Omega_{\rm b}) = \pm\kappa_0$$

(Binney & Tremaine 1987) where m is equal to 2 for a barred potential ($m = 5$ for a five arm spiral potential). The inner Lindblad resonance refers to the condition $\Omega_{\rm b} = \Omega_0 - \kappa_0/2$ while the outer Lindblad resonance occurs at $\Omega_{\rm b} = \Omega_0 + \kappa_0/2$. Most 'real' rotation curves allow for two ILRs and the one nearest the nucleus is sadistically called the inner inner Lindblad resonance (IILR) while the second ILR is often called the outer inner Lindblad resonance (OILR).

It has been shown (*e.g.* Kenney *et al.* 1992) that the location of the ILR is often coincident with the double peaks of molecular gas often seen in barred spiral galaxies. The barred spiral galaxies M101, NGC 3351, and NGC 6951 (Kenney *et al.* 1992) have double peaked molecular emission located at the same radius as the location of the ILRs and are not undergoing nuclear starbursts. NGC 3504 is a barred spiral that is undergoing a nuclear starburst, and it does not exhibit the double peaked structure in the molecular gas. Calculations indicate that ILRs do exist in NGC 3504, but the molecular emission does not appear to be accumulating there. This seems to suggest that accumulation of gas at ILRs is a way of inhibiting nuclear starburst in barred spiral galaxies, while the mere existence of ILRs is not sufficient to prevent starbursts.

Calculations of the locations of ILRs require knowledge of the rotation curve of the galaxy as well as the bar pattern speed. The value of κ_0 can be calculated from the rotation curve using

$$\kappa_0 = \sqrt{R\frac{d\Omega_0^2}{dR} + 4\Omega_0^2}$$

(Binney & Tremaine 1987) but since $\Omega_0 = V_{\rm rot}/R$ this reduces to

$$\kappa_0 = \sqrt{4\Omega_0^2 + 2\Omega_0 \frac{dV_{\rm rot}}{dR}}.$$

The nucleus of M83 has very peculiar, non-circular and streaming motions (Handa *et al.* 1990) which made it difficult to obtain a reliable rotation curve from our CO data. To get an estimate of the overall rotation curve for the inner 45″ of M83, we fitted the inner rotation curve (derived from H I data) of Tilanus & Allen (1993) with a velocity $\propto$ radius$^{1/4}$ profile. While there is no physical justification for this, it did provide a smooth fit to the data out to 90″. The bar pattern speed ($\Omega_{\rm b}$) is estimated by assuming that the corotation resonance ($\Omega_0 = \Omega_{\rm b}$) occurs just past the end of the bar. Using the rotation curve of Tilanus & Allen (1993) and adopting a bar radius of 105″ (Kenney & Lord 1991) gives $\Omega_{\rm b} = 61$ km s^{-1} kpc^{-1}. This indicates an OILR at a radius of $\sim$0.25 kpc (11″). This is the same radius that we see the double peak molecular emission indicating evidence for a build-up of gas at an ILR. This shows that *a nuclear starburst may occur even in galaxies that appear to have a build up of gas at an ILR.* A rotation curve based on observations rather than fitted curves will provide the true location on the ILRs, thus proving or disproving the above result.

High resolution ^{12}CO J=1−0 maps by Handa, Ishizuki & Kawabe (1994) show that the double peaked structure of M83 straddles a nuclear star formation complex (as traced by radio continuum, Cowen & Branch 1985). They do not see strong ^{12}CO J=1−0 emission from between the peaks, within the star forming region. They reinforce this by showing a CO channel map of the nucleus at a LSR velocity of 523 km s^{-1}. If we compare this to our ^{12}CO J=3−2 channel map (Figure 2.7), we can see a similar structure at 520 km s^{-1}, a double peak in ^{12}CO J=3−2 straddling the star forming region located at origin (0″, 0″). Now if we look at the ^{12}CO J=4−3 channel map (Figure 2.8), we see a very different structure at 520 km s^{-1}. The ^{12}CO J=4−3 emission *peaks* at the centre of the star forming region. This suggests that there *is* molecular gas in the nuclear regions of M83, but it is heated by the nuclear starburst so that most of the CO is excited to the higher rotational (J) states by energetic collisions with H_2. Double peaked accumulations of ^{12}CO J=4−3 emission are still seen in the integrated intensity maps (Figure 2.5) which suggests that the CO gas is gathering at the ILR, then slowly flows into the nucleus where the starburst occurs. The gas at the ILRs is heated less intensely by the starburst than the gas that made it into the nucleus, so in the double peaks we see emission from cooler gas (as traced by ^{12}CO J=1−0 emission) as well as hotter gas (as traced by ^{12}CO J=3−2 and ^{12}CO J=4−3 emission), while in the nucleus most of the gas is in the $J = 4$ and $J = 3$ states. This may indicate that ^{12}CO J=1−0 *emission is not always a good tracer of the molecular gas in starburst galaxies.* The edge-on starburst galaxy M82 indicates a similar structure with the ^{12}CO J=4−3 data filling in the torus of rotating gas traced by the ^{12}CO J=3−2 emission (White *et al.* 1994, Tilanus *et al.* 1991). It should be noted however that the ^{12}CO J=4−3 maps were *very* undersampled and the result was a map with a resolution of $>25''$, which may be too low to determine the fine structures of the inner $20''$.

The above discussion suggests that there may be an evolutionary sequence for starbursts in barred spiral galaxies. The first stage would be molecular gas flowing in along the bar and collecting at ILRs. At the early stages, there would be little molecular gas inside the ILRs. This stage corresponds to galaxies similar in appearance to M101, NGC 3351, and NGC 6951 (Kenney *et al.* 1992) where the double peaked structure is observed but there is no nuclear starburst. The next stage is reached when some of the collected gas is perturbed (*e.g.* Shlosman *et al.* 1989) and falls further into the nucleus, allowing a nuclear starburst to occur (M83, this work). Eventually all of the molecular gas may move into the nucleus, eliminating the double peaked structure seen in molecular emission and fueling the nuclear starburst further (NGC 3504, Kenney *et al.* 1992). This scenario is supported by the assertion that most starburst galaxies may contain bars (Jackson *et al.* 1987). It should be noted that no ^{12}CO J=4$-$3 data exist for M101, NGC 3351, NGC 6951, or NGC 3504 so the existence of ^{12}CO J=4$-$3 emission from the nucleus cannot be ruled out.

2.3.2 Rotating Gas Disk and Torus Out of the Plane of the Galaxy?

While the above scenario seems to explain the observations quite well, there is another possible configuration that can explain the double peaked structure seen in the integrated intensity and channel maps that should be addressed. If we were to consider the existence of a rotating torus of gas seen edge on, the CO emission would appear strongest from the edges, where we are looking through more of the gas than we are in the centre where the void is. The side moving away from us would appear to have a greater velocity than the side moving toward us (as is seen in the channel maps). The channel map for a rotating torus of gas would show an emission peak at velocities higher than the systemic velocity ($V_{\rm sys}$) on the side of the torus moving away from us, a peak at velocities lower than $V_{\rm sys}$ on the side moving towards us, and very weak emission at $V_{\rm sys}$ where the void is centred (*cf.* M82, Tilanus *et al.* 1991, NGC 253, Israel *et al.* 1995; both also starburst galaxies that exhibit the double peaked structure). This structure is indeed seen in the ^{12}CO J=3$-$2 data. The additional feature in our data that must be explained is the ^{12}CO J=4$-$3 emission that peaks at the centre of the channel maps at $V_{\rm LSR} \approx 520$ km s^{-1}. The ^{12}CO J=4$-$3 emission we see between the double peaked ^{12}CO J=3$-$2 structure in channel maps could be explained if the CO gas is actually a disk/torus combination. The channel map for a rotating disk of gas would appear as a peak of emission at velocities higher than the $V_{\rm sys}$ on the side of the disk moving away from us, an emission peak at velocities lower than $V_{\rm sys}$ on the side of the disk moving towards us, and peaks at all velocities in between that appear to move from the advancing side to the receding side as we look at increasing velocity intervals. This is what is seen in the ^{12}CO J=4−3 channel map. This seems to indicate the existence of a disk of hotter molecular gas located inside the molecular torus of gas with the ^{12}CO J=4−3 emission dominating in the middle parts of the disk (possibly excited to these higher J states by the presence of the nuclear starburst). The torus consists of slightly cooler gas that allows for the presence of the lower J states.

It has been proposed (*e.g.* Larkin *et al.* 1994) that a torus of gas may accumulate in the regions between the inner and outer ILRs. While this may be occurring in M83, the problem is that we require the torus/disk to be seen nearly edge on. M83 has an inclination angle of only 24°. This is nearly face on which indicates that if this torus is lying in the same plane as the rest of the galaxy, we are *not* seeing it edge on and hence should not be seeing enhanced emission from the sides of the torus. It should take inclination angles of $\gtrsim$45° to produce significant edge emission enhancement by looking through greater depths of gas. We would also need a much better rotation curve for the inner 30″ of M83 to confirm that the molecular emission peaks lie between the inner and outer ILR.

It is not unreasonable to believe that there is a torus/disk of gas that is lying out of the plane of the galaxy. Kinematically distinct subsystems have been found in at least three disk galaxies (NGC 3672, NGC 4826, and NGC 253. See Anantharamaiah & Goss 1996). This may be more common than the observations indicate due to a selection effect caused by the high levels of extinction in the nuclear regions of disk galaxies. M83 has long been believed to have a disk that is quite warped (Rogstad, Lockhart, & Wright 1974). More recent observations of dust lanes suggest that M83 is undergoing three-dimensional accretion in the nucleus and that dust lanes pass out of the plane of the galaxy (Sofue & Wakamatsu 1994). If we were looking at M83 from the edge, we would see the dust lanes passing over and under the nucleus. The result is that when seen nearly face-on, these dust lanes appear as a highly inclined ring ($\sim 70^{\circ}$ out of the plane of the galaxy) that runs from north to south with a radius of $\sim 8''$ (see Figure 4, Sofue & Wakamatsu 1994). This coincides with the out of the plane molecular gas torus explanation proposed above. Since dust tends to trace regions of high density and molecules need higher densities to be shielded from dissociation by UV flux, it is reasonable to believe that the two should be seen in the same environments. Hence, we may expect a ring of molecular gas to be coincident with the ring formed by the warped dust lanes that lie out of the plane of the galaxy.

One problem with the above discussion is explaining *how* the inner part of the disk of M83 could become misaligned with the rest of the disk of the galaxy. One possible explanation is that M83 has accreted a smaller companion galaxy. Models indicate that smaller elliptical galaxies can be accreted by larger elliptical galaxies and the cores of the smaller galaxies can remain nearly intact (Balcells & Quinn 1990). To the best of my knowledge, there are no models that can merge galaxies and maintain a large scale structure such as a bar. If it were possible, the rotation curve that would be created by the combination of the two rotating objects would appear very peculiar. It may appear discontinuous at the radius of the smaller galaxy that has been accreted to the core of the larger galaxy. Such a rotation curve has been predicted by the model of Handa *et al.* (1990) who fitted the *outer* rotation curve of M83 in an attempt to determine the rotation curve of the inner regions. If an accretion event is the cause of the proposed inner disk misalignment, it is not clear whether such a system would have Lindblad resonances where gas will collect. Better models of mergers of barred galaxies as well as observation of the inner rotation curve for M83 will yield a clearer picture of the dynamics at work.

2.4 Physical Conditions

Determining the physical conditions of molecular clouds in other galaxies can be very difficult. In the case of single dish observations, the beam size is often larger than the angular diameter of typical molecular clouds. This means the data are diluted by the regions without molecular emission that the large beam often covers. Molecular clouds are known to be very clumpy (*e.g.* Stutzki & Güsten 1990) which means that even for clouds that fill the beam, there are regions that are not emitting, resulting in a lower measured flux than the emitting regions of the clouds really produce. In addition, assumptions often have to made about the optical depth of the molecular clouds. For the most part, this is a difficult task. Good estimates for optical depth require observations using different transitions and isotopomers and a faith in models involving radiative transfer. Optical depth depends on the population levels of the various transitions, which allows us to make some initial assumptions. For example, in cooler gas the ^{12}CO J=4−3 transition is not as easy to excite as the ^{12}CO J=1−0 transition, thus we can say there are less J=4−3 transitions taking place than there are J=1−0. This means that it is more likely that the J=4−3 photon will escape the molecular clouds without being re-absorbed than it is that J=1−0 photon will escape. It then reasonable to believe that the optical depth (τ) of the ^{12}CO J=4−3 emission will lower than for the J=1−0 emission. In the discussion below, we initially assume that the ^{12}CO J=4−3 and rarer [C I] emission are optically thin ($\tau \ll 1$) and avoid measurements using ^{12}CO J=3−2 wherever possible since it is more likely to be optically thick than the J=4−3 and [C I] emission. These assumptions are not universal truths by any means and should be dropped or modified when evidence indicates it to be necessary. *NOTE: In the following section we will concentrate on the larger peak located at (+5″, +5″) because we have strong emission and good signal-to-noise ratios for all spectra including C I.*

2.4.1 Column Densities from Line Intensities

Not much is known about C I or the conditions in which it forms (*e.g.* Keene *et al.* 1985). Its emission is rather weak compared to CO emission (*e.g.* White *et al.* 1994, Israel *et al.* 1995) and is often thought to be optically thin. If this is the case then the column density can be expressed by

$$N(\mathrm{C}) = 1.9 \times 10^{15}(e^{E_1/kT_{\mathrm{ex}}} + 3 + 5e^{(E_1-E_2)/kT_{\mathrm{ex}}}) \int T_{\mathrm{MB}} dv \quad (\mathrm{cm}^{-2})$$

(Schilke *et al.* 1993, Phillips & Huggins 1981) where E_1/k is the energy of the $J =$ 1 level ($\sim$23.6 K), E_2/k is the energy of the J=2 level ($\sim$62.5 K), and T_{ex} is the excitation temperature of the gas. The last term is the integrated intensity of the [C I] line.

If we assume an excitation temperature of 24 K in M83 (Wall *et al.*1993), the strength of the [C I] line at (+5″,+5″) (71.3 K km s^{-1} (T_{MB})) indicates atomic carbon column densities of $N(\mathrm{C}) = 1{\times}10^{18}$ cm^{-2}. If we adopt a higher excitation temperature (T_{ex} = 50 K) the column density only increases by only 15%. This column density is slightly lower than is found in other starburst galaxies. For example, Israel *et al.* (1995) find atomic carbon column densities of 7.7 $\times 10^{18}$ cm^{-2} in NGC 253 and White *et al.* (1994) find $N(\mathrm{C})$ = 1.9 $\times 10^{18}$ cm^{-2} in the centre of M82. This may not be surprising since both NGC 253 and M82 are seen nearly edge on rather than face on like M83 ($i = 78^{\circ}\!.5$ for NGC 253, Pence 1981; $i = 80^{\circ}$ for M82, Shen & Lo 1995). This means that in M83 we are looking through less material and should then expect to see lower column densities. If we apply a simple correction term for the inclination angle, namely

$$N(\mathrm{C})_{\mathrm{face\ on}} = N(\mathrm{C})_{\mathrm{obs}} \cos\, i$$

we obtain $N(\mathrm{C})_{\mathrm{face\ on}} = 9\ \times 10^{17}$ cm^{-2} for M83, 1.5 $\times 10^{18}$ cm^{-2} for NGC 253, and 3.3 $\times 10^{17}$ cm^{-2} for M82. This indicates that C I column densities (corrected for inclination) are comparable to other starburst galaxies.

Another way to correct for the differences in the geometry between different galaxies is to compare the column density of one species to the column density of another. Since both species are likely subject to the same geometry within a galaxy, comparing the ratio of column densities between different galaxies will help reduce errors introduced by their different geometries. We would also like to calculate column densities using beams of comparable size to reduce the effects of beam dilution in the larger beam. Since both the ^{12}CO J=4−3 data and the [C I] data have approximately the same beam size (12″), we will use them to calculate the ratio $N(\mathrm{C})/N(\mathrm{CO})$.

It can be shown (White & Sandell 1995) that for the ^{12}CO J=4−3 transition, the column density can be expressed

$$N(\mathrm{CO}) = 4.3 \times 10^{14} \int T_{\mathrm{MB}} dv\, \frac{\tau}{1 - e^{-\tau}} \quad (\mathrm{cm}^{-2})$$

where τ is the optical depth of the ^{12}CO J=4−3 emission and assumes T_{ex} = 23 K.

For optically thin gas ($\tau \ll 1$), the $\tau/(1-e^{-\tau})$ term reduces to 1. The strength of the CO J=4−3 line in the region (+5″,+5″) indicates N(CO) = 1.5 $\times 10^{17}$ cm^{-2}. This column density is much lower than previously found in other starburst galaxies (*e.g.* M82 has N(CO) = 5 $\times 10^{18}$ cm^{-2}, Güsten *et al.* 1993; NGC 253 has N(CO) $\sim$3 $\times 10^{19}$ cm^{-2}, Israel *et al.* 1995). One possible explanation for this low CO column density could be our assumption that the gas is optically thin. We would require an optical depth $\tau \sim 30$ to obtain CO column densities similar to those in the starburst galaxy M82. This is not unreasonable given the high molecular gas densities believed to be required to fuel star formation, but it does add an extra uncertainty into the column density calculation, so we will abandon this technique.

Now we attempt to calculate CO column density in a manner that does not involve the knowledge of the optical depth of ^{12}CO J=4−3 emission. We use the relation (see Appendix B)

$$N(\mathrm{H_2}) = \alpha I_{\mathrm{CO}}$$

where $\alpha = 3 \times 10^{20}$ cm^{-2} (K km s^{-1})$^{-1}$ (the Galactic value) and I_{CO} is the integrated intensity of the ^{12}CO J=1−0 emission line (Young & Scoville 1991). Since we do not have ^{12}CO J=1−0 data from the JCMT, we will scale our ^{12}CO J=3−2 data down to a ^{12}CO J=1−0 intensity using published integrated intensity line ratios. The beam size of the ^{12}CO J=3−2 data is 14″ (comparable to the 12″ [C I] beam size) and we need not assume an optical depth for the ^{12}CO J=3−2 emission. Taking our ^{12}CO J=3$-$2 integrated intensity at (+5$''$, +5$''$) (201.4 K km s^{-1} ($T_{\rm MB}$)) and scaling it down to ^{12}CO J=1$-$0 intensity by adopting ^{12}CO J=3$-$2/J=2$-$1 = 1.1 (Wall *et al.* 1993) and ^{12}CO J=2$-$1/J=1$-$0 = 1 (Wiklind *et al.* 1990) and using the above equation gives $N(\rm H_2) = 6 \times 10^{22}$ cm^{-2}. It should be noted that the CO-to-H_2 conversion factor (α) in the above equation is calculated for our own Galaxy. It may be lower for starburst galaxies like M83 due to higher temperatures (see Appendix B), hence the above value of $N(\rm H_2)$ should be considered an overestimate. Now, adopting a CO/H_2 abundance ratio of 10^{-4} (Genzel 1992), we obtain N(CO) = 6 $\times 10^{18}$ cm^{-2}. This gives N(C)/N(CO) = 0.17 which is slightly lower than previously found for other starburst galaxies (0.2 – 0.3 for NGC 253, Israel *et al.* 1995; 0.5 for M82, White *et al.* 1994).

Another way of obtaining the CO column density is by modeling the CO line ratios. The ^{12}CO J=4$-$3 data were convolved to the same beam size as the ^{12}CO J=3$-$2 data using the data reduction package COMB. The integrated intensity line ratios for the nucleus of M83 are shown in Figure 2.9. We estimate a total uncertainty in the line ratios of 30%. We can use the line ratios at the region (+5$''$, +5$''$) to perform a Large Velocity Gradient (LVG, see Appendix D) analysis. If we adopt a kinetic temperature of 30 K, ^{12}CO J=3$-$2/J=2$-$1 = 1.1 (Wall *et al.* 1993), ^{13}CO J=3$-$2/J=2$-$1 = 0.2 (Wall *et al.* 1993) and ^{12}CO J=2$-$1/J=1$-$0 = 1 (Wiklind *et al.* 1990) and input the ^{12}CO J=4$-$3/J=3$-$2 ratio from Figure 2.9, we obtain a lower limit on the CO column density of N(CO) $\gtrsim 3 \times 10^{18}$ cm^{-2} at (+5$''$,+5$''$). This is

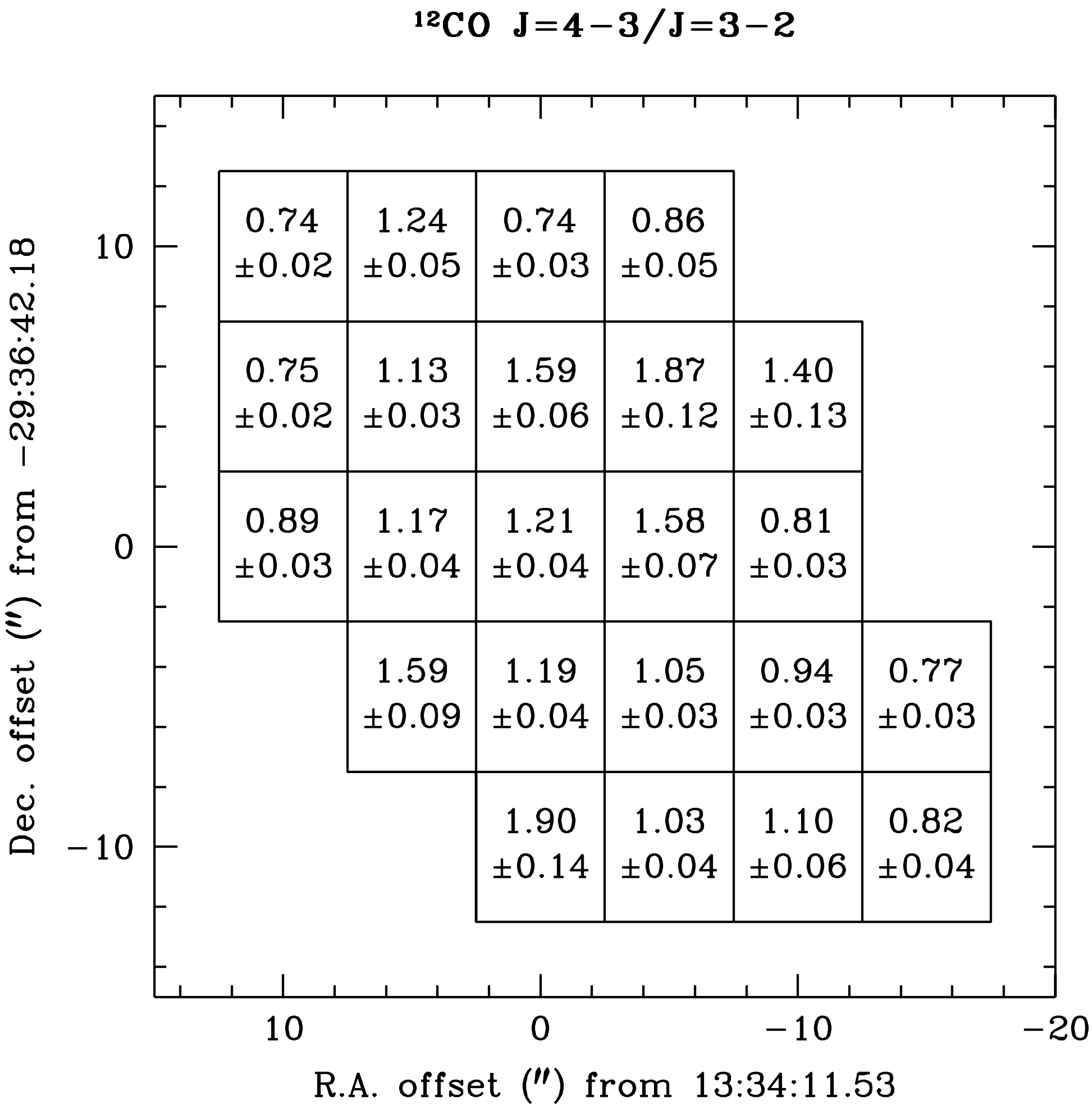

Figure 2.9: ^{12}**CO** J**=4−3/**^{12}**CO** J**=3−2 Line Ratios**

Integrated intensity line ratios for ^{12}CO J=4−3/^{12}CO J=3−2 at locations in M83. The ^{12}CO J=4−3 data has been convolved to the same beam size as the ^{12}CO J=3−2 data. The line ratio peaks in a rough line that runs from the upper right to the lower left corner of the diagram. This strip corresponds to a ring of active star forming regions.

consistent with the value calculated above (considering it is an upper limit). If we adopt a CO column density as the mean of our upper limit of 6 $\times 10^{18}$ cm^{-2} and our lower limit of 3 $\times 10^{18}$ cm^{-2} we obtain N(CO) = 4.5 $\times 10^{18}$ cm^{-2}. This gives us a ratio of N(C)/N(CO) = 0.22 which is similar to the value found for the starburst galaxy NGC 253 (Israel *et al.* 1995). We therefore adopt a N(C)/N(CO) ratio of 0.2 $\pm$ 0.03 for M83. It should be noted that this ratio is only for the region (+5$''$, +5$''$) while the values they are compared to for NGC 253 and M82 are average values over the nuclear region.

It is interesting to compare the N(C)/N(CO) ratios for these three galaxies to their star formation properties. Letting the surface brightness (Σ) of Hα flux (from H atoms ionized by hot young stars) per unit H surface density [(erg s^{-1} pc^{-2})/(M$_\odot$ pc^{-2})] be an estimate of the star formation activity in the inner 20$''$of each galaxy, Wall *et al.* (1993) find that M82 is the most active (log(ΣHα/ΣH) = 34.0) followed by M83 (log(ΣHα/ΣH) = 33.3) and NGC 253 (log(ΣHα/ΣH) = 31.8). This seems to indicate that the galaxy with the highest N(C)/N(CO) ratio is also the galaxy with the least active star formation. It should be noted that the Hα fluxes are *not* corrected for extinction and are not by any means the best way to measure star formation activity. If we wish to measure the strength of the starburst we could use the far-infrared (FIR) luminosity (caused by hot young stars heating dust grains; it is less prone to extinction). The FIR luminosity indicates that M82 and NGC 253 are stronger starbursts ($L_{\rm FIR}$ = 3 $\times$ 10^{10} L$_\odot$ and 1.5 $\times$ 10^{10} L$_\odot$ respectively) than

M83 ($L_{\mathrm{FIR}} = 4 \times 10^9$ $L_\odot$)(Telesco & Harper 1980, Wall *et al.* 1993). Thus, in our small sample (see a summary in Table 2.1), there seems to be no obvious correlation between N(C)/N(CO) and the intensity of star formation. Of course, observations of more starburst galaxies are required before any such conclusions are justified.

Table 2.1: **Properties of Starburst Galaxies**

Galaxy	i	N(C)	N(CO)	N(C)/N(CO)	L_{FIR}	log(Σ Hα/ΣH)
		cm^{-2}	cm^{-2}		$L_\odot$	$\log(\frac{\mathrm{erg\ s^{-1}\ pc^{-2}}}{\mathrm{M_\odot\ pc^{-2}}})$
M83	24°	1×10^{18}	4.5×10^{18}	0.2±0.02	4×10^{9}	33.3
M82	80°	1.9×10^{18}	5×10^{18}	0.5	3×10^{10}	34.0
NGC 253	78.°5	7.7×10^{18}	3×10^{19}	0.2 – 0.3	1.5×10^{10}	31.8

All references are given in the text.

2.4.2 Line Ratios

Another method of determining the physical conditions in a molecular cloud or distant galaxy is through the use of integrated intensity line ratios. By assuming the same regions in space are emitting the observed radiation, dividing the measured integrated intensities of two emission lines eliminates the unknown filling factor of the molecular gas in the beam (as long as the beam sizes are the same). Knowledge of how these line ratios vary in different conditions (such as cold dark clouds or hot star forming regions) as well as radiative transfer models allows determination of the conditions required to produce the observed line ratios.

The ^{12}CO J=4−3/^{12}CO J=3−2 integrated intensity line ratios (shown in Figure 2.9) vary substantially over the central region of M83 with the highest ratios occurring towards the edges of the emission peaks. If all the gas had the same optical depth, we would expect the ^{12}CO J=4−3 emission to be enhanced near the hotter regions of star formation in the centre of the galaxy. The ^{12}CO J=4−3/J=3−2 line ratio is highest to the right and left of the upper and lower peak of Figure 2.4 respectively. The highest ^{12}CO J=4−3/J=3−2 line ratios seem to run from the upper right to the lower left of Figure 2.9. This corresponds nicely with the arc of active star forming regions found by Gallais *et al.* (1991, also see Figure 4 of Sofue & Wakamatsu 1994). We thus conclude that the peak ^{12}CO J=4−3/J=3−2 line ratios are excited by the high temperatures associated with the arc of active star forming regions that encircles the nucleus of M83. Assuming local thermodynamic equilibrium (LTE, see Appendix C), the high line ratios (>1) indicate that the higher J transitions of CO are optically thin and are likely the result of the high temperatures and/or densities associated with star formation. According to the LTE approximation, ^{12}CO J=4−3/J=3−2 line ratios of no greater than 1.7 are predicted for optically thin gas at an excitation temperature of 50 K. Line ratios cannot exceed one if both transitions are optically thick (see Appendix C). This indicates that the ^{12}CO J=4−3 emission at (−5″, +5″) and (−10″, 0″) is likely optically thin while the emission at (+5″, +5″) may be optically thick as suggested in the previous section.

As mentioned above, little is known about the conditions that create C I. As a result, there are few (if any) models that can calculate exactly what gas conditions can be derived from measures line ratios. For this reason, we will restrict our analysis to comparing our values to those measured in our own and other galaxies.

Since the ^{12}CO J=4−3 and [C I] data have the same beam size, we are able to directly divide the integrated intensities to obtain line ratios. Ratios were only calculated for the regions where the integrated intensity was three times the rms noise. The results are shown in Figure 2.10. The [C I]/^{12}CO J=4−3 integrated intensity line ratios are uniform at the 2σ level and have an average value of 0.25 ± 0.03. This is similar to those found in the starburst galaxy NGC 253 (0.27, Israel *et al.* 1995). In order to compare our value to the [C I]/^{12}CO J=1−0 ratio, which is the most commonly published value, we must scale down our ^{12}CO J=4−3 data to ^{12}CO J=1−0 line strengths. We will again focus on the peak of the [C I] emission at (+5″, +5″). Taking the [C I]/^{12}CO J=4−3 line ratio of 0.21 (see Figure 2.10) and using the ^{12}CO J=4−3/J=3−2 line ratio of 1.02 (see Figure 2.9), the ^{12}CO J=3−2/J=2−1 ratio of 1.1 (Wall *et al.* 1993), and the ^{12}CO J=2−1/J=1−0 ratio of 1.0 (Wiklind *et al.* 1990) we obtain a [C I]/^{12}CO J=1−0 ratio of 0.24. This is higher than the value found in the starburst galaxy M82 (0.11, Schilke *et al.* 1993), the non-starburst spiral galaxy M33 (0.04-0.18, Wilson 1997), the spiral galaxy with a moderate nuclear starburst, IC 342 (Büttegenbach *et al.* 1992), and our own Milky Way (0.16, Wright *et al.* 1991, assuming ^{12}CO J=2−1/J=1−0 = 0.7, Sakamoto *et al.* 1994). It is lower than that of the starburst galaxy NGC 253 (Israel *et al.* 1995). This possibly indicates that there is more C I being produced in M83 than there is in M82, M33, IC 342, and the Milky Way or (if we assume all [C I] emission is optically thin

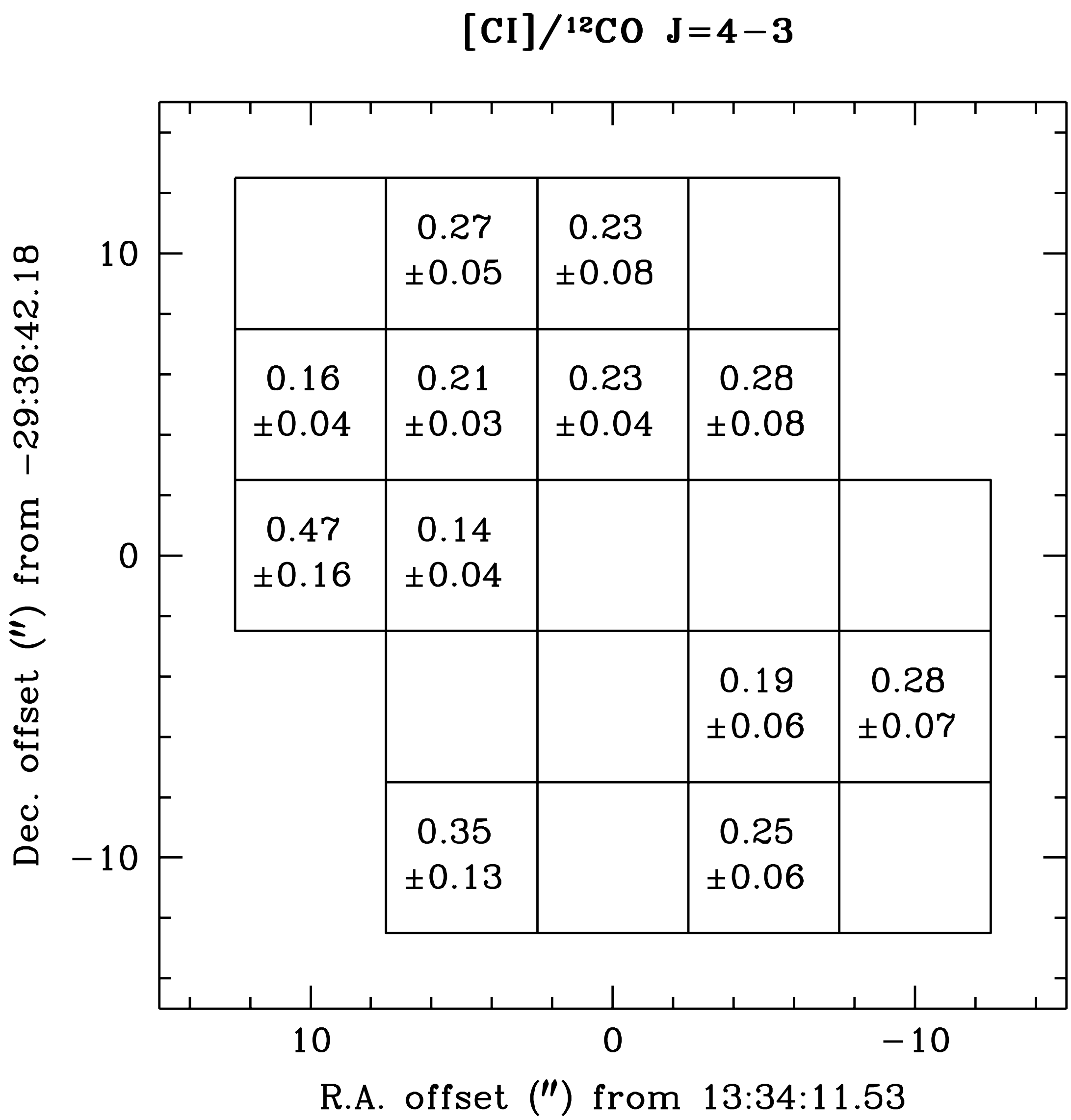

Figure 2.10: **[C I]/^{12}CO J=4−3 Line Ratios**
Integrated intensity ($T_{\rm MB}$) line ratios for [C I]/^{12}CO J=4−3 at locations in M83. Only those locations where the signal to noise in the [C I] and ^{12}CO J=4−3 integrated intensity was greater than three are shown. The data were taken with comparable beam sizes at the JCMT. The line ratios are uniform at the 2σ level, indicating that the processes creating and destroying C I and CO in the $J = 4$ state are comparable throughout the nucleus of M83.

and all ^{12}CO J=1−0 emission optically thick) that there is more CO in these other galaxies, reducing the [C I]/CO line ratio. Since we know little about the formation of C I, it is important to build up a database to compare with models.

While the actual value of the [C I]/CO line ratio may not yet tell us much about the conditions in the different regions of the galaxy, we can learn about the relative strengths of the processes creating and destroying C I and CO by comparing the [C I]/CO line ratio over different regions of the galaxy. If we neglect optical depth effects, the [C I]/CO ratio is a measure of the relative quantities of the emitting material. The relative quantities are related to the relative strengths of the processes creating and destroying them. As shown in Figure 2.10, the line ratio is uniform at the 2σ level, while the ^{12}CO J=4−3/J=3−2 ratio varies substantially (up to $\sim 50\sigma$, see Figure 2.9). While we do not know exactly what conditions are required to produce high concentrations of C I, we can say the uniformity of the [C I]/^{12}CO J=4−3 line ratios likely indicates that the processes creating and destroying CO in the $J = 4$ state and C I are comparable throughout the nucleus of M83. This indicates that C I may be created in the hot photodissociation regions surrounding massive stars that form inside the nuclear starburst of M83.

2.5 Conclusions

This chapter presents [C I], ^{12}CO J=4−3, and ^{12}CO J=3−2 maps of the nucleus of the barred spiral galaxy M83 taken at the JCMT. The main results are summarized below.

1. We observe a double peaked structure in the molecular emission consistent with gas inflow along the bar collecting at the inner Lindblad resonance. The ^{12}CO J=4−3 emission suggests that some of the molecular gas has made it into the nucleus and is being heated by, and possibly fueling the nuclear starburst. This indicates that nuclear starbursts may occur even in galaxies where gas collects at ILRs.

2. We observe different morphologies in the ^{12}CO J=4−3 channel maps than in the ^{12}CO J=3−2 and ^{12}CO J=1−0 channel maps. This indicates that ^{12}CO J=1−0 emission is not always a good tracer of molecular gas.

3. The observations cannot rule out that the double peaked emission is the result of a molecular ring out of the plane of the galaxy nearly perpendicular to the main disk. This torus of cooler gas contains a disk of hotter gas that fills its central void.

4. The [C I] line strength indicates carbon column densities of 1×10^{18} cm^{-2} while CO emission indicates CO column densities of $\sim 4.5 \times 10^{18}$ cm^{-2} and H_2 column

densities of 6×10^{22} cm^{-2}. The $N(\mathrm{C})/N(\mathrm{CO})$ ratio at the peak of the emission is 0.20 $\pm$ 0.02 which is lower than that found in most other starburst galaxies and is likely the result of a high column density of CO.

5. The twelve [C I]/^{12}CO J=4$-$3 line ratios in the inner $24'' \times 24''$ are uniform at the 2σ level and have an average value of 0.25 $\pm$ 0.03 similar to those of other starburst galaxies. The uniformity of the line ratios may indicate that the processes creating and destroying CO in the $J = 4$ state and C I are comparable throughout the nucleus of M83.

6. The ^{12}CO J=4$-$3/^{12}CO J=3$-$2 integrated intensity line ratios vary substantially over the central region of M83 with the highest ratios occurring towards the edges of the emission peaks. The ^{12}CO J=4$-$3/J=3$-$2 line ratios seem to be enhanced along an arc of active star forming regions. The high line ratios (>1) indicate that the higher J transitions of CO are optically thin and are likely the result of the high temperatures and/or densities associated with star formation.

Chapter 3

The Effect of Star Formation on Molecular Clouds in Dwarf Irregular Galaxies: IC 10 and NGC 6822

3.1 Introduction

Dwarf irregular galaxies are rather simple systems, free from the complicated dynamics that accompany bars or spiral density waves. This simplicity makes them useful for studying the interactions between star formation and the interstellar medium (ISM). Temperature, density, and abundance may all affect the star formation process, and thus, determining the physical conditions inside molecular clouds is important for understanding how the properties of the molecular gas affect the type and amount of stars formed. Unfortunately, extragalactic molecular clouds have low filling factors even within beams as small as $15''$ and so their true temperatures cannot be deduced from the observed peak temperature of the spectral line. Instead, observations of many rotational transitions of CO and its isotopomers can be combined with radiative transfer models to constrain the physical conditions inside these clouds. As it is necessary to observe some of the rarer isotopomers such as ^{13}CO, these techniques have been primarily applied to starburst galaxies (*e.g.* Tilanus *et al.* 1991).

Relatively few dwarf galaxies have been detected in CO and the lines that are observed are much weaker than those found in spiral galaxies (Combes 1986; Tacconi & Young 1987; Arnault *et al.* 1988). The weakness of these lines is likely due to a lower CO emissivity per unit mass of gas relative to spiral galaxies, which is caused by the low metallicity of most irregular galaxies (12 + log(O/H) = 8.16 for IC 10, 8.20 for NGC 6822, Lequeux *et al.* 1979). IC 10 is one of the few dwarf galaxies in which strong CO lines have been detected (Becker 1990), with line strengths that are greater than those of the LMC, SMC, and NGC 6822 (*e.g.* Israel *et al.* 1993; Wilson 1994; Israel 1997). The simplest explanation of these strong CO lines is that IC 10 contains large amounts of molecular gas (Wilson & Reid 1991). Unfortunately, except for the strong CO lines, there is no additional evidence to support this explanation. In fact, IC 10 has a rather low gas-to-dust ratio for a dwarf irregular galaxy (Schmidt & Boller 1993). A more likely answer lies in the star forming activity. Massey & Armandroff (1995) found that IC 10 has a *global* surface density of Wolf-Rayet stars three times as high as any other Local Group galaxy, comparable to the surface density found within active star forming regions of M33. This high concentration of Wolf-Rayet stars reinforces the idea that IC 10 is undergoing a rather strong burst of star formation. It has been shown both observationally and theoretically that CO emission depends on the conditions in the molecular clouds. Maloney & Black (1988) find that the ratio of CO intensity to excitation temperature is constant for ensembles of identical clouds. Hence, higher temperatures will result in brighter CO emission. The high star formation rates could increase the temperature of the molecular gas and more readily excite the CO molecules. Such a process would be able to produce the strong CO lines observed in IC 10.

In this chapter we study the physical properties of molecular clouds in environments with different amounts of star forming activity located in two Local Group dwarf irregular galaxies, IC 10 and NGC 6822. IC 10 appears optically as a patchy nebulous region extending approximately $3' \times 4'$. It has been classified as a dwarf irregular of the Magellanic type (IBm; de Vaucouleurs & Ables 1965). It is rather close to the Galactic plane (b $\sim -3°$), which indicates that there is heavy obscuration at visual wavelengths. It is considered a Local Group member based on its distance of 0.82 Mpc (Wilson *et al.* 1996). The bright H 2 regions (*e.g.* Sandage & Tammann 1974) indicate that IC 10 is undergoing massive star formation.

NGC 6822 is also a dwarf irregular galaxy relatively close to the Galactic plane (b $\sim -18°$). It has a bar-like appearance extending approximately $10' \times 20'$ north-south with a prominent "wing" located to the southeast. Its distance of 0.49 Mpc (McGonegal *et al.* 1983) also places it in the Local Group. In §3.2 we discuss the observations and the data reduction process. In §3.3 we discuss the results found for the individual molecular clouds in IC 10 and NGC 6822 based on the line ratios and models. We also compare masses obtained from flux measurements with virial masses and discuss the validity of the assumptions made to aid in the interpretation of the data. In §3.4 we discuss the implications of these new data and the physical conditions of the molecular clouds for the CO-to-H_2 conversion factor. The chapter is summarized in §3.5.

3.2 Observations and Data Reduction

Four regions centered on giant molecular clouds in IC 10 were observed using the James Clerk Maxwell Telescope (JCMT) over the period of 1994 October 20 – 24. The regions were selected from both interferometric CO J=1−0 surveys (Wilson & Reid 1991; Wilson 1995) and a single dish ^{12}CO J=2−1 and J=1−0 survey (Becker 1990). All four of the regions were observed in ^{12}CO J=2−1 with follow-up observations for 2 of these regions (containing clouds IC 10:MC 1/2 & IC 10:MC 6/7/8) in ^{12}CO J=3−2 and ^{13}CO J=2−1. A final ^{13}CO J=3−2 observation was obtained at a single position located at the peak of the ^{13}CO J=2−1 emission in IC10:MC 1/2. The half-power beamwidth of the JCMT is 22″ at 230 GHz (^{12}CO J=2−1) and 15″ at 345 GHz (^{12}CO J=3−2). Data were obtained on a five-point cross offset by 11″ for the J=2−1 data and 8″ for the J=3−2 data. One giant molecular cloud in NGC 6822 was observed during service observing at the JCMT on the nights of 1996 May 5 (^{12}CO J=3−2) and 1994 June 8 (^{12}CO J=2−1). The cloud was observed at a single position in the J=2−1 transition and a five-point cross offset by 8″ in the J=3−2 transition. All observations were obtained using the Dwingeloo Autocorrelation Spectrometer.

The data were reduced using the Bell Labs data reduction package COMB. The data were binned to 1.5 km s^{-1} resolution and first to seventh degree baselines were removed. The lines were quite narrow ($<$ 30 km s^{-1}) and the spectrometer bandwidth was at least 450 km s^{-1}, so the removal of rather high degree baselines for some spectra do not introduce significant errors into the final line intensities. Third and seventh degree baseline removal on the same data yielded line parameters that agreed to within 1σ. The ^{12}CO J=3−2 data were then convolved to simulate a 22″ beam. The spectra for each cloud are shown in Figures 3.1 and 3.2. The data were then binned to the same resolution and shifted to the same $V_{\rm LSR}$ (when necessary). This allowed the calculation of line ratios for each channel within the spectral line. The ratios for each channel were averaged to obtain the final line ratios. Only those channels with a signal-to-noise ratio of at least two in the line ratio were used in the calculation. This method helps reduce errors introduced by the existence of poor baselines or weak signals. The uncertainty in the value for the line ratio is taken as the standard deviation of the mean. As a final step, the line ratios were scaled to the main beam temperature scale using the appropriate values for $\eta_{\rm MB}$ (see below). A summary of the line ratios is given in Table 3.1 and a channel by channel histogram of the ratios is shown in Figure 3.3. The calibration of the IC 10 data was monitored

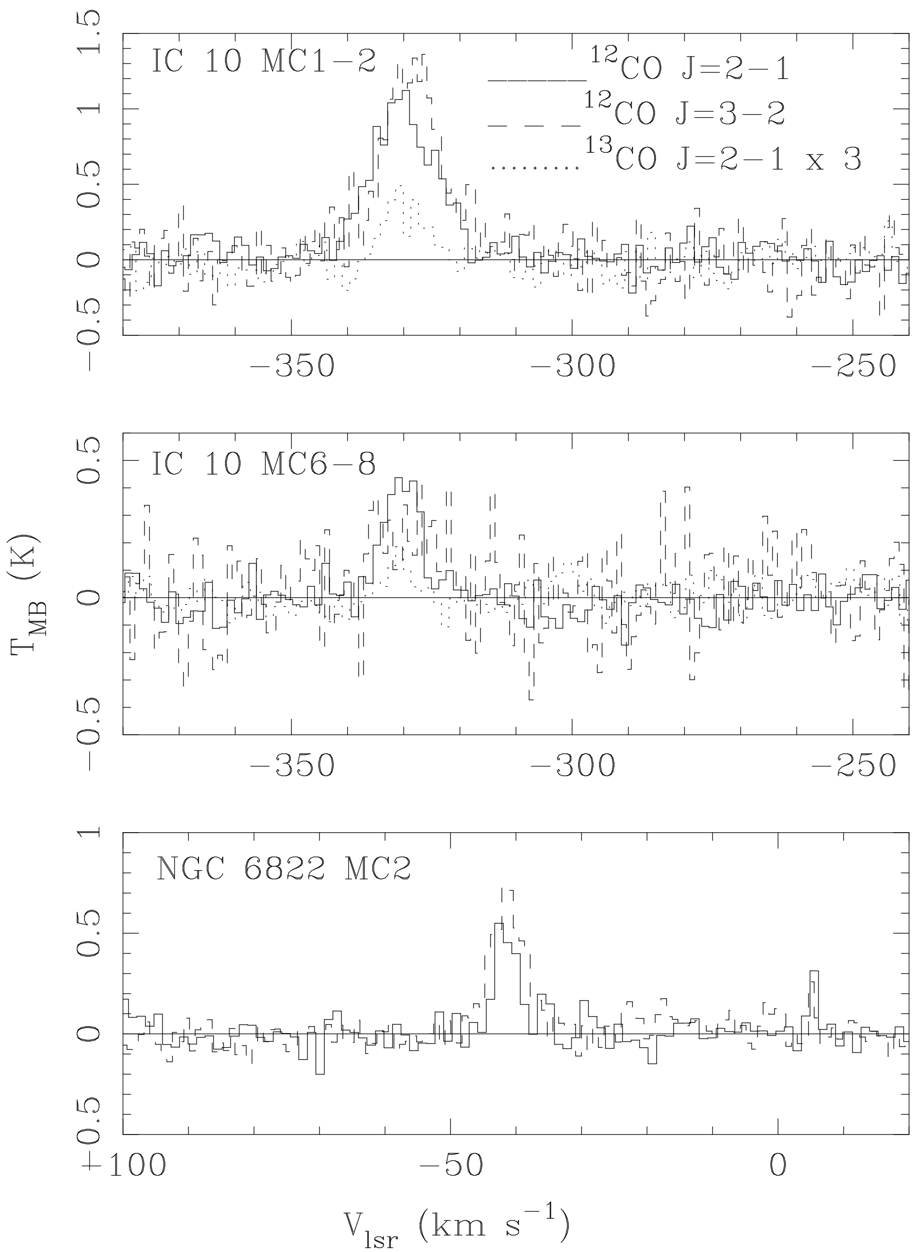

Figure 3.1: **CO Spectral Lines**

The ^{12}CO J=2−1 (solid line), ^{13}CO J=2−1 (dotted line), and ^{12}CO J=3−2 (dashed line) spectra observed in 3 regions in IC 10 and NGC 6822. The J=3−2 data have been convolved to match the 22″ beam of the J=2−1 data. The ^{13}CO J=2−1 line has been scaled up by a factor of three.

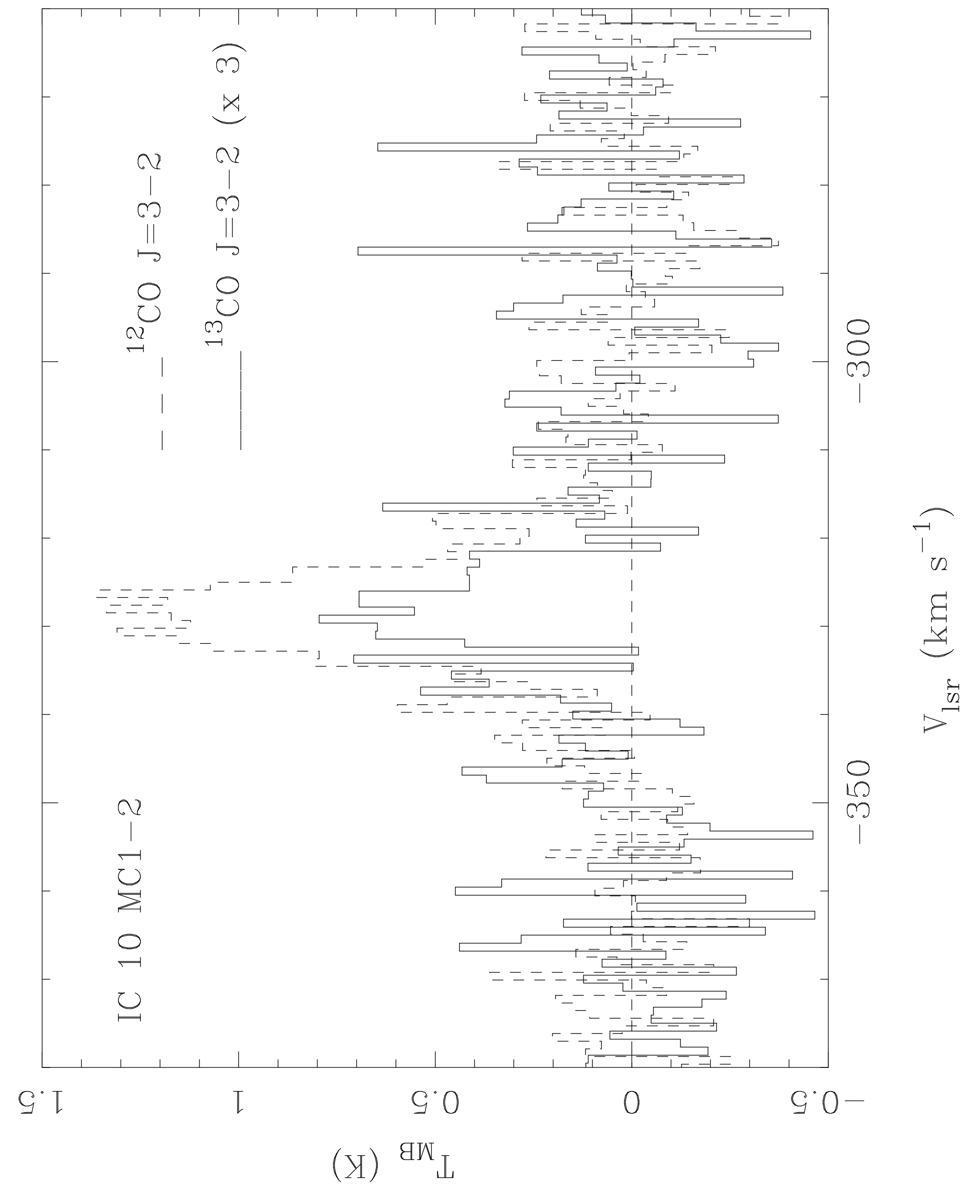

Figure 3.2: ^{13}**CO** J**=3−2 Emission from IC 10:MC 1/2**
The ^{12}CO J=3−2 (dashed line) and ^{13}CO J=3−2 (solid line) spectra observed towards the region MC 1/2 in IC 10. The spectra were obtained with a 15″ beam. The ^{13}CO J=3−2 spectrum is scaled up by a factor of three.

Table 3.1: **CO Line Ratios of Molecular Clouds in IC 10 and NGC 6822**

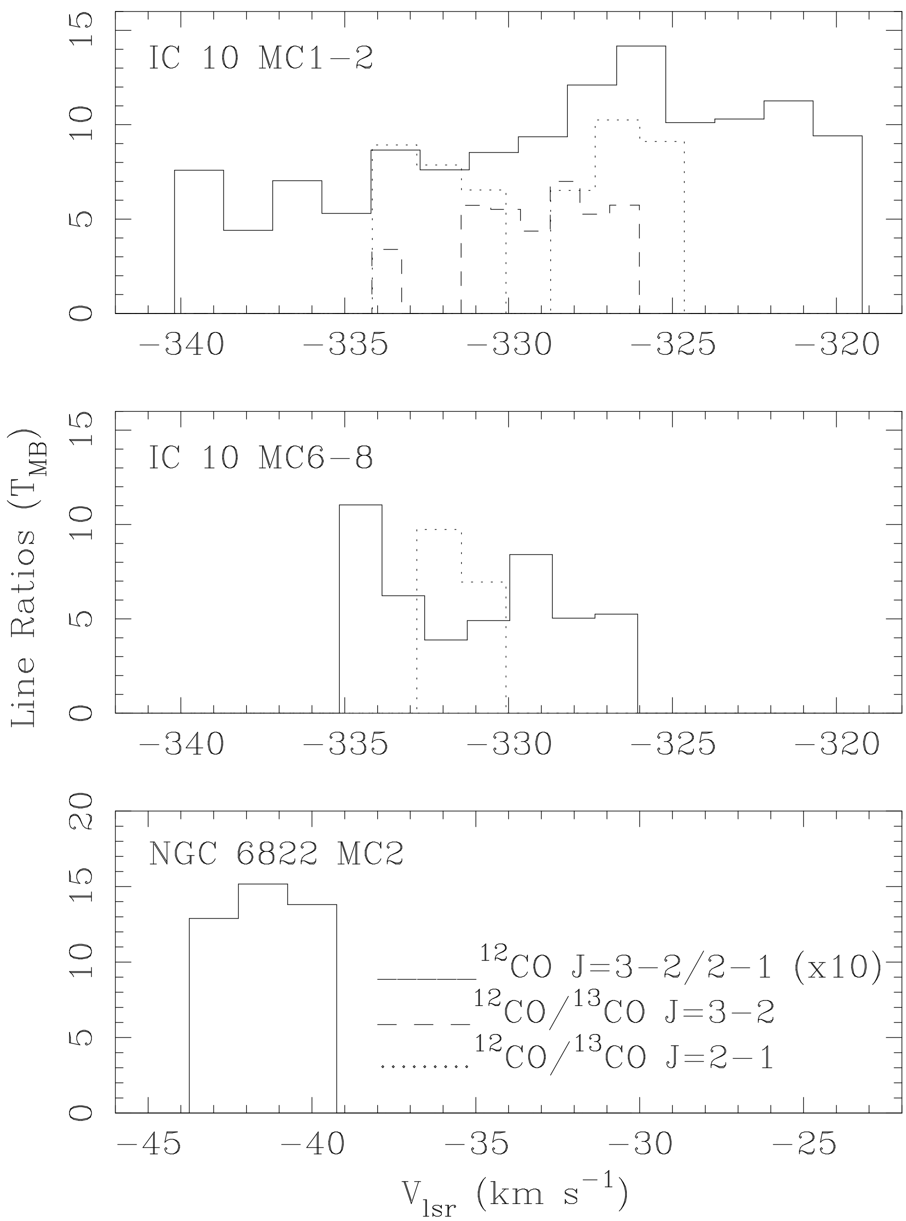

Figure 3.3: **CO Line Ratios**

Channel by channel line ratios (in $T_{\rm MB}$) for the 3 regions observed. The solid line represents the ^{12}CO J=3−2/J=2−1 line ratio (scaled up by a factor of 10), the dashed line represents the ^{12}CO/^{13}CO J=3−2 line ratio, and the dotted line represents the ^{12}CO/^{13}CO J=2−1 line ratio. Only those channels with a signal to noise ratio greater than two are shown.

by frequently observing both planets and spectral line calibrators. Unfortunately, it was later determined that the beam of the telescope was decidedly non-circular during 1994 October (see JCMT Newsletter No. 4, March 1995), enough to affect our calibration. Although the spectral line calibrators showed considerable scatter, with individual measurements differing by as much as $\pm 40\%$ from standard spectra, observations of a given source were repeatable to within $\sim 5\%$. The wide scatter of the spectral line calibrators may be understood given the large ellipticity of the beam and the range in diameter of the calibrators, from compact carbon stars to more extended emission in H 2 regions. Depending on the size of the source, the measured line strength may be larger or smaller with the elliptical beam compared to that measured with a circular beam. The main beam efficiencies determined using Saturn were 0.60 ± 0.02 at 220/230 GHz and 0.36 ± 0.01 at 345 GHz. Both efficiencies are substantially lower than normal values. Since Saturn had a diameter of $18''$ during these observations, it provides a reasonable match to the size of the emission regions in IC 10. This assumption was confirmed by observing the molecular cloud MC 20 in M33, for which observations obtained with the JCMT in a more normal state were available; the ^{12}CO J=2$-$1 line from this source was indeed low by about 20%. Thus, we adopt these observed efficiencies to convert our data to the main beam temperature scale. For the NGC 6822 data (taken at a different dates under normal calibration conditions), observations of CRL 2688 agreed with the published values, and so we adopt the normal main beam efficiencies from the JCMT Users Guide of

0.72 at 230 GHz and 0.58 at 345 GHz.

Since the line strengths we are comparing are measured with the same beam diameter, using the T_R^* temperature scale would ensure that our observed line ratios are equal to the true radiation temperature ratios. However, conversion to T_R^* from T_A^* requires knowledge of the forward scattering and spillover (η_{FSS}), which is difficult to measure and was not attempted during the observing run. As a result, we do not know how to correct the published values of η_{FSS} to take into account the calibration problems discussed above. On the other hand, we do have good values for the main beam efficiencies and so an accurate conversion to main beam temperature (T_{MB}) is possible. Using the T_{MB} scale instead of T_R^* scale only changes the ^{12}CO J=3−2/J=2−1 line ratio by ∼5% under normal calibration conditions. For this reason, we will use the main beam temperature scale for the line ratios throughout this thesis.

3.3 Molecular Cloud Properties

3.3.1 MC 1/2 and MC 6/7/8 in IC 10

The clouds MC 1/2 are located 60″ (240 pc at a distance of 0.82 Mpc) from the center of the brightest H 2 region in IC 10 (no. 111, Hodge & Lee 1990; Shostak & Skillman 1989). This H 2 region has an Hα luminosity of 4×10^{38} erg s^{-1}. Conversely, MC 6/7/8 is not located near a large H 2 region; it is 86″ (340 pc) away from the edge of even the nearest moderate sized one (no. 50, Hα luminosity of $\sim 10^{37}$ erg s^{-1}, Hodge & Lee 1990). For these two regions (MC 1/2 and MC 6/7/8), the ^{12}CO/^{13}CO J=2−1 ratios agree very well, which suggests similar ^{12}CO/^{13}CO abundances in these clouds. Although the ^{12}CO J=3−2/J=2−1 ratios also agree within the large uncertainties, the larger ratio of 0.90 is found for the cloud nearer the bright H 2 region, while the lower ratio of 0.66 is found in the more quiescent cloud.

Wilson, Walker, & Thornley (1997) found that the giant molecular cloud NGC 604-2, located in the very intense star formation environment of the giant H 2 region NGC 604 in M33, had a ^{12}CO J=3−2/J=2−1 ratio that was higher than average for M33 (1.07 ± 0.17 compared to 0.64 ± 0.07 for clouds without optical H 2 regions). They also found that a cloud located only 120 pc (31″) away from NGC 604 did not show an increase in the ^{12}CO J=3−2/J=2−1 ratio. In IC 10, MC 1/2 does exhibit an enhanced ^{12}CO J=3−2/J=2−1 line ratio, even though it is further away from the weaker H 2 region no. 111. This result suggests that if a similar line ratio enhancement is taking place as in M33, the ISM in the metal-poor dwarf irregular galaxy IC 10 must be more porous to UV radiation. This effect could allow the line ratio enhancement to occur at greater distances from weaker H 2 regions than is possible in the higher metallicity spiral galaxy M33 (12 + log(O/H) = 8.48 in NGC 604, Vilchez *et al.* 1988).

The IC 10 data and the NGC 6822 data (see §3.3.2) support the conclusions of Wilson *et al.* (1997) that the ^{12}CO J=3−2/J=2−1 line ratio increases towards the centers of bright H 2 regions. The higher transitions can be more readily excited by higher temperatures or higher densities, either of which will produce higher line ratios. It is believed that higher temperatures are present near star-forming regions, but without accurate densities for these clouds, we cannot assess the extent to which both of these factors contribute to the elevated line ratios. Independent temperature information on these clouds (*e.g.* from the new bolometer array SCUBA on the JCMT) should yield a clearer picture of the processes at work.

For the clouds for which we have observed more than one line ratio, we can use models to help constrain the physical conditions of the clouds. We will use the large velocity gradient (LVG) model, which assumes that the clouds in the beam have internal velocities large enough to Doppler shift the CO emission from one part of the cloud sufficiently to prevent reabsorption by other CO molecules in other parts of the cloud (Scoville & Solomon 1974). We used the LVG code RAD written by Dr. L. Mundy and implemented as part of the MIRIAD data reduction package. Model grids were run for kinetic temperatures $T_{\rm K}$ = 10, 15, 20, 30, 50, 100, 200, 300 K, abundance ratios $[^{12}{\rm CO}]/[^{13}{\rm CO}]$ = 30, 50, 70, and covering a range of densities of $\log[n_{\rm H_2}({\rm cm^{-3}})] = 1 - 6$ and ^{12}CO column densities per unit velocity of $\log[N(^{12}{\rm CO})/\Delta v\ \ ({\rm cm^{-2}\ km^{-1}\ s})] = 15 - 20$. To calculate the ^{12}CO column densities from $N/\Delta v$, we use the full-width half maximum velocity.

Figure 3.4 shows one of the two solutions found for the line ratios of IC 10:MC 1/2. The three ratios obtained using the JCMT (^{12}CO/^{13}CO J=3−2, ^{12}CO

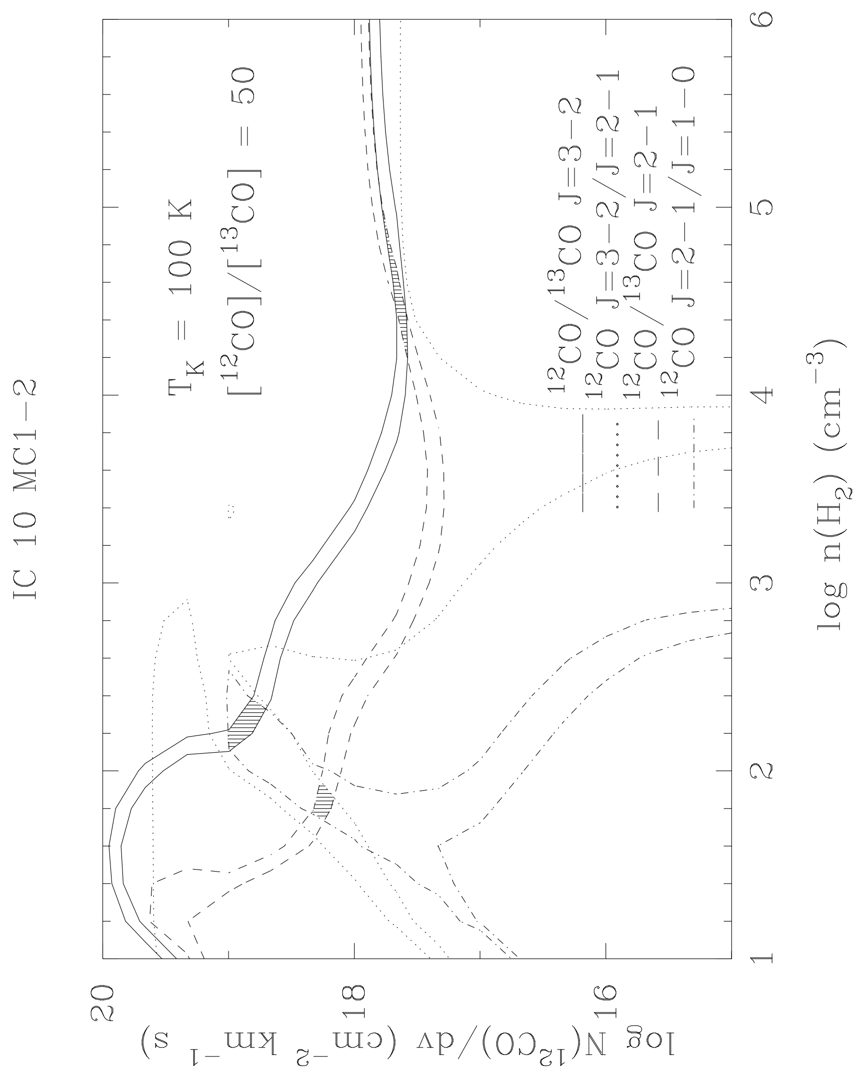

Figure 3.4: **LVG Solutions for IC 10:MC 1/2**

Solutions for the density and column density for the region MC 1/2 in IC 10 using a large velocity gradient code. This figure shows the solution for the three JCMT line ratios at a kinetic temperature of 100 K and a $[^{12}CO]/[^{13}CO]$ abundance of 50. The solid lines indicate the 1σ limits of the $^{12}CO/^{13}CO$ J=3−2 line ratio of 5.3 ± 0.4. The dotted lines represent the ^{12}CO J=3−2/J=2−1 line ratio of 0.9 ± 0.11 and the dashed lines represent the $^{12}CO/^{13}CO$ J=2−1 line ratio of 8.2 ± 0.6. Also included is the ^{12}CO J=2−1/J=1−0 line ratio of 0.64 ± 0.05 (J=1−0 data from IRAM, Becker 1990), shown as the dot-dashed lines. Solutions are indicated by the shaded regions where the line ratios overlap. In this case there are three separate regions where three of the four line ratios overlap which may indicate two distinct emission regions within the clouds.

J=3−2/J=2−1 and ^{12}CO/^{13}CO J=2−1) are shown as bands that indicate the 1σ upper and lower limits of the line ratio. Solutions are indicated by the locations where the regions of the different ratio boundaries overlap. Of the 24 possible models, this only occurred twice for the JCMT line ratios of IC 10:MC 1/2, at $T_{\rm K}$ = 100 K and for the abundances [^{12}CO]/[^{13}CO] = 50 and 70. Both cases indicate a density of $10^4 - 10^5$ cm^{-3} and column densities per unit velocity of about $10^{17.7}$ cm^{-2} (km s^{-1})$^{-1}$. The average full-width half maximum of the emission lines in IC 10:MC 1/2 is 12.2 ± 1.4 km s^{-1}, which gives a true column density of 6×10^{18} cm^{-2}.

We have also calculated the ^{12}CO J=2−1/J=1−0 ratio by combining our JCMT ^{12}CO J=2−1 data (22″ beam) and the IRAM 30-m telescope ^{12}CO J=1−0 data (21″ beam) obtained by Becker (1990). The similarity in the beam sizes at these two frequencies allows a straightforward combination of the data sets without the use of convolution algorithms. In an attempt to constrain the abundance better, we then included the ^{12}CO J=2−1/J=1−0 line ratio into the LVG model. However, instead of overlapping with one of the other two existing solutions, the ^{12}CO J=2−1/J=1−0 line ratio provided two additional solutions for each abundance at lower density (n(H$_2$) = $10^{1.5} - 10^{2.5}$ cm^{-3}). There is no region where all four line ratios overlap. This result may indicate the existence of separate high and low density regions that contribute to the emission. The high density region dominates the upper J emission while the lower J emission would originate predominantly from the lower density region (as would be predicted by the Boltzmann equation). We know that Galactic molecular clouds are clumpy (*e.g.* Stutzki & Güsten 1990), and there is every reason to believe that extragalactic molecular clouds are clumpy as well. If this is the case we can perhaps interpret the two distinct emitting regions as representing the high density clumps and the less dense inter-clump regions. Unfortunately, the lack of data with resolution better than 7″or 28 pc (Wilson & Reid 1991; Ohta *et al.* 1992; Wilson 1995) precludes further discussion of the degree of substructure within molecular clouds in IC 10.

With only two line ratios (^{12}CO J=3−2/J=2−1 and ^{12}CO/^{13}CO J=2−1), it is not possible to put very strong constraints on the physical conditions in IC 10 MC 6/7/8 without making some assumptions. For example, if we assume a moderate temperature of 20 K and a [^{12}CO]/[^{13}CO] abundance of 50 (as found for IC 10:MC 1/2), we can estimate upper and lower limits for the densities in the cloud. The results of this model are shown in Figure 3.5. There is a rather broad range of allowed values for density ($10^{1.6} - 10^4$ cm^{-3}) and for ^{12}CO column densities per unit velocity ($10^{16.5} - 10^{18.5}$ cm^{-2} (km s^{-1})$^{-1}$). The full-width half maximum of the emission lines in MC 6/7/8 is 7.1 ± 1.6 km s^{-1}, which gives true column densities ranging from 2×10^{17} to 2×10^{19} cm^{-2}. If we assume a [^{12}CO]/[^{13}CO] abundance of 70 (as is also allowed by the more complete IC 10:MC 1/2 model) the only change is that the lower limit on column density increases from 2×10^{17} cm^{-2} to 7×10^{17} cm^{-2}, narrowing the allowed range of column density slightly. The range in density and the upper limit in column density remain essentially the same. Adopting a higher kinetic temperature

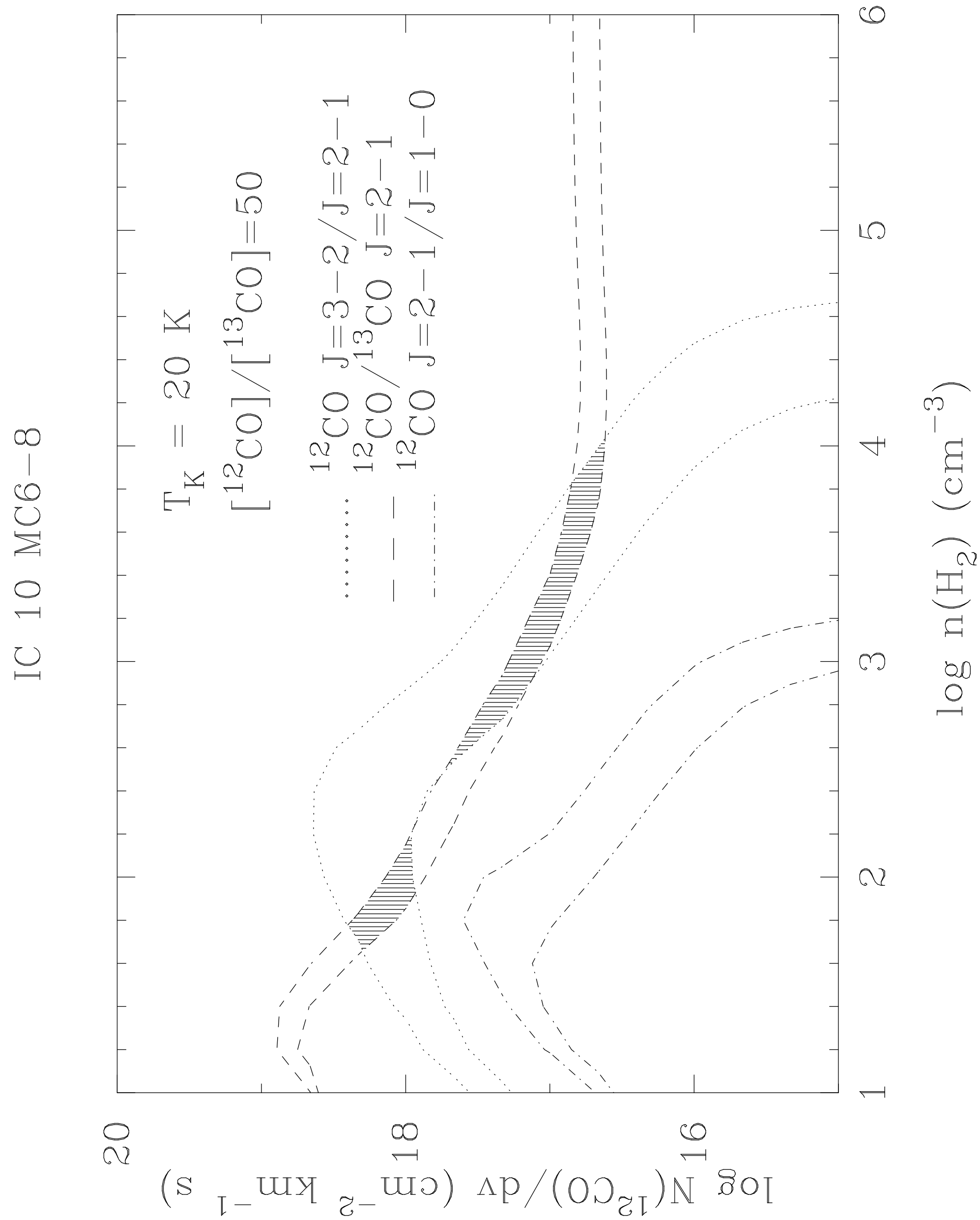

Figure 3.5: **LVG Solutions for IC 10 MC 6/7/8**

Typical LVG solution for the region MC 6/7/8 in IC 10 for a kinetic temperature of 20 K and a [^{12}CO]/[^{13}CO] abundance of 50. The dotted lines represent the 1σ limits of the ^{12}CO J=3−2/J=2−1 line ratio of 0.66 ± 0.11 while the dashed lines indicate the ^{12}CO/^{13}CO J=2−1 line ratio of 8.3 ± 1.4. The shaded region indicates the solutions for the JCMT data. Also included is the ^{12}CO J=2−1/J=1−0 line ratio of 0.50 ± 0.06 (^{12}CO J=1−0 data from Becker 1990). The ^{12}CO J=2−1/J=1−0 line ratio does not overlap with either of the JCMT line ratios.

of 30 K results only in a slightly lower upper limit on H_2 density ($10^{3.6}$ cm^{-3} instead of 10^4 cm^{-3}). Adopting a cooler kinetic temperature of 10 K indicates that H_2 densities greater than 10^4 cm^{-3} are required to produce the observed ^{12}CO J=3−2/J=2−1 and ^{12}CO/^{13}CO J=2−1 line ratios. As in IC 10:MC 1/2, the ^{12}CO J=2−1/J=1−0 line ratio for MC 6/7/8 does not overlap with the JCMT line ratios, which again suggests we may be seeing a combination of high and low density gas in this region.

3.3.2 MC 2 in NGC 6822

The molecular cloud MC 2 in NGC 6822 is located almost in the very center (within 1″) of the brightest H 2 region in NGC 6822. Discovered by Hubble (1925), and designated H 5 by Hodge *et al.* (1988), this H 2 region has an Hα luminosity of 4×10^{38} erg s^{-1} (Hodge, Lee & Kennicutt 1989). The ^{12}CO J=3−2/J=2−1 ratio (1.40 $\pm$ 0.07) is significantly higher than either of the IC 10 line ratios. The H 2 region H 5 is weaker than the giant H 2 region NGC 604 in M33 (Hα luminosity of 5×10^{39} erg s^{-1}, Kennicutt 1988) yet we see a much higher ^{12}CO J=3−2/J=2−1 line ratio in NGC 6822:MC 2. Again, as in IC 10, we see that in the low metallicity environment of NGC 6822, molecular clouds associated with H 2 regions can attain line ratios higher than in higher metallicity galaxies such as M33.

High J transitions can be readily excited by high temperatures, high densities, or some combination of the two. We would expect the temperature of molecular clouds near H 2 regions to be higher than those unassociated with H 2 regions. These higher temperatures would more readily excite the higher J transitions even in relatively low density regions. In the low density, hot gas there will be less CO in the lowest rotational levels and hence a lower probability of being reabsorbed (*i.e.* lower optical depth). Without separate constraints on the density, it is difficult to assess the role that density plays in producing this high line ratio. However, it can be shown from the virial theorem that for clouds with a relatively constant surface pressure the product of density and temperature ($\rho\ T$) is approximately constant (*e.g.* equation (2.8d), McLaughlin & Pudritz 1996). This result implies that for virialized clouds, an increase in temperature results in a decrease in density. It is likely that this cloud in NGC 6822 is in virial equilibrium (Wilson 1994, and next section). It also seems likely in the case of MC 2 that the temperature should be higher than in typical interstellar molecular clouds because of its close proximity to the OB stars generating the large H 2 region. We therefore conclude that in MC 2 the high line ratio is most likely the result of the high temperatures due to the proximity of the bright H 2 region.

With only one line ratio, a detailed LVG analysis is not possible. If we assume the cloud is in local thermodynamic equilibrium (LTE), we would expect line ratios no greater than unity for optically thick gas, while optically thin gas can produce much larger ratios (*e.g.* Walker 1991). The observed line ratio indicates that the ^{12}CO gas is optically thin in MC 2. CO is the most abundant molecule after H_2 and is generally found to be optically thick in giant molecular clouds. Optically thin ^{12}CO is quite rare, and likely the result of special physical conditions inside an H 2 region or possibly in starburst galaxies.

For gas to be molecular, it must be shielded by dust or have a high enough column density to be self-shielding. For molecular gas to collapse into stars, it is believed that the column density must exceed some critical value (*e.g.* Mouschovias & Spitzer 1976; Herbig & Terndrup 1986). In starbursts, the gas density may vary depending on how long ago the burst of star formation began. Initially, the collapse of the molecular clouds could give a higher than average gas density. The density should decrease as the gas is used up, new hot stars heat and expand the gas, and stellar winds blow gas out of the galaxy. This heating and expansion of the gas in a molecular cloud will decrease the density while leaving the column density unchanged (McLaughlin & Pudritz 1996). But, increasing the temperature excites more molecules to higher rotational levels, which decreases the opacity in the lower rotational levels. We should then expect to see optically thick gas in gravitationally sub-critical molecular clouds unless the clouds are heated sufficiently by external sources such as the active star forming regions we see in NGC 6822.

This heating effect may be amplified in the low metallicity environment of NGC 6822. Lower metallicity suggests a lower dust content, which would reduce the amount of shielding by dust from UV radiation from the star forming regions. With this reduced shielding, the UV radiation is able to heat the molecular gas more efficiently than is possible in higher metallicity (higher dust content) environments, which could contribute to the reduced optical depth seen in this galaxy. We might also expect optically thin gas in regions where there is simply less molecular gas. There is evidence for a deficit of molecular gas in the weak CO line strengths of NGC 6822. We thus attribute the low optical depth of the molecular gas in NGC 6822 to the low molecular gas content in this metal-poor environment. Our data are insufficient to sort out the extent to which each factor (namely low gas content and low metallicity) contribute to the low optical depth.

Optically thick gas (assuming LTE) can only produce CO line ratios ≤ 1 whereas optically thin gas can produce ^{12}CO J=3−2/J=2−1 line ratios of $\gtrsim 2.5$ for temperatures greater than 100 K (Walker 1991). It is possible that only a fraction of the gas in MC 2 is optically thin. For example, the cloud could be a mixture of 10% optically thin gas and 90% optically thick gas. Assuming the optically thin CO emission is not blocked by the optically thick emission, we would then expect our line ratios to be on the order of $1\times0.9 + 2.5\times0.1 = 1.15$ for a 100 K cloud. A rigorous calculation of the effect of mixtures of optically thin and thick gas is complicated and beyond the scope of this thesis. However, this simple calculation suggests that MC 2 contains at least ~25% optically thin gas. For simplicity, we will assume that the observed high ^{12}CO J=3−2/J=2−1 line ratio indicates that the entire cloud is optically thin.

With only one line ratio for MC 2 (^{12}CO J=3−2/J=2−1), we can only place crude limits on the temperature and density. However, we do not need to make any assumptions about the abundance ratio, since our data do not include any ^{13}CO observations. Figure 3.6 shows a possible solution for a temperature of 100 K. This temperature seems reasonable, considering MC 2 is located within a massive star forming region. If we assume a temperature any lower than 50 K, we would require densities greater than 10^6 cm^{-3} to achieve the observed line ratios. While this is not impossible, it seems more likely that this line ratio is a result of higher temperatures. For a temperature of 100 K, we can put a lower limit of $10^{4.2}$ cm^{-3} on density and an upper limit of 10^{17} cm^{-2} (km s^{-1})$^{-1}$ on column density per unit velocity. The full-width half maximum velocity of the emission lines in NGC 6822 is 5.4 ± 0.9 km s^{-1} which implies a true upper limit on column density of 5×10^{17} cm^{-2}.

If we increase the temperature above 100 K, we see that lower H_2 densities are allowed by the models. The observed line ratios can be produced with H_2 densities as low as 100 cm^{-3} with temperatures of 200 K, but the CO column densities increase to $> 5 \times 10^{18}$ cm^{-2}. Assuming a number density ratio of $n(\mathrm{CO})/n(\mathrm{H_2})$ of 10^{-4} (*e.g.* Genzel 1992) we obtain an H_2 column density of about 5×10^{22} cm^{-2}. This column density is uncomfortably close to the critical column density for molecular cloud collapse of $\sim 10^{22}$ cm^{-2}. As it seems unlikely that we are fortunate enough to observe a cloud that is on the brink of collapse, we will use the above value of the CO column density of 5×10^{17} cm^{-2} in further calculations.

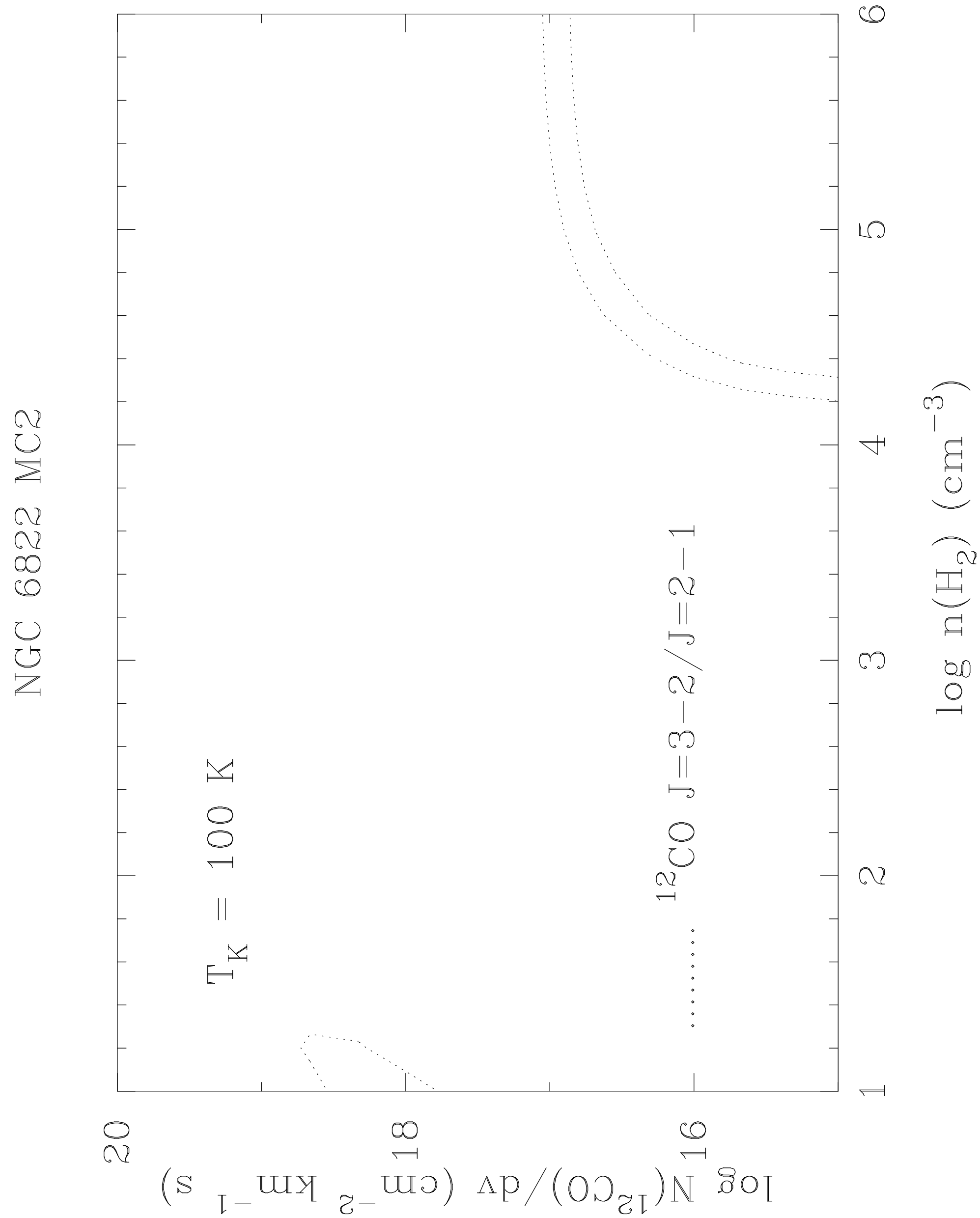

Figure 3.6: **LVG Solutions for NGC 6822 MC 2**

This figure shows one possible temperature (100 K) solution for the region MC 2 in NGC 6822. The dotted lines show the 1σ limits of the ^{12}CO J=3−2/J=2−1 line ratio of 1.4±0.07. With only a single line ratio, it is only possible to place lower limits on the temperature (> 50 K) and density (> 10^4 cm^{-3}).

3.3.3 Molecular Masses

The intensity of the CO emission can be related to the molecular mass of a cloud using the equation

$$M_{\rm mol} = 1.61 \times 10^4 \left(\frac{\alpha}{\alpha_{\rm Gal}}\right) \left(\frac{115\ \rm GHz}{\nu}\right)^2 d^2_{\rm Mpc}\, \frac{S_{\rm CO}}{R}\ \rm M_\odot \tag{3.1}$$

(Wilson & Scoville 1990; Wilson 1995) where $S_{\rm CO}$ is the ^{12}CO J=2−1 flux in Jy km s^{-1}, R is the ^{12}CO J=2−1/J=1−0 line ratio, ν is the frequency of the emission (230 GHz for the J=2−1 transition), $d_{\rm Mpc}$ is the distance to the cloud in Mpc, α is the CO-to-H_2 conversion factor for the galaxy, and $\alpha_{\rm Gal}$ is the Galactic value ($3 \pm 1 \times 10^{20}$ cm^{-2}(K km s^{-1})$^{-1}$, Strong *et al.* 1988; Scoville & Sanders 1987). The IC 10 ^{12}CO J=2−1/J=1−0 line ratio was calculated by combining Becker's (1990) IRAM ^{12}CO J=1−0 (21″ beam) with our JCMT ^{12}CO J=2−1 data (22″ beam)(see Table 3.1). For NGC 6822, a ^{12}CO J=2−1/J=1−0 ratio of 0.7 is assumed. The CO-to-H_2 conversion factor (α) is a globally averaged property of the galaxy and hence there are uncertainties involved in its use in one specific region of the galaxy. However, the conversion factor has been measured in these regions of the two galaxies, and so we adopt $\alpha/\alpha_{\rm Gal} = 2.7 \pm 0.5$ for IC 10 and 2.2 ± 0.8 for NGC 6822 (Wilson 1995). We use 34.6 Jy K^{-1} ($\eta_{\rm ap} = 0.45$) and 29.4 Jy K^{-1} ($\eta_{\rm ap}$= 0.53) to convert the JCMT data from Kelvins (T^*_A) to Janskys in IC 10 and NGC 6822 respectively (Kraus 1986). We assume a coupling efficiency (η_c) of 0.7 to correct our observed fluxes to true fluxes. The virial masses from Becker (1990) were corrected to the new IC 10 distance of 0.82

Mpc. The CO-to-H_2 conversion factor is only accurate to within $\sim$ 30% while our fluxes are typically accurate to about 10%. We therefore adopt a total uncertainty of 40%. The results are shown in Table 3.2.

It is interesting that the masses calculated here for the IC 10 regions are larger than the virial masses ($M_{\rm vir}$) found by Becker (1990). Our beam size of 22″ covers a diameter of 88 pc at the distance of IC 10. Although this beam is smaller than the dimensions of the clouds in IC 10 as measured by Becker using a comparable (21″) beam size (*e.g.* IC 10:MC 1/2 measured 107 pc $\times$ 98 pc), the IRAM dimensions are not much larger than the beam and were not deconvolved from the beam. Thus our single position measurements probably detect most of the emission in each region. Given the large uncertainties, the molecular mass of all the clouds in IC 10 lie within 2σ of the virial masses calculated by Becker (1990). If the clouds were not gravitationally bound, the virial masses would be larger than the molecular masses. We thus conclude that these quite large structures are gravitationally bound.

The mass of IC 10:MC 1/2 ($\sim 5 \times 10^6$ M$_\odot$) indicates that it may be either a large giant molecular cloud (GMC, $M = 10^5 - 10^6$ M$_\odot$, Sanders; Scoville, & Solomon 1985) or a small giant molecular association (GMA, $M = 10^7 - 10^8$ M$_\odot$ Rand & Kulkarni 1990). For star formation to occur, we would naturally expect that the molecular clouds in which the stars form must be gravitationally bound. All of the GMCs observed in IC 10 appear to be gravitationally bound (Wilson & Reid 1991; Wilson 1995). The larger region IC 10:MC 1/2 also appears to be gravitationally

Table 3.2: **Masses of Molecular Clouds in IC 10 and NGC 6822**

bound. Small GMAs seen in M33 all appear unbound by factors of about five *except* in giant H 2 regions (Wilson & Scoville 1989; 1992). In M51, the star formation efficiency is enhanced in the spiral arms where GMAs are seen (Rand & Kulkarni 1990). Individual GMCs inside the potential wells of the bound GMAs may be colliding at a much higher rate than isolated GMCs, which could increase the star formation rate and the star formation efficiency. Thus the presence of large bound molecular structures in IC 10 may provide a possible explanation for the high star formation rate in IC 10.

For NGC 6822:MC 2, the molecular mass is a factor of 3.4 larger than the virial mass calculated by Wilson (1994) using the Owens Valley Millimeter-Wave Interferometer. This large mass measurement may be caused by the larger $22''$ beam overlapping portions of the nearby cloud (NGC 6822:MC 1), which is approximately $17''$ away. Also, the virial masses for NGC 6822 are taken from interferometer data, which are insensitive to diffuse structures that can be detected by single dishes such as the JCMT. Finally, in determining the molecular mass for NGC 6822:MC 2, we assumed a ^{12}CO J=2$-$1/J=1$-$0 value of 0.7. Given the rather high ^{12}CO J=3$-$2/J=2$-$1 ratio, we might expect this cloud to have an unusually high ^{12}CO J=2$-$1/J=1$-$0 ratio as well. Increasing the ^{12}CO J=2$-$1/J=1$-$0 line ratio to a value of $\sim$1.0 would give molecular and virial mass estimates that agree within the uncertainties.

The CO-to-H_2 conversion factor relative to the Galactic value is determined by assuming the clouds are virialized and setting the molecular mass $M_{\rm mol}$ from equation (3.1) equal to the virial mass $M_{\rm vir}$. This method gives the relation $M_{\rm vir}/M_{\rm mol} = \alpha/\alpha_{\rm Gal}$ (*e.g.* Wilson 1995). Equation (3.1) assumes that the gas is optically thick and emission comes from the surface. However, MC 2 in NGC 6822 appears to be optically thin. For an optically thin cloud, the emission from the entire volume of the cloud can escape and we can get a much higher flux. This effect would result in an overestimate of the molecular mass found using equation (3.1), which in turn would result in an underestimate of $\alpha/\alpha_{\rm Gal}$. Even if only part of the cloud were optically thin, we would still be overestimating molecular masses. Because the clouds in NGC 6822 were not fully resolved, the derived virial masses were only upper limits and hence the value of $\alpha/\alpha_{\rm Gal}$ derived by Wilson (1994) is also an upper limit. Since NGC 6822:MC 2 is optically thin, we now see that $M_{\rm mol}$ was also overestimated, which would work to balance the previous uncertainty and make the value of $\alpha/\alpha_{\rm Gal}$ found by Wilson (1994) more reliable. However, since we do not know the extent of each mass overestimate, we cannot make precise corrections to the previously published values of α.

Given that the ^{12}CO emission from the cloud NGC 6822:MC 2 is optically thin, we have a rare opportunity to calculate the mass of the cloud directly. Using the upper limit on column density determined from the LVG analysis, we can estimate the mass by adopting a number density ratio of $n(\rm CO)/n(\rm H_2) = 10^{-4}$ (Genzel 1992) and multiplying by the area of the cloud πab, where a and b are the major and minor axes of the elliptical cloud. It is probably most appropriate to use the dimensions of the cloud obtained in the interferometry maps ($36\times < 13$ pc, Wilson (1994)) instead of the JCMT beam size. The LVG model indicates that the CO column density can be at most 5.3×10^{17} cm^{-2} (at temperatures of 100 K) to produce the observed line ratio, which leads to a total mass of H_2 of $< 1.2 \times 10^5$ $M_\odot$. This mass is in good agreement with the molecular mass derived using equation (3.1), and agrees with the virial mass to within a factor of two. As discussed in §3.3.3 we expect the mass derived from single dish flux to be overestimated. Since the virial mass is comparable to the mass derived from the column density, it is likely that the molecular cloud MC 2 in NGC 6822 is gravitationally bound.

3.4 Implications for the CO-to-H_2 Conversion Factor

It has been proposed that the CO-to-H_2 conversion factor (α) is not only dependent on density and brightness temperature ($\propto \sqrt{\rho}/T_{\rm b}$) but also on the metallicity (Dickman, Snell, & Schloerb 1986; Maloney & Black 1988; Sakamoto 1996). It is possible that the lower metallicity in irregular galaxies may change the typical temperatures and densities of the molecular clouds they contain. Although this effect may confuse any observed relation between α and metallicity, in essence it will simply introduce interrelationships between ρ, $T_{\rm b}$ and metallicity. Overall, the expression for α will still be a function of metallicity.

The line ratios for the clouds in IC 10 agree with those found in M33 by Wilson *et al.* (1997) within the measurement uncertainties (see Table 3.1). If we assume that the line widths are the same for both transitions, then the line ratios are essentially ratios of radiation temperature $T_{\rm R}$ (*e.g.* Walker 1991). The radiation temperature is related to the cloud excitation temperature and density by

$$T_{\rm R} = [J_\nu(T_{\rm ex}) - J_\nu(T_{\rm bg})]\,(1 - e^{-\tau}) \tag{3.2}$$

where $J_\nu(T)$ is the Planck function, $T_{\rm bg}$ is the background temperature, and $T_{\rm ex}$ is the excitation temperature of the cloud. The optical depth of the cloud is given by

$$\tau = \int_0^D K\rho\; dr \tag{3.3}$$

where D is the depth of the cloud, ρ is the density profile of the cloud and K is the absorption coefficient. For the optically thin case where $\tau \ll 1$, the ^{12}CO J=3−2/J=2−1 line ratio becomes

$$\frac{T_{\rm R}^{3-2}}{T_{\rm R}^{2-1}} = \frac{f^{3-2}\,[J_\nu(T_{\rm ex}^{3-2}) - J_\nu(T_{\rm bg})]\,\tau^{3-2}}{f^{2-1}\,[J_\nu(T_{\rm ex}^{2-1}) - J_\nu(T_{\rm bg})]\,\tau^{2-1}} \tag{3.4}$$

where f is the beam filling factor of the emission and the superscript 3-2 indicates those values pertaining to the J=3−2 transition. For the optically thick case, $\tau \gg 1$, the line ratio has the form

$$\frac{T_{\rm R}^{3-2}}{T_{\rm R}^{2-1}} = \frac{f^{3-2}\,[J_\nu(T_{\rm ex}^{3-2}) - J_\nu(T_{\rm bg})]}{f^{2-1}\,[J_\nu(T_{\rm ex}^{2-1}) - J_\nu(T_{\rm bg})]} \tag{3.5}$$

Both these line ratios are a complicated function of the excitation temperature. Thus to produce similar line ratios in clouds with different physical conditions would require a pathological interdependence of density and temperature to produce the same excitation temperature for the low-J CO transitions. We feel that the similarity in the line ratios in the clouds in IC 10 and M33 indicates similar physical conditions (namely similar ρ and T), and thus the difference in the measured value of α (Wilson 1995) can be attributed to the difference in metallicity of the spiral galaxy M33 and the metal poor dwarf irregulars IC 10 and NGC 6822.

3.5 Conclusions

We have observed the ^{12}CO J=2$-$1 and J=3$-$2 lines at a few locations in the dwarf irregular galaxies IC 10 and NGC 6822. In addition, we have observed the ^{13}CO J=2$-$1 and J=3$-$2 lines for molecular clouds in IC 10. The clouds are located in a variety of star formation environments. In general, the clouds in IC 10 show line ratios similar to those found in M33 by Wilson *et al.* (1997). We find that the ^{12}CO J=3$-$2/J=2$-$1 ratio increases with increasing proximity to H 2 regions as previously found by Wilson *et al.* (1997) in M33. This result may indicate a general relation that holds true for all galaxies (and galaxy types) and is likely the result of a combination of extreme temperature and density conditions near star-forming regions. In this low metallicity (and in NGC 6822, low CO column density) environment, this effect is more conspicuous than it is in the higher metallicity spiral galaxy M33.

Combining the JCMT line ratios in IC 10:MC 1/2 with large velocity gradient models indicates that this region has a kinetic temperature of 100 K, densities of $10^4 - 10^5$ cm^{-3} and a column density of 6×10^{18} cm^{-2}. The [^{12}CO]/[^{13}CO] abundance is between 50 and 70. The inclusion of the IRAM data from Becker (1990) suggests that there are two distinct emitting regions, a high density region where the upper J transitions dominate, and a lower density region where the lower J transitions dominate. For IC 10:MC 6/7/8, if we assume a temperature of 20 K and [^{12}CO]/[^{13}CO] = 50, we obtain densities of $10^{1.6} - 10^4$ cm^{-3} and column densities of $2 \times 10^{17} - 2 \times 10^{19}$ cm^{-2}.

We find an unusually high ^{12}CO J=3−2/J=2−1 line ratio in NGC 6822 which we attribute to optically thin CO emission resulting from the combination of a low molecular gas content in a low metallicity environment. An LVG analysis of the ^{12}CO J=3−2/J=2−1 line ratio in NGC 6822:MC 2 indicates the presence of hot (T $\geq$ 100 K), optically thin gas. The density of this cloud is likely greater than $10^{4.2}$ cm^{-3} and its column density is less than 5×10^{17} cm^{-2}.

The optically thin CO emission in NGC 6822 allows a rare opportunity to calculate the mass of molecular gas directly. Mass calculations from two separate techniques determine the molecular mass to be $1.2 - 2.1 \times 10^5$ $M_\odot$. This agrees with the virial mass to within a factor of ~3. Flux measurements yield masses for the cloud complexes in IC 10 which indicate that these regions are gravitationally bound. The masses of the clouds range from $0.83 - 5.2 \times 10^6$ $M_\odot$. These regions may represent either large giant molecular clouds or small giant molecular associations. The presence of these large gravitationally bound structures may help explain the high star formation rate in IC 10.

The similarity in the line ratios between IC 10 and M33 is most easily understood if the physical conditions in these clouds are also similar, in which case any variation in the CO-to-H_2 conversion factor between these two galaxies can be attributed to differences in their metallicity. The increase in the ^{12}CO J=3−2/J=2−1 ratio near star forming regions may be a result of either higher temperatures, higher densities or some combination of the two. Upcoming SCUBA observations will provide temperature measurements which will enable us to better determine the physical processes at work.

The JCMT is operated by the Royal Observatories on behalf of the Particle Physics and Astronomy Research Council of the United Kingdom, the Netherlands Organization for Scientific Research, and the National Research Council of Canada. This research has been supported by a research grant to C. D. W. from NSERC (Canada).

Chapter 4

Summary

This thesis presents [C I], ^{12}CO J=4−3, and ^{12}CO J=3−2 maps of the nucleus of the barred spiral galaxy M83, as well as a variety of CO spectra of molecular cloud complexes in the dwarf galaxies IC 10 and NGC 6822. We have used the observations of the molecular and atomic gas to study the dynamics and physical conditions in two very different types of galaxies, all undergoing starbursts of varying strengths. The central results are summarized below.

(1) In M83, we observe a double peaked structure in the molecular emission consistent with gas inflow along the bar collecting at the inner Lindblad resonance (ILR). The ^{12}CO J=4−3 emission suggests that some of the molecular gas has made it into the nucleus and is being heated by, and possibly fueling, the nuclear starburst. This indicates that nuclear starbursts may occur even in galaxies where gas collects at ILRs. The observations cannot rule out that the double peaked emission is the result of a molecular ring out of the plane of the galaxy nearly perpendicular to the main disk. This torus of gas contains a disk of hotter gas that fills the void at the

centre of the torus of cooler gas.

(2) We observe different morphologies in the ^{12}CO J=4−3 channel maps of M83 than in the ^{12}CO J=3−2 and ^{12}CO J=1−0 channel maps. This suggest that contrary to popular belief, ^{12}CO J=1−0 emission is not always a good tracer of molecular gas.

(3) The twelve [C I]/^{12}CO J=4−3 line ratios in the inner $24'' \times 24''$ of M83 are uniform at the 2σ level and have an average value of 0.25 ± 0.03, similar to those of other starburst galaxies. The uniformity of the line ratios may indicate that the processes creating and destroying CO in the $J = 4$ state and C I are comparable throughout the nucleus of M83. This in turn may indicate that the atomic carbon is is being created in the same hot environment that is capable of producing ^{12}CO J=4−3 emission, possibly the hot photon dominated regions around regions of active star formation.

(4) The ^{12}CO J=4−3/J=3−2 integrated intensity line ratios vary substantially over the central region of M83 with the highest ratios occurring towards the edges of the emission peaks. The ^{12}CO J=4−3/J=3−2 line ratios seem to be enhanced along an arc of active star forming regions. The high line ratios (>1) indicate that the higher J transitions of CO are optically thin and are likely the result of the high temperatures and/or densities associated with star formation.

(5) In general, the clouds in IC 10 show CO line ratios similar to those found in M33 (Wilson *et al.* 1997). We find that the ^{12}CO J=3−2/J=2−1 ratio increases

with increasing proximity to H II regions as previously found by Wilson *et al.* (1997). This may indicate a general relation that holds true for all galaxies (and galaxy types) and is likely the result of a combination of the extreme temperatures and densities near star-forming regions more readily exciting the higher J transitions of CO.

(6) The similarity in the line ratios between IC 10 and M33 is most easily understood if the physical conditions (namely density and temperature) in these clouds are also similar, in which case any variation in the CO-to-H_2 conversion factor between these two galaxies can be attributed solely to differences in their metallicity. The increase in the ^{12}CO J=3−2/J=2−1 ratio near star forming regions may be a result of either higher temperatures, higher densities or some combination of the two. Upcoming SCUBA observations will provide temperature measurements which will enable us to better determine the physical processes at work.

(7) Combining the JCMT line ratios in IC 10:MC 1/2 with large velocity gradient models indicates that this region has a kinetic temperature of 100 K, and that there exist two distinct emitting regions; a high density region where the upper J transitions dominate the emission, and a lower density region where the lower J transitions dominate. The ^{12}CO J=3−2/J=2−1 line ratio in NGC 6822:MC 2 indicates the presence of hot (T $\geq$ 100 K), optically thin gas, which is rare for CO.

(8) Flux measurements yield masses for the cloud complexes in IC 10 and NGC 6822 that agree with virial masses to within a factor of two, which indicates that these regions are gravitationally bound. The region MC 1/2 in IC 10 is massive

and may represent either a large giant molecular cloud or a small giant molecular association. The presence of these large gravitationally bound structures may help explain the high star formation rate in IC 10.

Future work will include analysis of the SCUBA data on the dust temperatures of molecular cloud complexes in the various star forming environments of IC 10. This will hopefully help unravel the coupling between high temperatures and densities in producing the observed high line ratios near star forming regions. It would also be interesting to obtain ^{12}CO J=3$-$2 and ^{12}CO J=4$-$3 maps of the other galaxies that exhibit the double peaked structure in the ^{12}CO J=1$-$0 namely M101, NGC 3351, and NGC 6951. The data would be analyzed to determine if a similar 'seepage' of gas into the nucleus is seen in these other galaxies. This may be an important factor in determining the triggering and fueling mechanisms of nuclear starbursts.

Appendix A

Spectral Line Calibration and Temperature Scales

Unfortunately, there are *many* different temperature scales in radio and submillimeter astronomy. It is also unfortunate that each of these has a purpose, so they cannot be eliminated and replaced with a 'standard' temperature scale. The secret to comparing data in one temperature scale to data in a different temperature scale is knowing how to convert from one to the other. These conversions usually only require knowledge of the telescopes efficiencies (η's). This section will describe the techniques for converting the temperature scale output by the telescope ($T_{\rm A}^{\star}$) to different temperature scales and how the telescope efficiencies are measured. An explanation of how the telescope obtains this original data is well documented and the reader is referred to Kraus (1986) for an exhaustive review.

The antenna temperature ($T_{\rm A}^{\star}$) is the temperature that the telescope measures. The $\star$ indicates that the data is corrected for atmospheric opacity through the chopper wheel calibration. This technique uses measurements from a blank region of the sky, in conjunction with hot loads placed in front of the receiver to determine the temperature of the source being observed. The $T_A^\star$ scale is useful because for any telescope, regardless of the elevation or atmospheric conditions, line strengths in $T_A^\star$ are repeatable to rather high precision at that telescope. The problem with the $T_A^\star$ scale is that it depends on the telescope being used and observations of the same source taken with different telescopes give different line strengths. Comparing data taken at different telescopes requires conversion from $T_A^\star$ to a source flux. The first step is to convert $T_A^\star$ (in K) to an observed source flux ($S_{\rm obs}$) in janskys (1 Jy = 10^{-26} W m^{-2} Hz^{-1}). This requires the relation

$$S_{\rm obs} = \frac{2kT_A^\star}{A_{\rm e}} = \frac{2kT_A^\star}{A_{\rm p}\eta_{\rm ap}} \tag{A.1}$$

(Kraus 1986) where k is the Boltzmann constant, $A_{\rm e}$ is the effective area of the telescope dish, $A_{\rm p}$ is the physical aperture of the dish, and $\eta_{\rm ap}$ is the telescope aperture efficiency. The value of $\eta_{\rm ap}$ can be determined by observing planets (which are considered uniform disks of known size and brightness) and assuming a Gaussian beam power pattern. These assumptions can be used to evaluate the observed brightness of the planet through

$$S_{\rm obs}^{\rm planet} = \int\int B^{\rm planet} P(r,\theta)\ d\Omega \tag{A.2}$$

where $B^{\rm planet}$ is the brightness of the planet (published) and $P(r,\theta)$ is the Gaussian power pattern of the telescope. The value of $S_{\rm obs}^{\rm planet}$ can be substituted along with the observed $T_A^\star$ for the planet into Equation A.1 to find $\eta_{\rm ap}$. Using this value for $\eta_{\rm ap}$

allows the rest of the data to be converted into observed fluxes.

The last step is to convert the observed flux ($S_{\rm obs}$) to an absolute flux using $S_{\rm true} = S_{\rm obs}/\eta_{\rm c}$ where $\eta_{\rm c}$ is the source-beam coupling efficiency which for a uniform source is the ratio of beam size to source size. Since most sources are not uniform, high resolution interferometry maps may be used to estimate $\eta_{\rm c}$. It should be noted that Equation A.1 is the source of the Jy-to-Kelvin conversion factor of 24.8 Jy/K adopted for the JCMT.

The above discussion allows for the conversion of temperatures to absolute fluxes in order to compare data from different telescopes. It is often the case that all of the data are taken with the same telescope. In this situation, any of the following temperature scales are acceptable as long they are used consistently, especially for data convolved to the same beam size. Some temperature scales have more physical meaning in certain situations, as will be pointed out.

It is commonly believed that the radiation temperature scale ($T_{\rm R}^\star$, Kutner & Ulich 1981) is most closely related to the 'true' temperature of the gas and is given by

$$T_{\rm R}^\star = \frac{T_{\rm A}^\star}{\eta_{\rm FSS}}. \tag{A.3}$$

This scale requires knowledge of the forward spillover and scattering efficiency ($\eta_{\rm FSS}$) which is a measure of how much of the radiation gathered is the result of reflection off the ground, support legs of the telescope and other such things. It is thus difficult to measure accurately and is not used in this thesis.

If it is possible to obtain a value for η_{FSS}, it is possible to scale the data to the true source brightness temperature (see Appendix C) given by

$$T_{\mathrm{B}} = \frac{T_{\mathrm{R}}^{\star}}{\eta_{\mathrm{c}}}. \tag{A.4}$$

For very large objects that fill the beam (*e.g.* Galactic giant molecular clouds) the brightness temperature is approximately the same as the radiation temperature.

The final temperature scale I will mention is the main beam temperature (T_{MB}) which is used throughout this thesis. It is given by the relation

$$T_{\mathrm{MB}} = \frac{T_{\mathrm{A}}^{\star}}{\eta_{\mathrm{MB}}} \tag{A.5}$$

where η_{MB} is the main beam efficiency. It can be determined from the relation

$$\eta_{\mathrm{MB}} = \frac{\Omega_{\mathrm{M}} A_{\mathrm{p}} \eta_{\mathrm{ap}}}{\lambda^2} \tag{A.6}$$

where Ω_{M} is the main beam solid angle. If one assumes a Gaussian beam and observes a object of known geometry and brightness (such as a planet), the FWHM of the main beam can be estimated by deconvolution, giving Ω_{M}. The JCMT has published values for the sizes of the main beam at different frequencies. The main beam temperature scale is approximately the brightness temperature for objects comparable in size to the main beam.

It can seen from the above discussion that line ratios in T_{MB} will differ from line ratios in $T_{\mathrm{R}}^{\star}$ by the factor

$$\left(\frac{\eta_{\mathrm{MB}}}{\eta_{\mathrm{FSS}}}\right)_{43}\left(\frac{\eta_{\mathrm{MB}}}{\eta_{\mathrm{FSS}}}\right)_{32}$$

(where the 43 subscript denotes values appropriate for the ^{12}CO J=4−3 transition) which for ^{12}CO J=4−3/J=3−2 line ratio with data taken at the JCMT is equal to 0.897. Thus we can see that line ratios in T_{MB} will differ from line ratios in $T_{\mathrm{R}}^{\star}$ by approximately 10%.

Appendix B

The CO-to-H_2 Conversion Factor

Since H_2 has no permanent electric dipole moment, it emits no dipole radiation. Thus, indirect techniques must be used to estimate its abundance. Despite its high optical depth, ^{12}CO J=1−0 emission is generally believed to trace the mass of molecular gas in luminous galaxies (see a review by Young & Scoville 1991). It is confirmed empirically in our own Galaxy through a variety of techniques (see §1) which all seem to obtain values of $N(\mathrm{H_2})/I_{\mathrm{CO}} = 1 - 5 \times 10^{20}$ cm^{-2}[K km s^{-1}]$^{-1}$. The most reliable technique for determining the CO-to-H_2 conversion factor (α) is the virial theorem analysis discussed in §3.4 which gives α for the Milky Way of $\sim 3 \times 10^{20}$ cm^{-2}[K km s^{-1}]$^{-1}$. The following discussion shows a simple explanation for the existence of a CO-to-H_2 conversion factor (Young & Scoville 1991).

The CO luminosity can be defined as

$$L_{\mathrm{CO}} = D^2 \int I_{\mathrm{CO}} d\Omega \tag{B.1}$$

where D is the distance to the cloud, I_{CO} is the CO integrated intensity ($\equiv \int T_{\mathrm{CO}} dv$), and Ω is the beam solid angle. For a spherical, uniform cloud with radius R, $L_{\rm CO}$ can be expressed

$$L_{\rm CO} = \pi R^2 T_{\rm CO} \Delta v \tag{B.2}$$

where Δv is the linewidth and $T_{\rm CO}$ is the peak brightness temperature of the cloud. For self-gravitating clouds with mass M in virial equilibrium, we have

$$\Delta v = \sqrt{\frac{GM}{R}}. \tag{B.3}$$

Substituting Equation B.3 into Equation B.2 and solving for M gives

$$M = \frac{L_{\rm CO}^2}{\pi^2 \; G \; T_{\rm CO}^2 \; R^3} \tag{B.4}$$

Substituting $R^3 = 3M/4\pi\rho$ into Equation B.4 and taking the square root gives

$$M = L_{\rm CO} \sqrt{\frac{4\rho}{3\pi G}} \frac{1}{T_{\rm CO}}. \tag{B.5}$$

This indicates there is a simple relation between CO luminosity and the mass (hence column density) of the molecular cloud which is proportional to $\sqrt{\rho}/T_{\rm CO}$.

It has been shown (*e.g.* Sakamoto 1996) that the factor $\sqrt{\rho}/T_{\rm CO}$ is the dominant factor in the CO-to-H_2 conversion factor (α). Cloud geometry and distribution within the beam play a very small role when observing clumps of clouds gathered in a telescope beam. The factor $\sqrt{\rho}/T_{\rm CO}$ is essentially a measure of the physical conditions inside the cloud. It is believed that metallicity will play a role in modifying the conditions in a cloud, hence it will modify the value of α (Young & Scoville 1991, Dickman, Snell & Schloerb 1986, Maloney & Black 1988). Higher metallicities will provide more shielding from UV rays that dissociate molecules, which act to decrease the CO-to-H_2 conversion factor by decreasing the CO luminosity (per unit molecular gas mass) in the optically thick gas.

Sakamoto (1996) found that the value of α can be expressed analytically in terms of the physical conditions inside the cloud under three extreme circumstances. His results are summarized below.

1. For dense ($\gtrsim 10^{3.5}$ cm^{-3}), metal-rich environments, the CO becomes optically thick and thermalized ($T_{\rm B} = T_{\rm K}$, see Appendix C). In this case, α becomes independent of the CO abundance and the conversion factor is expressed as

$$\alpha \propto \frac{\sqrt{\rho}}{T_{\rm K}} \tag{B.6}$$

2. For dense molecular gas under metal-poor environments, the gas becomes optically thin and thermalized. In this case the brightness temperature is proportional to the kinetic temperature, the CO column density per velocity width ($N(\mathrm{CO})/dv$), and the population at the lowest rotational level ($\propto 1/T_{\rm K}$). Thus, we have

$$\alpha \propto \frac{1}{Z(\mathrm{CO})} \tag{B.7}$$

   where $Z(\mathrm{CO})$ is the fractional abundance of CO to H_2 which is a measure of the metallicity of the gas.

3. For low density, metal-poor gas, the CO emission becomes optically thin and subthermal ($T_{\rm K} < T_{\rm ex}$, but collisions can still excite emission). In this case, the brightness temperature is proportional to the rate of collisional excitation throughout the line of sight per unit velocity width ($[N({\rm CO})/dv]n({\rm H_2})\sqrt{T_{\rm K}}$) and the CO-to-$H_2$ conversion factor is given as

$$\alpha \propto \frac{1}{n({\rm H_2})Z({\rm CO})\sqrt{T_{\rm K}}} \tag{B.8}$$

It is difficult to disentangle the above relations since we rarely know all the information required in the above relations. It is possible to make comparisons that eliminate the need to know some of the elements. For example, CO line strengths (hence, line ratios) depend on the physical conditions within the molecular gas (namely density and temperature). If we observe similar line ratios in two different galaxies (as we do in IC 10 and M33) we can pretty safely say that the molecular clouds in each galaxy have similar physical conditions. We can then say that any difference in the measured CO-to-H_2 conversion factor can be attributed to the differences in metallicity between these two galaxies. By measuring the physical conditions of molecular gas and the CO-to-H_2 conversion factor in different metallicity environments we can test the above hypotheses (*cf.* Wilson 1995).

Appendix C

Local Thermodynamic Equilibrium

Our interpretation of integrated intensity line ratios depends greatly on the use of models. One of the models used in this thesis is the Local Thermodynamic Equilibrium (LTE) approximation. Before I discuss the details of the model, I will start with a brief overview of radiative transfer.

Consider a cloud that is emitting (emission coefficient ϵ_ν) and absorbing (absorption coefficient κ_ν) at some frequency ν. We denote $\epsilon_\nu d\omega$ as the radiation energy emitted per unit time, volume, and frequency in the solid angle $d\omega$ towards the observer. Let I_ν be the intensity of the radiation such that $I_\nu d\omega$ is the energy per unit time and frequency, flowing across a unit area within the solid angle $d\omega$. Along the path element from s to $s + ds$ the intensity increases by $\epsilon_\nu d\omega ds$ and conversely undergoes absorption proportional to I_ν along the same path length, expressed as $\kappa_\nu I_\nu d\omega ds$. The balance of emission and absorption $dI_\nu d\omega \equiv \epsilon_\nu d\omega ds - \kappa_\nu I_\nu d\omega ds$ leads to the equation of radiative transport

$$\frac{dI_\nu}{ds} = -\kappa_\nu I_\nu + \epsilon_\nu. \tag{C.1}$$

If we define the optical depth such that $d\tau_\nu = -\kappa_\nu ds$ then Equation C.1 can be written

$$\frac{dI_\nu}{d\tau_\nu} = I_\nu - \frac{\epsilon_\nu}{\kappa_\nu}. \tag{C.2}$$

In order to determine I_ν mathematically, we need to know the last term in the above equation, called the source function S_ν $(= \epsilon_\nu/\kappa_\nu)$. Multiplying by the integration factor $e^{-\tau_\nu}$ allows direct integration, yielding

$$I_\nu(\tau_\nu)e^{-\tau_\nu} = -\int^{\tau_\nu} S_\nu(\tau'_\nu)e^{-\tau'_\nu}d\tau'_\nu \quad . \tag{C.3}$$

Writing this equation once for $\tau_\nu = 0$ (cloud surface facing observer) and once for the optical thickness of the whole cloud ($\tau_\nu^{\rm tot}$) and subtracting the two gives

$$I_\nu(\tau_\nu = 0) - I_\nu(\tau_\nu^{\rm tot})e^{-\tau_\nu^{\rm tot}} = -\int_{\tau_\nu^{\rm tot}}^{0} S_\nu(\tau_\nu)e^{-\tau_\nu}d\tau_\nu \quad . \tag{C.4}$$

Letting the background intensity $I_\nu(\tau_\nu^{\rm tot}) = I_{\nu,\rm bg}$, we can write the observed intensity at the side of the cloud nearest the observer $(\tau_\nu = 0)$ as

$$I_\nu = I_\nu(\tau_\nu = 0) = \int_0^{\tau_\nu^{\rm tot}} S_\nu(\tau_\nu)e^{-\tau_\nu}d\tau_\nu + I_{\nu,\rm bg}e^{-\tau_\nu^{\rm tot}}. \tag{C.5}$$

Assuming $S_\nu(\tau_\nu)$ as roughly constant over the cloud, integration yields

$$I_\nu = S_\nu[1 - e^{-\tau_\nu^{\rm tot}}] + I_{\nu,\rm bg}e^{-\tau_\nu^{\rm tot}} \quad . \tag{C.6}$$

The observations we obtain from the telescope have been sky subtracted through observations on an source free part of the sky (assumed equal to $I_{\nu,\mathrm{bg}}$). This means the observed intensity can be expressed

$$I_\nu^{\mathrm{obs}} = I_\nu - I_{\nu,\mathrm{bg}} = [S_\nu - I_{\nu,\mathrm{bg}}](1 - e^{-\tau_\nu^L}) \tag{C.7}$$

In LTE we assume that the gas is collisionally dominated and hence the relative populations between molecular energy levels are only a function of one temperature. The definition of LTE is that the kinetic temperature (T_{K}) of the gas is equal to the excitation temperature (T_{ex}). In this approximation, the brightness of an object at a given temperature ($T = T_{\mathrm{ex}} = T_{\mathrm{K}}$) and frequency ($\nu$) is given by Planck's law, namely

$$S_\nu = B_\nu(T) = \frac{2h\nu^3}{c^2}\frac{1}{e^{h\nu/kT} - 1} \tag{C.8}$$

where c, h, and k are the speed of light, Planck and Boltzmann's constants, respectively.

The observed brightness can be expressed as an effective source radiation temperature $J_\nu(T)$ defined as

$$J_\nu(T) = \frac{c^2 B_\nu(T)}{2\nu^2 k} \tag{C.9}$$

which reduces to

$$J_\nu(T) = \frac{h\nu/k}{e^{k\nu/kT} - 1}. \tag{C.10}$$

(At radio wavelengths, we have that $h\nu \ll kT$ and Equation C.10 reduces to $J_\nu(T) = T$. This is not a good approximation for submillimeter wavelengths so it is not used in this thesis.) If we assume the background source can also be approximated by the Planck function, multiplying Equation C.7 by the term $c^2/2\nu^2 k$ and dropping the superscript L gives intensity of an emission line as follows (*e.g.* Walker 1991)

$$J_\nu(T_\mathrm{B}) = [J_\nu(T_\mathrm{ex}) - J_\nu(T_\mathrm{bg})]\,(1 - e^{-\tau}) \tag{C.11}$$

where T_B is the source brightness temperature, T_ex is the gas excitation temperature (= kinetic temperature in LTE), and the $J_\nu(T_\mathrm{bg})$ term accounts for brightness caused by any background temperature source (T_bg, usually the 2.7 K cosmic background radiation). The brightness temperature is defined as the blackbody temperature that produces the observed intensity, namely $I_\nu \equiv J_\nu(T_\mathrm{B})$. The $(1 - e^{-\tau})$ term accounts for absorption within the cloud of optical depth τ. The optical depth is a measure of how deep into the cloud we can see. The optical depth can range from values $\ll 1$ (optically thin, translucent) to $\gg 1$ (optically thick, opaque).

The effective source radiation temperature (T_R) is defined as the temperature that would be observed with a radio telescope having a perfect surface (no losses), above the atmosphere, with an infinitesimally small beam (Kutner & Ulich 1981). Since this scenario is not quite within reach yet, we must try to make the appropriate corrections. The atmosphere can be corrected for by taking the observations using the *chopper wheel* method and the telescope efficiencies can be measured. The remaining factor (called the filling factor, f_ν) is more difficult to evaluate. Even though we can calculate the size of our beam, we do not know the size of the object at which we are looking. Since molecular clouds are clumpy, even if the cloud dimensions are larger than the beam, we do not know how much of the cloud is emitting radiation. For this reason, the radiation temperature is written as follows

$$T_{\rm R} = f_\nu I_\nu = f_\nu \left[J_\nu(T_{\rm ex}) - J_\nu(T_{\rm bg})\right](1 - e^{-\tau}). \tag{C.12}$$

Intensities in terms of $T_{\rm R}$ are as close as we can get to "true" source intensities without knowledge of the structure of the source. As seen in the equation, in order to obtain the measured intensity in terms of radiation temperature, knowledge of the unknown filling factor f_ν is required.

One way of eliminating this problem is to create line ratios. For clouds with similar line widths for different frequency emissions, the ratio of integrated intensities is essentially the ratio of radiation temperatures, except for the unknown filling factors. Dividing the integrated intensities of two different molecular transitions (^{12}CO J=3−2/^{12}CO J=2−1 for example) gives

$$R_{32/21} = \frac{f_{32}[J_\nu(T_{32}) - J_\nu(T_{\rm bg})](1 - e^{-\tau_{32}})}{f_{21}[J_\nu(T_{21}) - J_\nu(T_{\rm bg})](1 - e^{-\tau_{21}})} \tag{C.13}$$

where T and τ are the excitation temperature and optical depth for the transition denoted in the subscript. If we assume that the same regions in the beam (namely, the molecular clouds) are emitting all the observed radiation that (*i.e.* $f_{32} = f_{21}$) the expression reduces to

$$R_{32/21} = \frac{[J_\nu(T_{32}) - J_\nu(T_{\rm bg})](1 - e^{-\tau_{32}})}{[J_\nu(T_{21}) - J_\nu(T_{\rm bg})](1 - e^{-\tau_{21}})}. \tag{C.14}$$

which is a direct relation between integrated intensities and radiation temperatures.

We now wish to determine what excitation temperature (or kinetic temperature) will produce the observed line ratios. As mentioned above, there are generally two limits with which we are concerned: the optically thick ($\tau \gg 1$) case and the optically thin ($\tau \ll 1$) case. For $\tau \gg 1$ we have $(1 - e^{-\tau}) \rightarrow 1$ and thus

$$R^{\rm thick}_{32/21} = \frac{[J_\nu(T_{32}) - J_\nu(T_{\rm bg})]}{[J_\nu(T_{21}) - J_\nu(T_{\rm bg})]} \tag{C.15}$$

which in LTE ($T_{32} = T_{21} = T_{\rm K} = T_{\rm ex} = T$) is just a weak function of frequency (contained in the definition of $J_\nu(T)$ and gives $R^{\rm thick}_{32/21} \approx 1$.

For the optically thin case ($\tau \ll 1$) we have that $(1 - e^{-\tau}) \rightarrow \tau$ and Equation C.14 reduces to

$$R^{\rm thin}_{32/21} = \frac{[J_\nu(T_{32}) - J_\nu(T_{\rm bg})]\tau_{32}}{[J_\nu(T_{21}) - J_\nu(T_{\rm bg})]\tau_{21}}. \tag{C.16}$$

which in LTE depends on frequency (as above) and τ_ν and can be expressed $R^{\rm thin}_{32/21} \approx \tau_{32}/\tau_{21}$.

Optical depth is a rather complicated function that depends on the frequency of the emission, the path length through the cloud (L), Einstein coefficients and many other things. An analytic expression has fortunately been derived by Scheffler &

Elsässer (1988, assumes density at an rotational energy level n_J and $T_{\rm ex}$ constant along the line of sight). For a diatomic molecule such as CO, the optical depth for the $J+1 \rightarrow J$ transition at the frequency $\nu_{J+1,J}$ is given by

$$\tau_{J+1,J} = \frac{8\pi^3 \nu_{J+1,J} \mu^2}{3hc} \frac{(2J+3)(J+1)}{(2J+1)^2} \left[1 - e^{-h\nu_{J+1,J}/kT_{\rm ex}}\right] n_J \; L \; \phi_{J+1,J} \tag{C.17}$$

where J is the lower rotational state, μ is the dipole moment of the molecule, and $\phi_{J+1,J}$ is the line profile function which is normalized to unity over the frequency range of the line. Using Equation C.17 to evaluate the last part of Equation C.16, we obtain

$$\frac{\tau_{32}}{\tau_{21}} = \frac{189}{250} \frac{\nu_{32} \; [1 - e^{-h\nu_{32}/kT_{\rm ex}}] \; n_2 \; \phi_{32}}{\nu_{21} \; [1 - e^{-h\nu_{21}/kT_{\rm ex}}] \; n_1 \; \phi_{21}}. \tag{C.18}$$

To calculate the n_2/n_1 term in Equation C.18, we use the equation

$$\frac{n_J}{n_{\rm tot}} = (2J+1) e^{-\frac{Jh\nu_{J+1,J}}{2kT_{\rm ex}}} \left(\frac{hB}{kT_{\rm ex}}\right) \tag{C.19}$$

where $B = \nu_{J+1,J}/[2(J+1)]$ is the rotational constant of the molecule. Equation C.19 can be used to calculate $n_2/n_{\rm tot}$ and $n_1/n_{\rm tot}$. The ratio of these can be used to obtain n_2/n_1 which can be substituted into Equation C.18, allowing expression of the ratio of optical depths (hence line ratios) as a function of temperature and laboratory measured frequencies and constants.

Appendix D

Large Velocity Gradient

The observed width of interstellar molecular lines (a few tens of km s^{-1}) is much larger than is predicted for plausible thermal velocities ($<$ 1 km s^{-1}) within the molecular cloud (Goldreich & Kwan 1974). This suggest the existence of either sizable velocity gradients or non-thermal supersonic motions in dense clouds. (The non-thermal supersonic motions are not likely the cause since they would require a strong source of mechanical energy to sustain them.) Interpretation of observed line strengths in clouds that are not optically thin involves the formidable task of solving the equations of radiative transfer in a moving medium. This problem was first approached by Sobolev (1958) for the expanding envelopes of Wolf-Rayet stars. It was adapted to clouds undergoing gravitational collapse by Goldreich & Kwan (1974) and also to clouds with large random internal motions by Scoville & Solomon (1974).

The basic assumption in this model is that the clouds have random internal velocities that are large enough to Doppler shift the emission to a different frequency such that if it does not get re-absorbed locally, it cannot be re-absorbed by another region of the cloud. In this assumption, solving the equations of radiative transfer becomes a local problem and the source function (see Appendix C) can be expressed as

$$S = \frac{2h\nu^3}{c^2} \frac{1}{g_{ul} n_l / n_u - 1} \tag{D.1}$$

(Scoville & Solomon 1974) where n_i is the number density of molecules in the i^{th} energy level and g_{ul} $[= (n_u/n_l)e^{h\nu/kT_{ul}} = (2J+3)/(2J+1)]$ is the statistical weight ratio of the molecules in the upper and lower energy levels (denoted by the subscripts u and l respectively). Recall that the observed emission line intensity will be given by

$$I = (S - I_0)(1 - e^{-\tau}) \tag{D.2}$$

(Appendix C) where I_0 is the background intensity and τ is the optical depth, in this approximation given by

$$\tau = \frac{g_{ul} c^3}{8\pi\nu^3 dv/dz} A_{ul} (1 - e^{-h\nu/kT_{ul}}) n_l \tag{D.3}$$

(Scoville & Solomon 1974) where ν is the frequency of the emission, v is the velocity (assumed to be equal to the observed line width), z is the depth into the cloud, A_{ul} is the Einstein coefficient for the $J = u \to l$ transition, and T_{ul} is the excitation temperature for this transition.

Notice that the above equations depend on gas densities and the relative energy level populations of the gas. After adopting a kinetic temperature T_{K}, one can solve the rate equations (which utilize collision probabilities, collisional cross sections and other such terms) to determine the relative populations of the energy levels. A detailed explanation of collision probability and excitation is given in de Jong, Chu, & Dalgarno (1975) and will not be reproduced here. There is no need to assume thermodynamic equilibrium as we did in Appendix C because the excitation temperature can be calculated from the Boltzmann equation, namely

$$\frac{n_u}{n_l} = g_{ul} e^{-(E_u - E_l)/kT_{\mathrm{ex}}} \tag{D.4}$$

where E_i is the excitation energy of the i^{th} energy state. This model allows the excitation temperature to be different from the kinetic temperature, which is much more realistic than assuming they are equal.

The model can be run for a range of H_2 densities ($n(\mathrm{H_2})$, which dominate the collisional processes) and range of CO column densities ($N(\mathrm{CO})$, which govern the level populations for the emitting gas) at a given kinetic temperature (T_{K}). Note that term $n_l/dv/dz$ in Equation D.3 can be re-expressed as $n_l dz/dv = N/dv$ which is the column density per unit velocity, which is the variable on the x-axis of the LVG plots shown in this thesis.

References

Anantharamaiah, K. R., & Goss, W. M., 1996, ApJ, 466, L13

Arnault, P., Casoli, F., Combes, F., & Kunth, D., 1988, A&A, 205, 41

Balcells, M., & Quinn, P., 1990, ApJ, 361, 381

Becker, R., 1990, Ph.D. thesis, Bonn

Binney, J., & Tremaine, S., 1987, Galactic Dynamics (Princeton: Princeton Univ. Press)

Bloeman, H., 1989, ARA&A, 27, 469

Bohlin, R. C., Cornett, R. H., Hill, J. K., Smith, A. M., & Stecher, T. P., 1983, ApJ, 274, L53

Combes, F., 1986, in Star Forming Dwarf Galaxies and Related Objects, ed. D. Kunth, T. X. Thaun, & J. Tran Thanh Van (Singapore: Kim Hup Lee Printing Co.), 307

Combes, F., Encrenaz, P. J., Lucas, R., & Weliachew, L., 1978, A&A, 67, L13

Combes, F., 1988, in Galactic and Extragalactic Star Formation, ed. R. E. Pudritz & M. Fich (Dordrecht: Kluwer), 475

Comte, G., 1981, A&AS, 44, 441

Cowen, J. J., & Branch, D., 1985, ApJ, 293, 400

de Jong, T., Chu, S.-I., & Dalgarno, 1975, ApJ, 199, 69

Dickman, R. L., Snell, R. L., & Schloerb, F. P., 1986, ApJ, 309, 326

Elmegreen, B. G., & Lada, C. J., 1977, ApJ, 214, 725

Elmegreen, B. G., Elmegreen, D. M., & Morris, M., 1980, ApJ, 240, 455

Elmegreen, B. G., 1989, ApJ, 338, 178

Gallagher, J. S., Hunter, D. A., Gillett, F. C., & Rice, W. L., 1991, ApJ, 371, 142

Gallais, P., Rouan, D., Lacombe, F., Tiphene, D., & Vauglin, I., 1991, A&A, 243, 309

Genzel, R., 1992, in The Galactic Interstellar Medium, ed. D. Pfenniger, P. Bartholdi (Berlin: Springer-Verlag), 275

Goldreich, P., & Kwan, J., 1974, ApJ, 189, 441

Green, S., & Thaddeus, P., 1976, ApJ, 205, 766

Güsten, R., Serabyn, E., Kasemann, C., Schinckel, A., Schneider, G., Schultz, A., & Young, K., 1993, ApJ, 402, 537

Handa, T., Nakai, N., Sofue, Y., Hayashi, M., & Fujimoto, M., 1990, PASJ, 42, 1

Handa, T., Ishizuki, S., & Kawabe, R., 1994, in Astronomy with Millimeter and Submillimeter Wave Interferometry, IAU Colloquium No. 140, ed. M. Ishiguro & W. J. Welch, 341

Herbig, G. H., & Terndrup, D. M., 1986, ApJ, 307, 609

Hodge, P. W., Kennicutt, R. C., & Lee, M. G., 1988, PASP, 100, 917

Hodge, P. W., Lee, M. G., & Kennicutt, R. C., 1989, PASP, 101, 32

Hubble, E. P., 1925, ApJ, 62, 409

Hunter, D. A., Gallagher, J. S., Rice, W. L., & Gillett, F. C., 1989, ApJ, 336, 152

Ishizuki, S., Kawabe, R., Ishiguro, M., Okumura, S. K., Morita, K.-I., Chikada, Y., & Kasuga, T., 1990, Nature, 344, 224

Israel, F. P., 1991, in Dynamics of Galaxies and Their Molecular Molecular Cloud Distribution, IAU Symposium No. 146, eds F. Combes & F. Casoli (Dordrecht: Kluwer), 13

Israel, F. P., *et al.*, 1993, A&A, 276, 25

Israel, F. P., White, G. J., & Baas, F., 1995, A&A, 302, 343

Israel, F. P., 1997, A&A, 317, 65

Jackson, J. M., Barrett, A. H., Armstrong, J. T., & Ho, P. T. P., 1987, AJ, 93, 531

Keene, J., Blake, G. A., Phillips, T. G., Huggins, P. J., & Beichman, C. A., 1985, ApJ, 299, 967

Kenney, J. D. P., & Lord, S. D., 1991, ApJ, 381, 118

Kenney, J. D. P., Wilson, C. D., Scoville, N. Z., Devereux, N. A., & Young, J. S., 1992, ApJ, 395, L79

Kraus, J. D., 1986, Radio Astronomy 2nd ed, (Ohio: Quasar-Cygnus)

Kutner, M. L., Ulich, B. L., 1981, ApJ, 250, 341

Larkin, J. E., Graham, J. R., Matthews, K., Soifer, B. T., Beckwith, S., Herbst, T. M., & Quillen, A. C., 1994, ApJ, 420, 159

Madden, S. C., Poglitsch, A., Geis, N., Stacey, G. J., & Townes, C. H., 1997, ApJ, 483, 200

Maloney, P., & Black, J. H., 1988, ApJ, 325, 389

Massey, P., & Armandroff, T. E., 1995, AJ, 109, 2470

McGonegal, R., McLaren, R. A., Welch, D. L., Madore, B. F., & McAlary, C. W., 1983, ApJ, 273, 539

McLaughlin, D. E., & Pudritz, R. E., 1996, ApJ, 469, 194

Morton, D. C., Drake, J. F., Jenkins, E. B., Rogerson, J. B., Spitzer, L., & York, D. G.,1973, ApJ, 181, L103

Mouschovias, T., & Spitzer, L., 1976, ApJ, 210, 326

Ohta, K., Sasaki, M., & Saito, M., 1988, PASJ, 40, 653

Ohta, K., Tomita, A., Saito, M., Sasaki, M., & Nakai, N., 1993, PASJ, 45, L21

Park, Y. -S., & Hong, S. S., 1995, A&A, 300, 890

Pence, W. D., 1981, ApJ, 247, 473

Phillips, T. G., & Huggins, P. J., 1981, ApJ, 251, 533

Plume, R., Jaffe, D. T., & Keene, J., 1994, ApJ, 425, L49

Rand, R. J., & Kulkarni, S. R., 1990, ApJ, 349, L43

Rogstad, D. H., Lockhart, I. A., & Wright, M. C. H., 1974, ApJ, 193, 309

Sakamoto, S., Hayashi, M., Hasegawa, T., Handa, T., & Oka, T., 1994, ApJ, 425, 641

Sakamoto, S., 1996, ApJ, 462, 215

Sandage, A., & Tammann, G. A., 1974, ApJ, 194, 559

Sanders, D. B., Scoville, N. Z., & Solomon, P. M., 1985, ApJS, 289, 373

Scheffler, H., Elsässer, H., 1988, Physics of the Galaxy and Interstellar Matter, eds. M. Harwit, R. Kippenhahn, J.-P. Zahn (Berlin: Springer-Verlag)

Schilke, P., Carlstrom, J. E., Keene, J., & Phillips, T. G., 1993, ApJ, 417, L67

Schmidt, K.-H., & Boller, T., 1993, Astron. Nachr., 314, 5, 361

Scoville, N. Z., & Sanders, D. B., 1987, in Interstellar Processes, eds. D. J. Hollenbach & H. A. Thronson (Dordrecht: Reidel), 21

Scoville, N. Z., & Solomon, P. M., 1974, ApJ, 187, L63

Shen, J., & Lo, K. Y., 1995, ApJ, 445, L99

Shlosman, I., Frank, J., & Begelman, M. C., 1989, Nature, 338, 45

Shostak, G. S., & Skillman, E. D., 1989, A&A, 214, 33

Sobolev, V. V., 1958, Theoretical Astrophysics, ed. V. A. Ambartsumyan, (London: Pergamon Press Ltd.), Ch 29

Sofue, Y., & Wakamatsu, K. -I., 1994, AJ, 107, 1018

Solomon, P. M., Rivolo, A. R., Barrett, J., & Yahil, A., 1987, ApJ, 319, 730

Sørensen, S. -A., Matsuda, T., & Fujimoto, M., 1976, Ap&SS, 43, 491

Spitzer, L., 1978, Physical Processes in the Interstellar Medium, (New York: Wiley)

Stark, R., & van Dishoeck, E. F., 1994, A&A, 286, 443

Strong, A. W., Bloeman, J. G. B. M., Dame, T. M., Grenier, I. A., Hermsen, W., LeBrun, F., Nyman, L. -A., Pollock, A. M. T., & Thaddeus, P., 1988, A&A, 207, 1

Stutzki, J., & Güsten, R., 1990, ApJ, 356, 513

Tacconi, L. J., & Young, J. S., 1987, ApJ, 332, 681

Tacconi, L. J., & Young, J. S., 1987, ApJ, 332, 681

Talbot, R. J., Jr., Jensen. E. B., & Dufour, R. J., 1979, ApJ, 229, 91

Telesco, C. M., & Harper, D. A., 1980, ApJ, 235, 392

Thronson, H. A., Hunter, D. A., Casey, S., & Harper, D. A., 1990, ApJ, 355, 94

Tilanus, R. P. J., Tacconi, L. J., Sutton, E. C., Zhou, S., Sanders, D. B., Wynn-Williams, C. G., Lo, K. Y., & Stephens, S. A., 1991, ApJ, 376, 500

Tilanus, R. P. J., & Allen, R. J., 1993, A&A, 274, 707

Tully, R. B., 1988, Nearby Galaxies Catalogue, (Cambridge: Cambridge Press)

Turner, B. E., 1988, in Galactic and Extragalactic Radio Astronomy, 2$^{\text{nd}}$ Edition, eds. G. L. Verschuur & K. I. Kellermann, (New York: Springer-Verlag), Ch 4

de Vaucouleurs, G., & Ables, H., 1965, PASP, 77, 272

Vogel, S. N., Kulkarni, S. R., & Scoville, N. Z., 1988, Nature, 334, 402

Walker, C. E., 1991, Ph.D. Thesis, University of Arizona

Walker, C. E., Bash, F. N., Martin, R. N., & Phillips, T. G., 1992, RMxAA, 27, 203

Wall, W. F., Jaffe, D. T., Bash, F. N., Israel, F. P., Maloney, P. R., & Baas, F., 1993, ApJ, 414, 98

White, G. J., Ellison, B., Claude, S., Dent, W. R. F., & Matheson, D. N., 1994, A&A, 284, L23

White, G. J., & Sandell, G., 1995, A&A, 299, 179

Wiklind, T., Rydbeck, G., Hjalmarson, Å., & Bergman, P., 1990, A&A, 232, L11

Wilson, C. D., & Scoville, N. Z., 1989, ApJ, 347, 74

Wilson, C. D., & Scoville, N. Z., 1990, ApJ, 363, 435

Wilson, C. D., & Reid, I. N., 1991, ApJ, 366, L11

Wilson, C. D., & Scoville, N. Z., 1992, ApJ, 385, 512

Wilson, C. D., 1994, ApJ, 434, L11

Wilson, C. D., 1995, ApJ, 448, L97

Wilson, C. D., Welch, D. L., Reid, I. N., Saha, A., & Hoessel, J., 1996, AJ, 111, 1106

Wilson, C. D., Walker, C. E., & Thornley, M. D., 1997, ApJ, in press

Wilson, C. D., 1997, ApJ, accepted

Wright, E. L., *et al.*, 1991, ApJ, 381, 200

Young, J. S., & Scoville, N. Z., 1991, ARA&A, 29, 581